Electron Transfer in Flavodoxin-based Redox Maquettes

Alagaratnam, S.

ELECTRON TRANSFER IN FLAVODOXIN-BASED REDOX MAQUETTES

Proefschrift

ter verkrijging van

de graad van Doctor aan de Universiteit Leiden,

op gezag van de Rector Magnificus Dr. D. D. Breimer,

hoogleraar in de faculteit der Wiskunde en

Natuurwetenschappen en die der Geneeskunde,

volgens besluit van het College voor Promoties

te verdedigen op maandag 24 october 2005

klokke 16.15 uur

door

Sharmini Alagaratnam

Geboren te Singapore in 1975

Promotiecomissie

Promotor:	Prof. Dr. G.W. Canters
Referent:	Prof. Dr. P. Kroneck
Overige leden:	Prof. Dr. J. P. Abrahams
	Prof. Dr. J. Brouwer
	Dr. Ir. C. P. M. van Mierlo

For my parents

Cover: Structure of the FMN cofactor of *A. vinelandii* flavodoxin and residues 57 to 60 of the adjoining turn, as determined by X-ray crystallography

Contents

Abbreviations

5-dRf	5-deazariboflavin
A. vinelandii	*Azotobacter vinelandii*
Cu-H117G azurin	copper-reconstituted His117Gly azurin
ε	extinction coefficient
E. coli	*Escherichia coli*
E_1	the sq/hq redox potential of flavin/flavodoxin
E_2	the ox/sq redox potential of flavin/flavodoxin
E_m	the two-electron redox potential of a flavin
EPR	electron paramagnetic resonance
ET	electron transfer
FAD	flavin adenine dinucleotide
FMN	flavin mononucleotide
Im-Cu-H117G azurin	imidazole- and copper-reconstituted His117Gly azurin
IPAR	8α-imidazolyl-(N-propylyl)-amino riboflavin
K_d	dissociation constant
k_{ese}	electron self-exchange rate
kDa	kilodalton
k_{et}	electron transfer rate
k_{obs}	observed rate
hq	hydroquinone
NHE	normal hydrogen electrode
NMR	nuclear magnetic resonance
ox	oxidised
PDB	Protein Data Bank
pK_a	dissociation constant
RMS	root mean square
sq	semiquinone
TUPS	thio-uredo-pyrene trisulphonate
UV-vis	ultraviolet-visible

Outline and scope of the thesis

Biological electron transfer (ET) is crucial for the running of the energy processes of the cell. The transfer of electrons occurs stepwise and results in a transmembrane proton gradient, which is coupled in the processes of oxidative phosphorylation and photosynthesis to ATP synthesis. This transfer is mediated by chains of protein-bound redox centres, where the proteins may be either membrane bound or soluble. In both cases, ET occurs by tunnelling between redox centres via the overlapping wave functions of the centres. In the case of soluble partners, the redox partners need not merely associate but rather bind in an orientation suitable for ET to take place. The ET efficiency is then determined both by the association constant of redox partners as well as the nature of the protein matrix separating the redox centres. The extent to which the process of ET is governed by the presence of pathways consisting of particular residues in the protein remains a matter of contention in the literature.

To address this question in the present project, an array of redox-active model systems has been created by combining various redox active molecules in both covalent and non-covalent complexes. The ET properties of the resulting maquettes were tested and characterised in terms of their structure, reactivity and ET rates. These systems are built around the redox protein flavodoxin, combined with flavin-based molecules as well as the blue copper protein azurin. **Chapter 1** of this thesis introduces these building blocks, focusing in particular on the structural and redox properties of flavodoxin, useful for later interpretation of the results. The other components are also described in brief, outlining the unique features that render them suitable for use in the constructs. In **Chapter 2** the Marcus theory that describes biological ET is summarized, describing the main factors that contribute to reaction rate. There remains some dispute on the exact role of the protein matrix in mediating electron transfer; the different theories on this are expanded upon. Finally, this chapter also reviews the main experimental techniques available for initiating and following ET within proteins.

Detailed structural information on the redox proteins is a prerequisite for predicting and understanding distance and/or pathway dependencies of the rates of ET between proteins. The structure of wild type azurin has been known for almost 25 years, and the structures of six flavodoxins have been published over the years. However the structure of the *A. vinelandii* flavodoxin was hitherto unknown. As such a crystallographic study of the Cys69Ala mutant of this flavodoxin - the protein at the core of this thesis - was undertaken, and its structure, reported in **Chapter 3**, determined to a resolution of 2.25 Å. In addition to being a vital resource for the work performed, several unique structural features close to the redox centre were revealed which could not have been predicted on the basis of structure-based sequence alignment of this flavodoxin with others. These features demonstrate how relatively conservative variations in amino acid sequence can affect interactions between the apoprotein and the flavin cofactor, and in so doing sensitively tune the redox potentials of the protein.

The characterisation of the initial ET reactions from external flavin electron donors to several different forms of azurin in **Chapter 4** is necessary groundwork for interpretation of the redox reactions observed in the more complex system linking the His117Gly (H117G) mutant of azurin with flavodoxin, described in **Chapter 5**. H117G is a cavity mutant of azurin in which an aperture exposing the copper ion to the solution has been created. Although reconstitution of this protein with imidazole restored wild type spectral properties, differences were noted in the reactivity of the various azurin forms for reduction, demonstrating the role of the native histidine ligand in efficient coupling and rearrangement of the redox active copper site (**Chapter 4**). Similarly, apoflavodoxin can bind external flavins, and the capacity of this and the H117G azurin for reconstitution by external ligands was exploited to form a heterodimeric non-covalent complex with flavodoxin, by means of a bifunctional linker made up of an imidazole moiety connected with an aminopropyl chain to a riboflavin group. The dissociation constants for the formation of this ternary complex were determined before studying its ET characteristics by laser flash photolysis. Direct reduction from the soluble donor could be distinguished from further (and slower) protein based redox reactions, although the latter showed complex behaviour, as detailed in **Chapter 5**.

The same two proteins, H117G azurin and flavodoxin, were also covalently linked by a flexible peptide. The azurin gene was cloned in frame after the gene for flavodoxin, separated by a region coding for a linker. Variants with three different linker lengths were constructed. ET has been shown to occur free in solution from reduced flavodoxin to oxidized azurin. As such, this peptide-linked construct was conceived with a view to increase the local concentrations of the partner proteins and as such enhance the probability for the formation of an encounter complex favourable for electron transfer. The resulting fusion heterodimers were successfully expressed, purified and characterised for reconstitution with imidazole and stability, and their ET behaviour was analysed by laser flash photolysis. The results, detailed in **Chapter 6**, show the importance of orientation of partners in a complex for electron transfer.

The last two experimental chapters, **7** and **8**, focus on the ET behaviour of flavodoxin, both intra- and intermolecularly. In **Chapter 7**, a total of four surface cysteine mutants of flavodoxin were created and a method developed for the labelling of these mutants by the photoactive compound TUPS with up to 80% efficiency. The reduction of TUPS-labelled protein through a novel route involving the formation of the TUPS reduced radical in the presence of ascorbate was identified and characterized by transient spectroscopy. The resulting rates of intramolecular ET from the TUPS label at different points around the flavodoxin were determined and compared. Finally, flavodoxin samples at different reduction levels were studied by ^{31}P NMR, where the phosphorus group of the FMN cofactor acts as a probe for the rate of intermolecular ET between flavodoxin molecules of different redox state. The results, described in **Chapter 8**, corroborate those from the intramolecular study, and overall present a picture where the structural details of the association complex plays a more vital role in controlling ET than the intrinsic rate from the redox centre to the exterior of the protein. Finally, **Chapter 9** discusses the main conclusions of this thesis and places them in the broader context of current opinion in the field of biological ET.

Chapter 1

Maquette building blocks

Abstract

This chapter introduces the three main players of this thesis, the flavin family of redox cofactors, the FMN-containing flavodoxin protein and the blue copper protein azurin. These molecules and their variants are used in different combinations to create maquettes of redox proteins for the study of biological electron transfer. The main characteristics of each of the components are described, and focus is given to the adaptability and malleability of the molecules that makes them amenable to application in the construction of such modular systems. Particular attention is paid to flavodoxin as it is the core element around which the studies described in this thesis are built, where its redox properties and reactions represent as a case study for the factors controlling protein-mediated electron transfer.

1.1 Flavins

The flavins are a group of redox active compounds with the three-ringed isoalloxazine group as the basis of their structure, where either natural or synthetic modifications at various positions on their benzene, pyrazine or pyrimidine rings expands the range of this family (see Fig. 1.1a). For example, lumiflavin and 5-deazariboflavin have a methyl and a ribose group respectively for the substituent R, and 5-deazariboflavin additionally has the nitrogen at position 5 replaced by a carbon, as its name suggests. The most abundant natural flavins however are riboflavin (Fig. 1.1b), or Vitamin B_2, and its two main derivatives, which all have a linearized molecule of ribose covalently attached to the N10 atom of the isoalloxazine ring. The simpler of the two derivatives, flavin mononucleotide or FMN, has a phosphate group attached to the 5' carbon atom of the ribose chain, and is shown in Fig. 1.1c. The other, flavin adenine dinucleotide, or FAD, is further derived from FMN, by addition of a diphospho adenosine moiety at the 5' phosphate terminal.

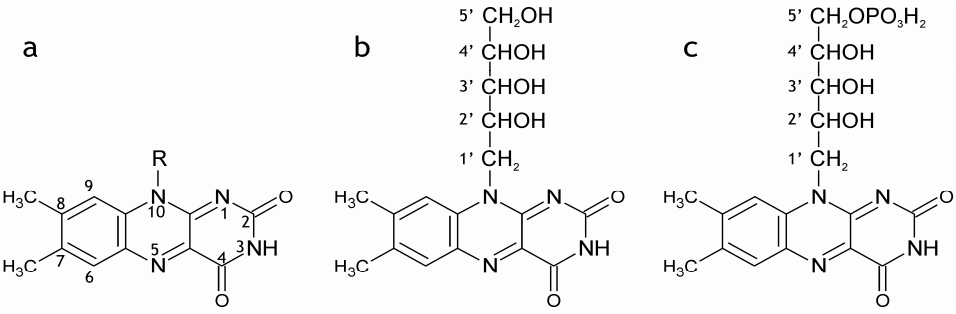

Fig. 1.1. (a) The general structure of flavins. (b) Riboflavin. (c) Flavin mononucleotide (FMN), or riboflavin 5'-phosphate. Numbers next to the atoms indicate their IUPAC-based nomenclature.

Flavins are particularly interesting in that via the action of two separate redox couples, they can exist in three different redox states, namely the oxidized quinone, the one-electron reduced semiquinone and the two-electron reduced hydroquinone (see Fig. 1.2). These states are spectroscopically distinct from each other, allowing the progression of electron transfer between the different states to be followed over time. As will be later

elaborated upon, this fact as well as the low E_2 reduction potentials of lumiflavin and 5-deazariboflavin has resulted in their wide application as external electron donors in the study of redox proteins.

1.2 Flavodoxins in context

1.2.1 Distribution and Function

The flavoprotein superfamily is defined by its members bearing a flavin cofactor, usually the FMN or FAD described above, either covalently or non-covalently bound to the protein coat. Slightly modified versions of these cofactors, involving for example a hydroxylation or a covalent link to an amino acid, have also been identified in flavoproteins, albeit less commonly. Through the action of these redox-active cofactors, flavoproteins carry out a myriad of reactions involving such molecules as glutathione, pyruvate and trimethylamine. These activities form the basis upon which the flavoproteins can be divided into groups according to their catalytic activity. These are the dehydrogenases/oxidases, dehydrogenases/oxygenases, transhydrogenases, dehydrogenases/electron transferases, and the pure electron transferases.

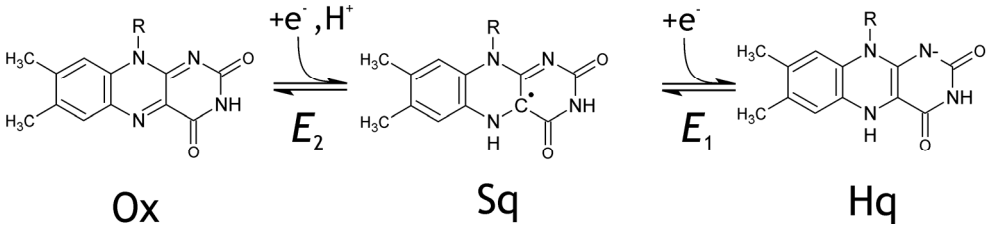

Fig. 1.2. The general reaction scheme showing the two sequential one-electron reduction reactions of oxidised (ox) flavin to the semiquinone (sq) with the redox potential E_2, and its reduction to the two-electron reduced hydroquinone (hq) flavin with the potential E_1.

The flavodoxins are a subgroup of small (14 - 23 kDa) acidic proteins within this superfamily which carry a single non-covalently bound FMN molecule, and act as pure electron transferases. They have been identified in a variety of prokaryotic organisms,

ranging from strict (*Azotobacter vinelandii*) to facultative anaerobes (*Klebsiella pneumoniae*), photosynthetic bacteria (*Anabaena*), blue-green algae (*Anacystis nidulans*), while in eukaryotes they have been found in both red (*Chondrus crispus*) and green (*Chlorella fusca*) algae (see [1] for an extensive review). In higher plants and organisms flavodoxin tends to be present as a domain of larger redox proteins, such as the flavorubredoxins [2] and flavocytochrome P-450 BM3 [3]. Despite being capable of two-electron transfer, *in vivo* flavodoxin acts as a one-electron carrier in low potential redox reactions, shuttling between the one-electron reduced semiquinone and the two-electron reduced hydroquinone states. Indeed there is evidence that the thermodynamics of flavodoxin reduction may disfavour the accumulation of the oxidised state in the cell [4]. In many organisms such as *Anabaena* and *A. nidulans* its expression is upregulated under low-iron growth conditions in order to assist in maintaining the transfer of electrons from Photosystem I to $NADP^+$ [5,6], with the reciprocal down regulation of ferredoxin expression [7]. It has been implicated in a broad range of redox reactions, such as the metabolism of pyruvate in *Helicobacter pylori* [8] and sulphate in *Desulfovibrio vulgaris*.

In several bacteria however flavodoxin is found constitutively expressed, for example in *Escherichia coli*, where in conjunction with flavodoxin $NADP^+$ oxidoreductase it provides reducing equivalents for a variety of metabolic pathways including glycolysis, biotin, ribonucleotide and methionine synthesis [9]. In the nitrogen-fixing *Azotobacter vinelandii*, the source of the flavodoxin used in this thesis, flavodoxin is also always present. Initial studies showed this flavodoxin to have extremely low activity in ferredoxin-dependent reactions, however it was eventually found to be one of the endogenous electron donors to nitrogenase [10]. Despite not being the unique physiological electron donor, flavodoxin is required for maximum *in vivo* nitrogenase activity [11]. In *A. vinelandii* strain 478, three distinct flavodoxins have been identified at different cellular concentrations under different growth conditions, on the basis of their phosphorylation and proteolytic digestion patterns. Purification showed that flavodoxin I and II were constitutively expressed although at varying levels, while flavodoxin III was found exclusively in cells that were grown on NH_4^+ [12]. The expression of flavodoxin II, used for the work in this

thesis, was found to be upregulated concurrently with nitrogenase upon transfer of cells to N_2-containing medium [13].

1.2.2 Sequence and structural features

By combining the known amino acid sequences of isolated flavodoxins with information becoming available in the burgeoning field of genomics, a large number of putative flavodoxins and proteins containing flavodoxin-like domains have been identified in organisms which have had their genomes sequenced. Almost 3000 entries for flavodoxin are found in the Entrez Protein Database at the National Centre for Biotechnology Information (NCBI) as of early 2005. However, by far the largest part of the structural, physiological and functional studies done on flavodoxins have focused on those isolated over the last forty years from a select few organisms, most of which have been discussed in Section 1.1.

The alignment of the amino acid sequences of the most extensively studied flavodoxins is shown in Fig. 1.3, and shows the basis of the sub-classification of flavodoxins into two groups, namely the short and the long chain flavodoxins. The short chain flavodoxins include those from *C. beijerinckii* and *D. vulgaris*, and lack a loop of sixteen residues (boxed in with a thin line in Fig. 1.3) compared to the long chain flavodoxins, all the others shown in the alignment. There are indications that the short chain flavodoxins in fact derive from long ones. In a recent experiment the excision of this loop in the long chain *Anabaena* flavodoxin, effectively converting it into a short chain flavodoxin, had little impact on its structural stability [14].

Flavodoxin II from *A. vinelandii* falls into the group of long chain flavodoxins, and at 180 residues is along with the flavodoxin from *Azotobacter chroococcum*, the longest of the best studied flavodoxins. Both these proteins have an additional 8-residue insertion (boxed in with a bold line in Fig. 1.3) from residues 64 to 71 compared to the other prokaryotic long chain flavodoxins. In the *A. chroococcum* flavodoxin this loop is alleged to play a role in complex formation with its physiological partner, the Fe protein of nitrogenase [15]. Although the same has not been demonstrated for the *A. vinelandii* flavodoxin, as the two

Azotobacter proteins show 94% identity, it is not unreasonable to assume a similar role for the same loop in *A. vinelandii*.

The FMN cofactor is bound towards one end of the molecule, with its dimethyl benzene edge solvent exposed, the pyrimidine ring more buried, and the ribityl chain extended into the interior of the protein. The loop that distinguishes the short from the long chain flavodoxins, coloured dark in Fig. 1.4, is located towards one side of the protein at the flavin-binding end. It does not make any direct contacts to the FMN cofactor, but appears to stabilize the FMN-binding 100's loop. The loop has been postulated to be primarily involved in partner protein recognition rather than fulfilling a structural role [16].

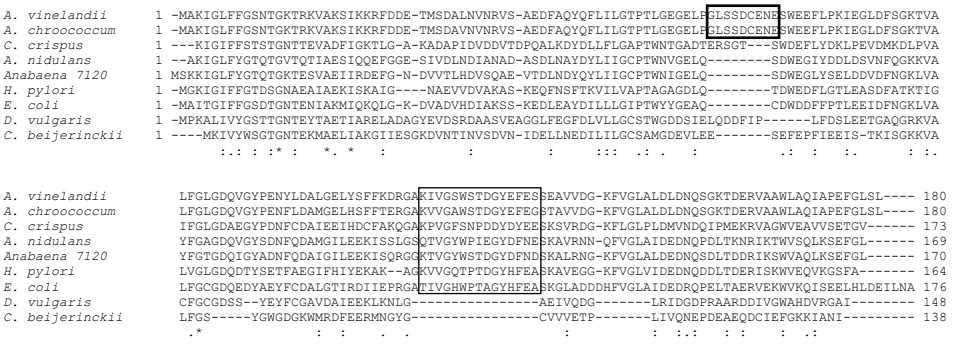

Fig. 1.3. Sequence alignment of flavodoxins performed using CLUSTALW v3.2 [17], where '*' denotes a single, fully conserved residue, ':' the conservation of a single residue, '.' conservation of a residue type and a space denotes no consensus. A thin-lined box is drawn around the loop of 16 residues which distinguishes the long from the short chain flavodoxins, while the thick-lined box indicates the eight-residue insertion in the *Azotobacter* flavodoxins.

The FMN cofactor is additionally stabilized in the apoprotein by hydrophobic stacking interactions, sandwiched as it is in most flavodoxins between two aromatic residues. A tyrosine is normally found stacked above the FMN's outer *si* face, while more often than not a tryptophan is found on its inner *re* face, interacting with the FMN at more of an angle (up to 45° out of plane for the *D. vulgaris* flavodoxin). Several variations on this

theme have been identified however, for example a methionine and an alanine have been found at the *re* face of the FMN in the flavodoxins from *C. beijerinckii* and *H. pylori* respectively, while from sequence alignments the *A. vinelandii* flavodoxin is expected to have a leucine at this position. The *C. beijerinckii* flavodoxin is also the only one to have a tryptophan instead of a tyrosine on its outer *si* face.

These hydrogen bonding and aromatic stacking interactions act in concert resulting in an FMN-apoflavodoxin complex with dissociation constants in the low nM range. Despite this tight association, methods have been developed whereby the FMN can not only be removed from the flavodoxins, but also replaced with an external, non-native flavin (see [18] for a summary) to form fully functional, reconstituted flavodoxin. The most common technique involves precipitation of the holoprotein using cold trichloroacetic acid, during which the FMN dissociates but remains in solution. The apoflavodoxin can be recovered after removal of the FMN by dissolving the precipitated protein in a suitable high pH buffer, after which simple incubation of the apoprotein with a flavin solution will result in the reconstituted flavodoxin. The tightness of the new complex formed will depend not only on the identity of the flavodoxin and flavin used, but also on conditions such as salt and pH, and can be quantified by fluorescence quenching studies [19]. This method has been applied with much success to introduce a variety of labelled and/or modified flavins into flavodoxins to address particular issues about the protein, and will be discussed more thoroughly in Chapter 2.2.2 (Cofactor reconstitution).

1.2.3 Redox properties

As previously touched upon, the FMN found in flavodoxins can exist in one of three redox states, namely oxidised (ox), the one-electron reduced semiquinone (sq), and the two-electron reduced hydroquinone (hq). Reducing equivalents can be provided by a variety of means, chemically using sodium dithionite [20], electrochemically with the use of either mediators [21] or poly-lysine linkers [4] to couple the protein to the metallic electrode, photochemically using 5-deazariboflavin [22] (see Chapter 2), by pulse radiolysis to generate the reducing CO_2^- radical [23], or enzymatically using for example its physiological partner in *E. coli* the FAD-containing protein NADPH:ferredoxin (flavodoxin)

oxidoreductase [24] or a hydrogen-hydrogenase system [7]. The extent to which flavodoxin can be reduced depends on the relative redox potentials of the electron donors and those of the flavodoxin. In general, dithionite and photoreduction using 5-deazariboflavin, with redox potentials below −500 mV, are capable of reducing flavodoxin to the hydroquinone state, while the other agents only reduce it to the semiquinone state.

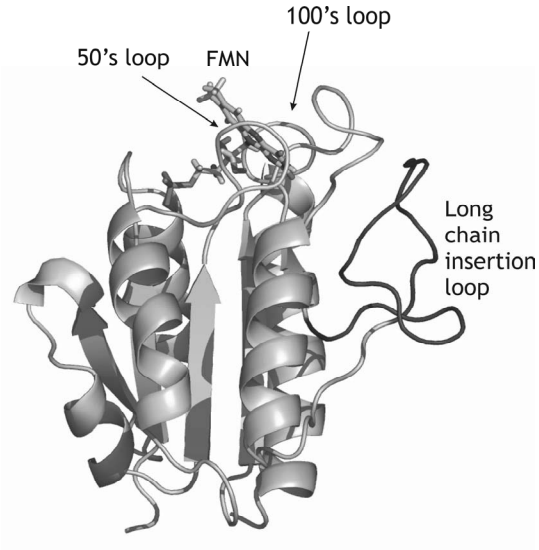

Fig. 1.4. Cartoon representation of the three-dimensional fold of the *Anabaena* flavodoxin, PDB Code 1RCF prepared using Pymol (http://www.pymol.org). The FMN cofactor is bound at one end of the protein, and is shown in stick form, while the sixteen-residue insertion that distinguishes long from short chain flavodoxins is the dark-coloured loop extending outwards from the main core of the protein.

As with free flavins, the redox state of flavodoxin can be monitored by its visible absorption spectrum (Fig. 1.5). One-electron reduction of the oxidised form of the protein to the semiquinone causes an almost four-fold decrease in the extinction coefficient at 450 nm from 11.3 mM^{-1} cm^{-1} to 3.0 mM^{-1} cm^{-1}, while a broad absorption band between 550 and 700 nm appears, with an extinction coefficient of 5.7 mM^{-1} cm^{-1} at its maximum of 580 nm. Upon further reduction to the hydroquinone, this broad peak disappears again, while absorption in the 450 nm region is also minimal (ε_{450} = 1.5 mM^{-1} cm^{-1}). The characteristic spectra for the different redox states allow the determination of redox potentials for the ox/sq and sq/hq couples, designated E_2 and E_1 respectively (see Fig. 1.2) by spectrophotometric redox titrations (see [25] for a recent example). An alternative to this would be an EPR-monitored redox titration, where the semiquinone radical has an EPR signal but not the oxidised or hydroquinone forms (see [26] for an example).

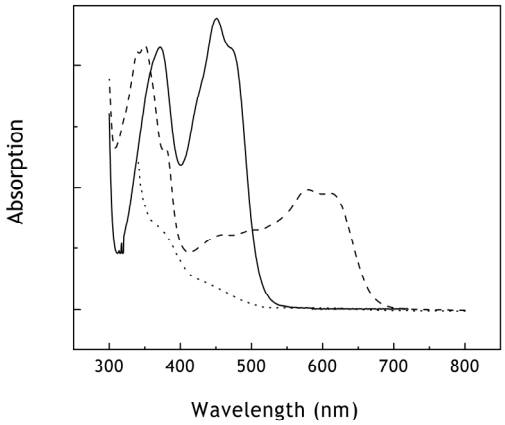

Fig. 1.5. Absorption spectrum of 50 μM C69A flavodoxin in the oxidised (solid line), semiquinone (dashed line) and hydroquinone (dotted line) state, in 20 mM MES buffer pH 6.0 and at 293 K. For the sake of clarity the intensity of the peaks have been rescaled, and do not represent equal concentrations of the three species.

Crucially, for FMN free in solution E_1 is higher than E_2, such that the semiquinone form is not usually observed, for example in redox titrations. When FMN is bound to the apoflavodoxin however, these potentials are inverted with respect to each other, in particular due to the specific stabilisation of the semiquinone state of the FMN by interactions with the apoflavodoxin. This stabilisation also effects a large separation between the two redox potentials; Table 1.1 summarizes E_1 and E_2 values known for various flavodoxins, as well as for FMN for comparison. In general, E_2 potentials are lower for the long chain than for the short chain flavodoxins, where several determinants have been identified for the value of both of these redox potentials.

1.2.3.1 E_2, *the ox/sq redox potential*

The structural basis for the stabilisation of the semiquinone form of FMN by apoflavodoxin, as previously alluded to, was elucidated on the basis of three-dimensional crystallographic structures of semiquinone flavodoxins from three different sources, *C. beijerinckii*, *D. vulgaris* and more recently *A. nidulans*. The visible spectrum of the flavodoxin semiquinone, in particular the broad band peaking at 580 nm, was an indication that the FMN semiquinone when bound to flavodoxin existed as a neutral species, protonated at the N5 position. This was confirmed by a number of structural studies of semiquinone and hydroquinone flavodoxins, from a number of different species. In all known structures of

oxidised flavodoxins, the two-residue 58-59 peptide (using the *A. vinelandii* numbering) is oriented in what has been defined as the 'O-down' conformation, where the backbone carbonyl oxygen of residue 58 points away from the flavin ring. In the three structures of semiquinone flavodoxins however, this peptide was found to undergo a backbone flip such that the O58 hydrogen bonds to the flavin N5H in the 'O-up' conformation [27,28,29].

This hydrogen bond is thought to be the main factor in preferential stabilisation of the semiquinone form that leads to the inversion of the E_1 and E_2 redox potentials of FMN bound to flavodoxin. The structure of the hydroquinone form was also determined for the flavodoxins from *C. beijerinckii*, *D. vulgaris* and *A. nidulans*. For the first two flavodoxins, reduction of the semiquinone to the hydroquinone form did not provoke any further structural changes, with the 58-59 peptide persisting in the 'O-up' conformation. This was different in the *A. nidulans* flavodoxin hydroquinone structure, in which the peptide was found to revert to the 'O-down' position characteristic of the oxidised structure [29]. It remains a matter of contention as to whether or not this last observation is an artefact resulting from the crystal packing of the protein.

Flavodoxin Source Organism	E_2, ox/sq, mV	E_1, sq/hq, mV
Short chain flavodoxins		
*Clostridium beijerinckii**	−92	−399
Clostridium pasteurianum	−132	−419
*Desulfovibrio vulgaris**	−143	−440
Megasphaera elsdenii	−115	−372
Long chain flavodoxins		
Anabaena 7120*	−196	−425
*Anacystis nidulans**	−221	−442
Azotobacter chroococcum	−103	−522
Azotobacter vinelandii	−165	−458
*Chondrus crispus**	−222	−370
*Escherichia coli**	−244	−455
Klebsiella pneumoniae	−170	−422

Table 1.1. Redox potentials of flavodoxins at pH 7.0 in mV, adapted from [28]. An asterisk (*) indicates that the three-dimensional structure of the flavodoxin has been determined.

Several other structural factors have been found to modulate the ox/sq E_2 redox potential, leading to the spread in values observed in Table 1.1, and in particular the lower values for long chain than short chain flavodoxins. In all the structures

of oxidised long chain flavodoxins, the backbone amide group of residue 59 was found in a favourable orientation for hydrogen bonding to the N5 of FMN, although at distances that were rather long, between 3.1 and 3.6 Å. It has been suggested however that the apolar environment of the FMN binding site may increase the relative strength of this interaction [30], compelling evidence for which exists in the direct measurement of the hydrogen bond strength [31,32]. The fact that this stabilizing interaction is completely absent in the oxidised short chain flavodoxin structures helps explains the higher E_2 value for these proteins, as without first having to break the hydrogen bond to the N5 in the oxidised form their reduction is comparatively easier. Additionally, residue 58 (in *A. vinelandii* numbering) in the peptide that undergoes the backbone flip upon reduction is also known to influence the value of E_2. This is most commonly a glycine in short chain and an asparagine in long chain flavodoxins; however from sequence alignments the *A. vinelandii* flavodoxin is found to have a glycine at this position. The lack of a side chain in glycine means that it can optimally accommodate the O-up conformation at that position of the type II' turn found in flavodoxin semiquinones [33], lowering the energy of the 'O-up' conformation found in the semiquinone state, and making it easier to reduce. In contrast, the bulky side chain of the asparagine found in the long chain flavodoxins induces very close contacts between the asparagine Cβ and the following amide group, raising the energy of the O-up conformation [29], thus lowering the redox potentials.

This effect was investigated with a series of site directed mutants at this position in various flavodoxins. Replacement of this asparagine residue by glycine in the *A. nidulans* flavodoxin raised the ox/sq potential by 46 mV [29], while a series of mutants of the short chain *C. beijerinckii* flavodoxin where the homologous Gly57 residue was replaced by alanine, asparagine, aspartate and proline all had ox/sq potentials that were reduced by approximately 60 mV and the Gly57Thr mutant with its bulkier β-branched side chain showed an even stronger effect, with an E_2 that was lowered by 180 mV [27]. Further support for the correlation between the size of the side chain at this position and E_2 comes from the long chain *E. coli* flavodoxin: the protein has a bulky tyrosine residue here, and displays the lowest the ox/sq potential of all those known [34] (see Table 1.1).

1.2.3.2 E_1, *the sq/hq redox potential*

As with the ox/sq potential, site-directed mutants have been instrumental in elucidating particular features of flavodoxin which determine the value of the sq/hq redox potential. In general the effects of charge and flavin environment have much greater influence on E_1 than E_2, as the FMN hydroquinone exists as an anion in flavodoxin, as shown by NMR experiments on the *M. elsdenii* flavodoxin [35]. This concept was reinforced by an experiment which showed that steric hindrance prevents protonation of the N1 FMN atom in the *C. beijerinckii* flavodoxin [36]. The hydroquinone is destabilized in the protein by a series of unfavourable flavin-apoprotein interactions, the extent of which ultimately determines the value of E_1.

Focusing on the anionic character of the FMN hydroquinone, Zhou and Swenson identified a cluster of six acidic resides within 15 Å of the charged N1 atom in the *D. vulgaris* flavodoxin that were uncompensated for by other charged groups, where they postulated that electrostatic repulsion between these residues and the anionic FMN lowers the E_1 potential. This was borne out by a series of mutants in which each of the acidic residues was neutralized in turn, the result of which was the increase in E_1 of approximately 15 mV per residue [37]. The negatively charged FMN phosphate group can also conceivably contribute to the charge repulsion effect, where mutants of the *D. vulgaris* flavodoxin which neutralized this charge were found to have E_1s that were slightly raised compared to wild type [38]. The effect was however relatively small, indicating that the phosphate charges do not dominate the sq/hq potential.

The overall polarity of the FMN binding site is also known to influence the sq/hq potential. In most flavodoxins, the FMN is sandwiched between two aromatic residues, shielding it from the solvent. In the oxidised and semiquinone form this arrangement provides for favourable coplanar stacking interactions that stabilize the flavin-apoprotein complex, however such an environment is much more unfavourable for the anionic hydroquinone. Replacement of the outer face flanking tyrosine in the *D. vulgaris* flavodoxin by an alanine raised the E_1 by 139 mV compared to wild type protein [39]. The

corresponding mutation in the Anabaena flavodoxin also shifted E_1 by 137 mV to a more positive value [40]. A similar situation exists in the flavodoxin for *C. beijerinckii*, where the wild type protein is flanked by a tryptophan on the outer *si* face, and a much smaller methionine residue on the inner *re* face of the FMN. As a result a solvent channel is formed leading from the FMN to the surface of the protein, where the increased polarity may stabilize the anionic hydroquinone, leading to this flavodoxin having the highest E_1 value of all flavodoxins known [41] (see Table 1.1). Such variations have multiple physical effects however, including elimination of the aromatic stacking interactions as well as increasing the solvent accessibility of the FMN binding site, while it remains difficult to ascribe the difference in E_1 observed solely to either one of these. In reality the factors described all act in concert, with additive or counteracting effects depending on the variation in the flavodoxin, leading to the spread of E_1 values observed.

1.2.4 Aspects of flavodoxin electron transfer

The ease of flavodoxin reduction, the relative stability of the semiquinone form in the presence of oxygen as well as knowledge of the spectral changes that accompany changes in redox state all make the study of the electron transfer reactions to and from flavodoxin ideal for the understanding of flavodoxin and flavoprotein reactivity in particular and redox proteins in general. The redox potential of the flavodoxin ox/sq couple, between –100 and –250 mV depending on its source organism, is low enough to reduce many other redox compounds, be they small inorganic molecules or other proteins. As such the majority of studies performed on electron transfer reactions of flavodoxin utilise this couple. At values of between –370 and –520 mV the sq/hq redox couple is even lower as well as being the physiologically relevant reaction, and for both these reasons is also of interest. However the fully reduced hq form of flavodoxin is more difficult to achieve and maintain for kinetic studies; despite that several successful reports of electron transfer studies involving the sq/hq couple of flavodoxin are found in the literature [5,42].

Facets of the electron transfer in flavodoxin that add to the general understanding of biological electron transfer include tuning of the flavodoxin redox potential that determines the driving force for electron transfer, as well the factors controlling productive

complex formation between flavodoxin and its partners, including electrostatic and hydrophobic interactions, the effects of ionic strength and pH, and the issues of orientation and accessibility. Many of these can be investigated more thoroughly by making slight modifications to the flavodoxin and the subsequent investigation of the effects of such changes on rates of electron transfer. These modifications can be effected at the redox heart of the protein by replacement of the FMN cofactor by a different or modified flavin group, but also specifically at points on the protein surface or in its interior by site-directed mutagenesis of particular residues. It is however vital to bear in mind that even the most conservative changes in amino acid sequence or flavin structure can affect more than one controlling aspect of the electron transfer reaction. As such any observed changes should be evaluated with care to determine the true influence of a particular factor, as will be demonstrated with recent examples from the literature.

1.2.4.1 Recognition and orientation of partner proteins

The electron transfer reaction between flavodoxins and its various different physiological redox partners from different sources has been studied, where examples of the partner proteins include Photosystem I (PS I) [43] in *Anabaena* and ferredoxin/flavodoxin NADP+ reductase (FNR) in *E. coli* [25]. Flavodoxin has also been shown to transfer electrons to a range of other, non-physiological protein partners. These tend to be small and generally well characterised redox proteins such as the blue copper protein azurin [44], the haem containing cytochrome *c* [45], and flavodoxin has even successfully been used to reconstitute an artificial redox chain by interaction with bovine adrenodoxin reductase [46]. Structural information both on flavodoxin and the partner proteins allows the modelling of interactions which may guide complex orientation and formation, generally based on the surface features and charge distribution on the partner proteins, and more recently further guided by NMR data on residues which are found at the complex interface [47]. These interactions can be evaluated by changing the ionic strength and measuring its effect on the kinetics of electron transfer. In one dramatic example, two cytochromes with the same redox potential but different surface charge distribution showed two orders of magnitude difference in rates of electron transfer to

flavodoxin, yet this large effect could even be reversed at high salt concentrations that shielded the repulsive charges on the partner proteins [48].

More subtle reorientation of flavodoxin with respect to its partner after the initial encounter complex is formed as is known for other protein-protein complexes [49] has also been documented. While an unresolved debate continues on the exact role of the protein matrix immediately surrounding the redox centre in determining the rates of reaction, in general electron transfer reactions have been shown to occur almost exclusively via specific ports of entry and exit from the protein-bound redox centres. Specific surface characteristics of charge, hydrophobicity and shape around these entry and exit points add a level of control in restricting the occurrence of redox events to desirable partners by limiting accessibility and orientation. For flavodoxin the electron transfer patch was thought to be the solvent exposed dimethylbenzene ring of FMN [7]. Rates of electron transfer from wild type flavodoxin and flavodoxins which had had the FMN cofactor replaced by analogues that had been modified at positions 7 and 8 on the ring (see Fig. 1.1) to cytochrome *c* were determined using stopped flow and flash photolysis methods [42,50]. The modifications were found to affect the rates dramatically, while the association of the flavodoxin to the electron acceptor was unaffected. This unequivocally demonstrated the role of these positions on the protein in the actual electron transfer reaction, as opposed to the disruption of the electron transfer complex.

Comparing the kinetics of electron transfer of wild type with site-directed mutants of flavodoxin with a variety of flavodoxin partner proteins also demonstrate the importance of electrostatic as well as hydrophobic interactions for the formation of a productive electron transfer complex [51,52]. Replacement of one or more of the negatively charged residues on the surface of flavodoxin caused decreases in the rate of electron transfer [53], while neutralization of a single charged group on the flavodoxin surface caused a decrease of 40% in catalytic a27ctivity of a bovine cytochrome P450 dependent on flavodoxin as its electron source [54]. Surface mutations of the partner proteins also affect the observed rates, where reversing the positive charge of just a single residue on PS I to negative reduced the rate of flavodoxin reduction 20-fold [55]. A general picture emerges where the net protein charge (that give rise to both attractive and repulsive electrostatic

interactions) plays a role in the initial recognition process for forming an encounter complex, while local charge in the vicinity of the electron transfer site has much more influence in the orientation of productive electron transfer complexes [44].

1.2.4.2 Redox potential, accessibility and reorganizational energy

One of the determinants of rate in biological electron transfer as given by the Marcus theory is the difference in redox potential between two redox active groups (see Chapter 2.). However a study of the second order rate constants of a flavodoxin semiquinone reacting with 12 different *c*-type cytochromes did not reveal any simple relationships on the basis of redox potential difference [48]. This indicated that the reaction between flavodoxin and other redox proteins is very much dominated by steric considerations instead, which manifest themselves in variations in the energy required to rearrange the proteins such that electron transfer can occur. This effect is larger with interactions between proteins than between proteins and small electron donors such as free flavins, where the latter pair demonstrates rate constants that are orders of magnitude larger, and more in tune with the difference in redox potential [56].

A more recent example also demonstrates the manifold effects that a single amino acid change can have on the kinetics of electron transfer. The aromatic residues flanking FMN in flavodoxin were mutated in turn to the much smaller alanine, which did not affect complex formation between flavodoxin and PS I or FNR, all isolated from *Anabaena* [57]. Electron transfer to flavodoxin from the two partner proteins was accelerated, due to the increased accessibility of FMN. However the reverse reaction of flavodoxin reoxidation was retarded, due to the change in flavodoxin E_2, which decreased the driving force for the reaction.

1.2.4.3 Kinetics of the protonation event

The backbone flip occuring upon reduction of flavodoxin to the semiquinone state that accompanies protonation of the FMN N5 (Chapter 1.3.1) has consequences for the kinetics of electron transfer to and from flavodoxin. That the rate for electron transfer

between the oxidised and semiquinone forms of flavodoxin is slower than between the semiquinone and hydroquinone has been demonstrated by a number of different experiments. The reduction rate of flavodoxin quinone using dithionite was found to be much slower than for the semiquinone from both *D. vulgaris* [58] and *M. elsdenii* [59]. ^{31}P NMR experiments with mixtures of oxidised, semiquinone and hydroquinone *M. elsdenii* flavodoxin estimated the electron self exchange rate between the oxidised and semiquinone forms to be much lower than that for the semiquinone and hydroquinone forms [60]. The rates were however quoted as first-order rate constants, while their correlation with the second-order electron self exchange reaction was unclear. Only the sq/hq couple of flavodoxin could be electrochemically observed, due to the slow ox/sq kinetics which prevented its detection at a carbon electrode [21].

A pulse radiolysis-transient spectroscopic study of the flavodoxin from *M. elsdenii* showed that the non-protonated semiquinone of flavodoxin was formed within 2 μs of the reducing pulse, before being protonated at the slower first-order rate of 10^5 s^{-1} to the blue neutral semiquinone form [23]. The observation of this protonation event was later confirmed by the biphasic character of the *Anabaena* flavodoxin reduction by 5-deazariboflavin. Reduction of the oxidised flavodoxin to the non-protonated semiquinone occurred rapidly with a second-order rate constant, but the blue neutral semiquinone was formed more slowly in a protein concentration independent manner [61].

From this it is clear that a slower step is involved in forming the neutral flavodoxin semiquinone, and that this is likely to be the basis for the slow rates observed for the ox/sq reaction. Electron transfer for this step is effectively coupled to protonation of the FMN N5, which is itself accompanied by the conformational change of the backbone peptide flip. The protonation and the conformational change are interrelated processes but represent two distinct steps, where the conformational change is not directly observable. This should be borne in mind when evaluating the spectrokinetic results of flavodoxin electron transfer reactions. A recent electrochemical study of flavodoxin immobilised on tin dioxide electrodes succeeded in characterising both redox couples of flavodoxin individually, and showed that deprotonation of the semiquinone is the rate limiting step in the overall equilibrium between the three redox states [4]. The authors propose that this

mechanism provides thermodynamic control over the ox/sq equilibrium that prevents cycling of the flavodoxin between these states while the sq/hq couple is the physiologically relevant one.

1.3 Azurin

The small (14 kDa) well-characterised blue copper protein azurin from *Pseudomonas aeruginosa* was chosen as a partner protein for flavodoxin in the construction of heterodimers. Its true physiological role has yet to be ascertained, although recent *in vivo* experiments have disproved its originally proposed role as electron donor to nitrite reductase under stress situations [62]. Due to its ease of expression and stability however, azurin has been used as a model protein for a large number of studies ranging from protein folding [63,64,65] to the visualization and characterization of the physical and mechanical properties of proteins on gold surfaces by electrochemistry and microscopy [66,67].

Fig. 1.6. Cartoon representation of the three-dimensional fold of azurin from *P. aeruginosa*, PDB Code 1AZU prepared using Pymol. The copper atom is shown as a sphere at the top of the molecule, and the histidine 117 ligand that shields it from the solvent is shown as sticks.

Structurally, azurin folds to form two β-sheets in a Greek key motif, with an α-helix to one side of the main protein core. The single copper atom that gives azurin its functionality as a redox protein is co-ordinated at the so-called 'north' end of the molecule in a trigonal bipyramidal configuration by three co-planar ligands, the N^{δ} of histidines 46

and 117, and the S^{γ} of cysteine 112, as well as two axial ligands, the S^{δ} of methionine 121 and the carbonyl oxygen of glycine 45.

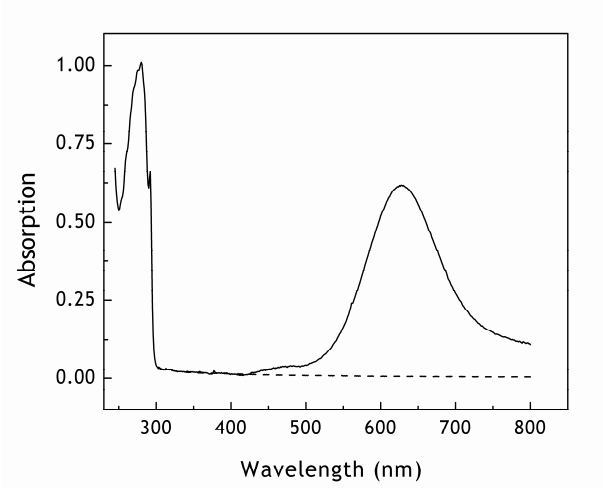

Fig. 1.7. Absorption spectrum of 110 μM azurin in the oxidized (solid line) and reduced (dashed line) state in 20 mM MES buffer pH 6.0 and at 293 K.

This absorption band is however absent in the Cu (I) reduced protein, as shown in Fig. 1.7. This striking change in colour, as with flavodoxin, provides a highly responsive sensor for the redox state of the protein, and has been used in the past in transient absorption spectroscopy to determine the rate of azurin reduction by pulse radiolysis [68,69], other reduced proteins [70] or azurin surface-attached electron donors [71].

1.3.1 The azurin cavity mutant His117Gly

Mutation of the surface-exposed copper ligand histidine 117 to a glycine introduces a cavity at the northern end of the protein that exposes the copper atom to the solvent. The changed co-ordination sphere of this mutant, H117G azurin, results in a green protein in which a water molecule co-ordinates the copper instead [72,73]. In this species, the absorption band at 630 nm is decreased five-fold in intensity (ε_{628} = 1.2 mM^{-1} cm^{-1}) as compared to the wild type protein, while a new absorption band appears at 420 nm with an ε_{420} of 2.2 mM^{-1} cm^{-1} [74] (see Fig. 1.8). Interestingly, the mutated site can be reconstituted by a range of compounds, including anionic ligands such as Cl^{-} and N_3^{-}, as well as imidazole- and histidine-based molecules [75].

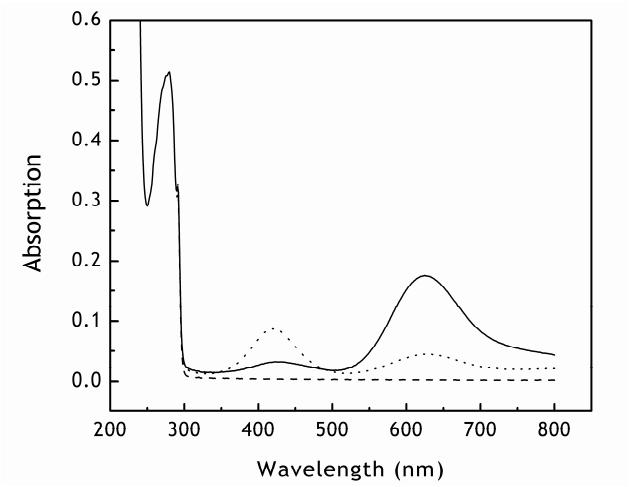

Fig. 1.8. Absorption spectrum of 55 μM H117G azurin in its apo form (dashed line), after reconstitution with 1.1 equivalents of copper (dotted line) and after reconstitution with 1.1 equivalents each of copper and imidazole (solid line), in 20 mM MES buffer pH 6.0 and at 293 K.

Reconstitution with imidazole was most successful in restoring the spectral characteristics of the mutant, where with ε_{628} of 5.3 mM^{-1} cm^{-1} the reconstituted protein was spectrally virtually indistinguishable from the wild type (Fig. 1.8). The extent to which functionality was restored to the mutant depended greatly on the reconstituting ligand, as judged by the rate of reduction of H117G reconstituted with different ligands by a hydroxylase enzyme [76]. In general the presence of imidazole-like ligands increased the rate of azurin reduction over water co-coordinating H117G azurin, however even the fastest rate, observed for imidazole-reconstituted H117G azurin was approximately an order of magnitude lower than the comparable rate for the wild type protein.

It has also been shown that, once reduced, that H117G has very low affinity for the external ligands; however under extremely high electrochemical scan rates the reduced ligand-bound H117G form could be trapped, and a reversible redox couple established [74]. This last has implications for the application of the H117G mutant in the complexation of the protein either with itself to form homodimers, or with other proteins to form heterodimers, as will be elaborated upon in Chapter 2. In one example, the addition of an alkane linker with imidazole at each end to copper-containing H117G azurin resulted in a homodimer of the protein, with each copper site co-ordinating one imidazole end of the linker [77]. While each of the reconstituted H117G molecules remains functional for

accepting electrons, upon reduction they dissociate from the imidazole ligand and hence each other, and remain as reduced monomers in solution.

Chapter 2

Protein engineering of redox proteins: Theory and methods

Abstract

This chapter first explains the theory of biological electron transfer, discussing in particular the most pertinent factors that ultimately determine rate. In particular the role played by the protein matrix remains a topic of discussion; the two main concepts describing this role are compared and contrasted. The chapter then explores the main experimental techniques available today for validation of the theory and further understanding of this process. In particular the various modifications that can be made to a protein, either by site-directed mutagenesis or (modified) cofactor replacement, are discussed. In addition, an overview is given of the methods currently used to introduce electrons into the system under study. A practical approach is taken to this with specific examples of which and how electron transfer proteins have been studied, and the conclusions can be drawn with regards to the theory from the results.

2.1 Theory of biological electron transfer

The donor and acceptor redox centres in proteins which mediate biological electron transfer (ET) are by nature relatively shielded from the solvent, so as to prevent the occurrence of unwanted redox reactions. This also means, however, that the donors and acceptors are electronically only very weakly coupled, where the product is only formed in a small proportion of the cases where the transition state is formed. This is in contrast to adiabatic reactions, where formation of the transition state by thermal collision of the reactants almost always leads to the product. Marcus theory presents the framework that describes the factors governing the rates of non-adiabatic biological ET [78], based around Fermi's golden rule:

$$k_{et} = \frac{2\pi}{\hbar}\left|H_{AB}\right|^2 FC \qquad (2.1)$$

where the rate of ET, k_{et}, is proportional to the product of the square of H_{AB}, the electronic coupling between the donor and acceptor states A and B, and FC, the nuclear Franck-Condon factor; with ħ as Planck's constant. For non-adiabatic reactions H_{AB} is smaller than k_BT, where k_B is the Boltzman constant and T the temperature.

The nuclear FC factor relates the free energy or driving force for the reaction ΔG° with the reorganization energy λ, that is required to distort the nuclear arrangement of the reactant and its surroundings to that of the product, without the occurrence of ET:

$$FC = \frac{1}{\sqrt{4\pi\lambda k_B T}} \exp\left[-\frac{\left(\Delta G^o + \lambda\right)^2}{4\lambda k_B T} \right] \qquad (2.2)$$

The sum of all the nuclear motions around the reactants R and products P can be approximated by a simple harmonic motion along the reaction co-ordinate Q, and represented graphically as a potential well (Fig. 2.1), with the equilibrium geometry at the bottom of the well. The product curve is identical to that of the reactant, but is shifted

along the reaction co-ordinate from Q_R to Q_P, and along the energy axis by $\Delta G°$, the free energy of the reaction. The activation energy of the reaction, $\Delta G^{\#}$, is dependent on the balance between $\Delta G°$ and λ:

$$\Delta G^{\#} = (\Delta G^{o} + \lambda)/4\lambda \qquad (2.3)$$

The diagram on the right of Fig. 2.1 shows the three possibilities for this balance that ultimately govern the rate of ET. The first so-called 'normal region' is defined by $-\Delta G° < \lambda$, where an increase in driving force results in increased k_{et}. Alternatively, the region where $-\Delta G° > \lambda$ is known as the Marcus inverted region, as increase in driving force results in the decrease of k_{et}.

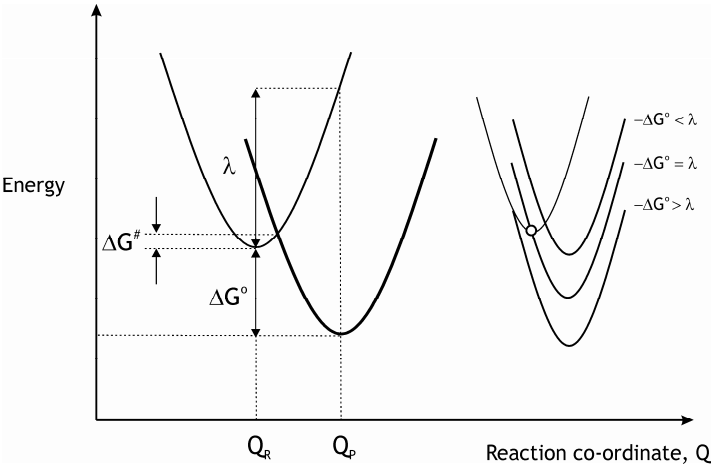

Fig. 2.1. Potential energy diagram for electron transfer, with the nuclear motion of the reactants R and the products P depicted as harmonic oscillators. *Right:* The relative values of $\Delta G°$ and λ determine the activation energy for the reaction.

Finally, when $-\Delta G° = \lambda$, the reaction is activationless and the rate is maximal. Under these conditions, k_{et} approaches its maximum value, and is governed only by the electronic coupling strength H_{AB}. This electronic factor describes how the exponential decay of electronic wave functions, β, affects rate over distance, R, as given by:

$$\left|H_{AB}\right| \propto \exp(-\beta R) \qquad (2.4)$$

In effect, β describes the efficiency of the medium between two buried redox centres in mediating ET. Describing this efficiency more mathematically for the prediction of ET rates has however been and remains a matter of hot contention in the field. One useful empirical approximation has been to treat protein as a homogenous matrix with a β value of 1.4 $Å^{-1}$, in between what has been determined for covalent systems (0.9 $Å^{-1}$) and vacuum (3-5 $Å^{-1}$) [79]. This allows the theoretical estimation of ET rates in s^{-1} with

$$\log_{10} k_{et} = 15 - 0.6(R - 3.6) - 3.1(\Delta G + \lambda)^2 / \lambda \qquad (2.5)$$

where R represents the edge-to-edge distance in Å, and ΔG and λ are the driving force and reorganization energy of the reaction, both in eV [80]. The same authors have further refined this model with known protein structures, allowing identification of the difference in local packing densities associated with secondary structure elements. Their extensive surveys of the structures of known redox proteins show that edge-to-edge distances appear to be a vital factor in determining redox protein architecture, extending from near van der Waals contact to approximately 13-14 Å, with few proteins exhibiting distances much beyond this limit. This was taken as an indication that this distance is the natural threshold for electron tunnelling, without limiting the natural turnover of enzymes (in the order of milliseconds) [81]. Electron conducting chains can then be built up of multiple redox centres, arranged within this maximum distance from each other, thus allowing for the transfer of electrons over large distances.

An alternative approach has been expounded based on the specific and discrete connections or pathways between two redox centres. The electronic coupling could then be conceived of as the product of the couplings of the individual components, namely covalent bonds, hydrogen bonds and through-space jumps, with each assigned a coupling decay value [82]. A number of programmes have been developed over the years that calculate the strength of the coupling of various pathways based on the structure of the protein. Results from a wide range of ET rate vs. distance measurements on redox proteins modified on the surface with ruthenium-based photolabels showed good correlation and strongly support this approach (see [83] and [84] for reviews of this work). Similar results

have emerged from pulse radiolysis experiments which compared the rate of ET from the native disulphide bridge in various mutants of azurin [69,85,86].

In their current states, neither model has managed to entirely describe the relationship between rate and distance in biological electron transfer. The uniform barrier model does not satisfactorily explain the scatter in ET rates for long-range coupling in proteins. The simple pathways model does not however address the issue of the multiple pathways (often in the order of $> 10^3$) identified within a single protein, and how they may interact and/or interfere. More recently attempts have been made to overcome this with the concept of 'tunnelling tubes', or families of pathways, the interference between which can be estimated [87]. In addition, tunnelling currents with which the probability of electron density in the region between donor and acceptor is considered are being taken into account in extending several models [88,89]. In general, uncertainty about whether edge-to-edge or centre-to-centre distances are more appropriate in the measurement of distances between donor and acceptor complicate the interpretation of experimental protein ET rate data and the evaluation of which model describes the role of the protein matrix more accurately.

2.2 Protein engineering of redox proteins

The engineering of redox proteins by the introduction of specific structural and/or functional changes has greatly extended the possibilities for the investigation of the factors controlling biological electron transfer as described above. Advances in molecular biology, *de novo* design of proteins and chemical modifications of cofactors allow the creation of redox proteins with characteristics absent in the native protein. Their study provides unique insights into the mechanisms and factors controlling electron transfer in living systems. This section provides an overview of the practical methods available for manipulation of redox proteins, and illustrates their application by means of specific examples.

2.2.1 De novo *protein design and site-directed mutagenesis*

As our understanding of protein folding and architecture broadens, *de novo* protein design has emerged as a viable alternative for creating redox-active models of physiological electron transfer systems. Simply put, this is the design of polypeptide sequences which fold into stable tertiary structures, based on the principles learnt from the study of protein assembly and structure. The first steps in this field were taken with the design of a self-assembling 4-helix bundle towards the end of the 1980s [90], but has since been extended to other secondary structures, globular proteins, as well as the introduction of specific metal and substrate sites to give *de novo* redox proteins. The use of self-assembling 4-helix bundles as a scaffold for such binding sites has been particularly successful, see [91] for an example of a di-iron helical protein. Both [92] and [93] are excellent references here. Rational design has also allowed the introduction of such sites into existing proteins, such as the iron and oxygen binding sites introduced into thioredoxin [94].

In addition, present-day molecular biology and protein chemistry methods have made it possible not only to rapidly introduce site-directed mutations into a protein of choice, but also to overexpress and purify the mutant protein relatively quickly. In combination with the rational design approach above, these methods have great potential for effecting small yet specific changes in either existing or *de novo* designed proteins. Within the context of redox proteins, the cofactor ligands are an obvious target for mutagenesis, for modulation of the redox potentials and reactivity of the proteins. An example was the exchange of the lysine haem ligand in cytochrome c-550 by a glutamate, which resulted in enhanced peroxidase activity upon unfolding compared to wild type protein [95]. A cavity mutant similar to His117Gly of azurin (Chapter 1.3.1) was created in nitrite reductase, resulting in a raised redox potential [96].

The possibility also exists of making bigger changes on the level of quaternary structure level through the creation of or changes to larger redox units. These may consist of multiple domains and redox centres as often found in nature, such as the haem and molybdenum centres found on different domains of chicken liver sulphite oxidase [97], or the iron-sulphur, molybdenum and FAD-containing milk xanthine oxidase [98]. The fatty

acid hydroxylase cytochrome P450 BM-3, which has its P450 haem domain linked to its FAD/FMN reductase domain [3], was subjected to such engineering. The FAD domain of the enzyme was removed by truncation of the encoding gene and subsequent expression and purification of the protein, thus eliminating the spectral and kinetic overlap of the FAD cofactor with the FMN during characterization [99]. Intramolecular electron transfer from the FMN to the haem group in the presence of carbon monoxide could be observed and characterized directly, as well as the subsequent fatty acid turn over [100]. Similarly, existing functional protein domains can also be fused on a genetic level with a linker module then expressed as a single polypeptide, thus creating artificial redox chains by what has been referred to by some authors as 'molecular Lego' [101]. Additional modifications such as biotinylation or the site-specific introduction of cysteines help in immobilization to solid supports or electrodes [102]. In this way the macromolecular properties of the protein can be adapted to the requirements of the system under study.

2.2.2 Cofactor reconstitution

The essential but non-amino acid molecules which assist redox proteins in their myriad functions are collectively known as cofactors. These relatively small molecules can be covalently attached to or non-covalently associated with the polypeptide chain, and include such atoms and molecules as metal ions (such as copper in azurin), flavins (FMN in flavodoxin), haem groups and nucleotides. The technique of cofactor reconstitution can be used to confer novel characteristics and activities onto existing proteins that carry such cofactors. The principle of the method, illustrated in Fig. 2.2, is based on the replacement of the protein's original cofactor by a modified version of the same cofactor, and is dependent first on the apoprotein remaining stable in the absence of cofactor, and its ability to then bind the non-native cofactor, or be reconstituted. Modifications to cofactors can also impart more global as well as activity-related traits upon the reconstituted proteins, where the technique has most widely been applied to haemo- and flavoproteins.

Although the cofactor may be only slightly modified relative to its native form, when bound to the apoprotein it may still have large effects on the macroscopic properties of the protein. In two different examples, long hydrophobic chains were attached to one of

the propionate ends of a haem group. In one case, the attached tail consisted of a simple alkyl chain [103,104], while in the other this was made up of a polystyrene chain [105]. The former was used to reconstitute apomyoglobin, upon which the semisynthetic protein was found anchored in a lipid bilayer in a highly ordered and oriented fashion. Horseradish peroxidase was reconstituted with the latter molecule, which then formed large amphiphiles that took on vesicular structures in aqueous solution.

Modifications can also be introduced that impart new binding properties to the protein. Boronic acid is known to bind particular sugar units in solution, thus a haem group bearing such a phenylboronic acid moiety as a sugar receptor was conceived of and synthesized. Myoglobin bearing the phenylboronic-appended haem was found to specifically bind certain sugars [106], thus an artificial receptor was successfully grafted onto the protein. This was further extended for certain phenylboronic acid derivatives, which showed enhanced aniline hydroxylase activity upon sugar binding, thus a functional semisynthetic enzyme could be created by modified cofactor reconstitution [107]. Myoglobin was also engineered to recognize both small and larger molecules by extending the haem group at the propionate positions by up to eight carboxylate groups, thus forming a novel negatively charged artificial binding face on the protein [108,109]. Reconstituted myoglobin was found to form complexes with the small electron acceptor methyl viologen [108], as well as the macromolecular cytochrome *c* [110]. In both cases complex formation was shown to be driven by electrostatic interactions between the binding face and the positively charged methyl viologen and the lysine rich patch on cytochrome *c*. Conversely, replacing the carboxylate groups by alkylamino groups caused the reconstituted myoglobin to bind anionic hexacyanoferrate instead [111].

Particular modifications of the haem group were also found to result in catalytic activity that was previously absent in the native proteins. Efforts were made in parallel to enhance the peroxidase activity of myoglobin, where eventually several approaches succeeded. In one, the haem with eight carboxylates appended to the propionate groups was used to reconstitute myoglobin, and the resulting molecule had increased specificity towards guaiacol oxidation that was 13-fold higher compared to native myoglobin [112]. Similarly, addition of histidine or arginine-alanine at one of the propionates allowed the

binding of and electron transfer to phenolic substrates in the presence of hydrogen peroxide [113].

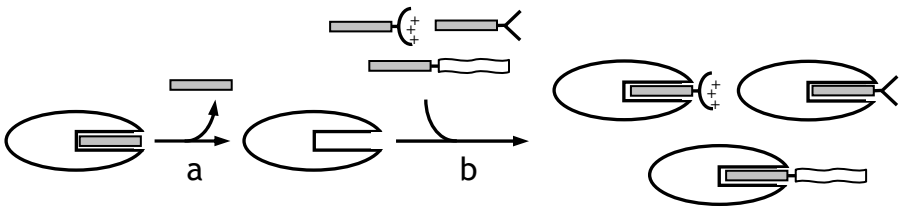

Fig. 2.2. The principle of cofactor reconstitution. In step (a) the native cofactor is removed from the protein, leaving the apoprotein. In step (b) the apoprotein is presented with a range of cofactors modified for added functionalities, where those illustrated here have characteristics ranging from a positively charged electrostatic face, a receptor for small molecules and a long attached tail. Binding of these modified cofactors by the apoprotein results in reconstituted proteins that carry the functionalities of both the protein with bound cofactor as well as the characteristics of the modification.

The electrochemistry of redox proteins is a challenging field due in the main to difficulties in establishing good and reproducible contacts between the redox site buried within the insulating protein and the solid electrode surface. While a number of diffusional mediators have been identified that can act to shuttle the electrons between the protein and the electrode, finding a suitable combination of these molecules is still a matter of trial and error, and may not even be possible for all redox proteins. Reconstitution of proteins with modified cofactors can however provide a viable alternative to solving this problem. Derivatizing cofactors with small electron transfer mediators was found to enhance the electrochemical contact between the reconstituted proteins and electrodes, where a FAD cofactor functionalized with ferrocene when bound to glucose oxidase was found to significantly improve electrical communication between the protein and a gold electrode compared to the protein when randomly functionalized with ferrocene [114]. In a series of experiments carried out by Willner and Katz, the FAD cofactor from glucose oxidase was replaced by a FAD-pyrroloquinolinoquinone (PQQ) dyad assembled on a gold electrode [115]. With PQQ acting both as a spacer and a relay to the gold electrode, the enzyme was successfully reconstituted such that it could efficiently turnover glucose with the electrode at rates similar to those obtained with molecular oxygen [114].

With particular reference to flavodoxins, the ease with which the FMN cofactor can be removed and replaced with an external flavin has been instrumental in many structural and functional studies of the protein. Modifications at particular positions of the FMN cofactor and their incorporation into flavodoxin allowed hypotheses on the importance of these positions in modulating the redox properties of the protein to be tested [36,116,117]. Specific interactions between the FMN and apoflavodoxin could be identified by NMR experiments with a flavodoxin reconstituted with ^{15}N-labelled flavins [35], while the tightness of the interaction between the apoflavodoxin and various flavins could be quantified by fluorescence quenching upon titration of the flavin with apoflavodoxin [19,118]. The physical pathways along which flavodoxin transfers electrons could also be probed by modifying the position on the FMN postulated to be involved, and investigating the effect of the modification on the kinetics of electron transfer from the reconstituted flavodoxin to an acceptor protein [50].

Although the ligands of an active site are not strictly speaking considered cofactors of redox enzymes, instances do exist where these can also be replaced, or reconstituted, affecting changes to the local and/or macromolecular of the protein, and as such merit a mention here. As previously described in Chapter 1.3.1, the mutant His117Gly of azurin could be reconstituted back to the wild type protein as judged spectroscopically, but this ability to bind imidazole was used to build a homodimer of azurin with the use of a bis-imidazole linker [77].

Finally, it has also been possible to replace the native metal ion in a number of proteins, and in so doing abolishing existing characteristics onto the protein, or conferring new ones depending on the replacing metal. Zinc-replaced azurin is redox inactive [119], and can act as a mimic for the oxidised copper (II) state of the protein. This allows NMR experiments to be done without the interference of paramagnetism of the oxidised copper. Furthermore, zinc-substituted haem proteins can be photoexcited to form a stable strongly reducing species (see below). However, it is worth bearing in mind that replacement of the metal can influence the fine structure of the metal binding site; X-ray diffraction and paramagnetic NMR studies showed different coordination geometries and dynamics for the metal sites of copper (II) and cobalt (II) azurin [120]. Binding studies of redox-inactive

silver- and cadmium-reconstituted amicyanin showed that structural changes in the metal site can have large effects on affinity for a redox partner [121]. A vanadate ion has even been incorporated into the active site of phytase, which does not naturally co-ordinate a metal ion, resulting in a semisynthetic enzyme with peroxidase activity [122].

2.2.3 Cross-linking

It is worth briefly discussing the technique of chemical cross-linking of proteins, as an alternative to the methods of introducing changes and the creation of new redox-active (multimeric) molecules already discussed. This method has in the past often been applied to stabilize complexes of redox proteins, which due to their transient nature can be difficult to study. The strategy often applied attempts to trap the natural encounter complexes formed between partner proteins by the addition of cross-linking agents that link carboxylate and amino groups on the opposing partner proteins. Many examples of this approach exist, such as complexes of flavodoxin and cytochrome *c* [123], and myoglobin and cytochrome b_5 [124]. The non-specificity of this form of linking generally leads to an ensemble of covalent complexes, which may resemble the true situation more closely.

To obtain more structurally well-defined complexes, surface cysteines may be introduced at predefined positions on the partner proteins. These can then be linked either directly via disulphide bridges, as was done for cytochrome *f* and plastocyanin [125], or with the use of sulphydryl-specific linkers, such as the maleimide-based linker used to form dimers of azurin [126]. The characterization of the electron transfer properties demonstrated amongst others the importance of protein rearrangement [125], electrostatic interactions [127] and other factors in regulating electron transfer. However, the various cross-linked complexes were also found to have very different and much slowed rates, despite prior indications that a particular orientation could be productive for electron transfer, for example for three different complexes of cytochrome *c* peroxidase and cytochrome *c* from yeast [128]. In extreme cases, electron transfer can even be abolished altogether [126]. From this it is clear that the experimental advantages afforded by covalent linking of redox protein partners also carry defined limitations and even shortcomings, in sometimes inadvertently locking proteins in unproductive conformations. By comparison,

the non-covalent approach of cofactor reconstitution allows more rotational freedom and higher (local) mobility, essential for circumventing these problems.

2.3 Photoinduced Electron Transfer

Over the years, gene identification and protein expression and purification methods have improved greatly so as to allow the isolation of many of the crucial players in the electron transfer chains that are key to respiration and photosynthesis. *In vitro* studies of the interactions and reactions of these proteins with their partners afford much information on the mechanisms that control and regulate these pathways. To study the often high rates of the electron transfer reaction between proteins however, the ability to co-ordinate initiation of the reaction with observation of the system is desirable. This requirement is addressed well by photoactive compounds, which donate an electron upon excitation by light, at which point the changes in the sample can be followed by spectroscopic or other means. A number of molecules and systems have been developed with particular regard to photoinduced electron transfer in proteins as discussed below, where the covalent attachment of such exciter molecules to the redox proteins has often proved to be of benefit.

2.3.1 Free and Bound Flavins

Towards the end of the 70's, it was noted that relatively small amounts of free flavin combined with extended white light illumination could catalyse the reduction of flavoproteins [22] when EDTA was also present. The derivative 5-deazariboflavin in particular was found to be especially efficient [129], due to the very low redox potential of its semiquinone state [130]. This method was extended to excitation of the flavins by a short laser pulse that reduces a fraction of the total sample, and allows averaging of the signal (see [131] and [132] for reviews). The laser generated flavin semiquinone has been widely used not only to study direct electron transfer to a range of redox proteins such as cytochromes [133,134] and blue copper proteins [135], but also to initiate electron transfer in chains of redox donor and acceptors which include small inorganic molecules [61,136] and larger protein partners [137,138].

With regards to the reduction of flavodoxin by photoexcitation methods, it should be noted that although in principle the flavin cofactors can also be excited by a laser pulse of the appropriate wavelength even when bound to flavoproteins, this does not result in stable reduced protein. The excited state is likely to be quenched by aromatic residues that commonly flank the flavin-binding site in the protein. A study of the FAD-containing enzyme glutathione reductase showed that 90% of the picosecond time-scale deactivation of the excited flavin molecules could be attributed to quenching by an adjacent tyrosine residue [139]. Furthermore, photoreduction in the absence of external free flavins is slow and inefficient, and is thought to be mediated by the small concentration of free flavin cofactors present in the solution by dissociation from the flavoprotein [22]. Hence, for efficient and stable reduction of flavodoxin external electron donors are required.

2.3.2 Ruthenium compounds

The transition metal ruthenium has been incorporated in a range of compounds for use as an initiator of electron transfer in biological systems, where photoexcitation of Ru(II) efficiently converts it to a strongly reducing form, the Ru(II*) metal-to-ligand charge-transfer state (see [140] for a review). Furthermore, the choice of ligands coordinating the ruthenium can modulate the reduction potential of the complex, and as a result a range of ruthenium-based compounds of varying potentials has been developed.

While these soluble compounds are continuously being applied to new systems (see [141,142,143] for recent examples), covalent attachment of the ruthenium compound at a predefined position on the surface of the protein crucially allows for control over the distance between the ruthenium electron donor and the redox centre acceptor (see [83] and [84] for reviews). Site-selective labelling of proteins by Ru-compounds was initially achieved by reaction of the ruthenium compound with histidine side-chains [71,144], however by chemical modification the reactivity of the different complexes has been extended to include lysines [145,146] and cysteines [147,148]. The latter residue, relatively rare in proteins, is of particular interest in light of the modern DNA manipulation methods where unique cysteines can be engineered at a position of choice on the protein of interest. As an alternative to protein surface attachment, several groups have covalently connected $[Ru(bpy)_3]^{2+}$ with an haem group using a linker, then inserting the modified haem into

apomyoglobin [149,150]. This combination of cofactor reconstitution with covalent ruthenium attachment represents an elegant method for creating a photoactive myoglobin with minimum perturbation to the enzyme structure. Another alternative involves ruthenium photosensitizer compounds linked to substrates for particular enzymes. The substrate then acts as a rapid delivery system of electrons to relatively buried active sites in the protein by excitation of the linked ruthenium [151].

Once properly positioned, ruthenium labels have subsequently been used to transfer electrons to a variety of redox active centres within these proteins, including haem groups [152], iron-sulphur clusters [153] and blue copper sites [154]. Redox events following the initiation of electron transfer from the ruthenium are most often followed using absorption spectroscopy and allow direct measurement of the rates of electron transfer between the ruthenium donor and the protein redox centre. In addition, a wealth of complementary information on the processes accompanying the electron transfer event has also been obtained. This includes estimation of reorganization energies [144] and distance-rate dependencies [155], kinetics of further electron transfer to other redox sites within the same protein (intramolecularly) [156] or to a different protein (intermolecularly) [157,158,159], with the additional possibility of following intermediates on the way [160]. The energy transfer kinetics from the Ru to redox sites can further be applied, in the case of cytochrome P450 as a 'molecular ruler' for the depth by which the haem group is buried in the protein [161].

2.3.3 Zinc-substituted haem proteins

In the case of haem proteins, the quenching of photoexcited states can be modulated by replacing the native iron of the haem group by other transition metals, where Zn, Sn and Mg in particular enhance the formation of a long-lived and strongly reducing triplet exited state. This species is capable of reducing a second redox centre, be it intra- or intermolecular. In a seminal experiment, rate constants for electron transfer from the zinc haem group of cytochrome *c* to the copper site of a cross-linked plastocyanin molecule were measured [162]. An example of an intramolecular reaction was the replacement of one of the two haem groups in the *P. aeruginosa* nirite reductase with a zinc porphyrin,

photoexcitation of which species induced the reduction of the native c haem by the replaced Zn-haem [163]. The technique has since been extended to intermolecular acceptors of different sizes. In the reaction of zinc myoglobin with binaphthyl bisviologen, comparisons of rate constants showed a stereospecificity in electron transfer [164]. For larger redox proteins, the reaction of zinc cytochrome *c* with the wild type and various mutants of azurin free in solution helped elucidate the importance of electrostatic interactions for complex formation [165].

Again, chemical modification of the cofactor and its reconstitution into the protein can extend the application of this method. A quinone group was attached to the zinc-substituted porphyrin in myoglobin using linkers of different lengths; upon excitation of the zinc, reduction of the quinone could be detected spectroscopically and the efficiency of different linkers compared [166,167]. Electron transfer could also be detected from zinc-containing myoglobin modified on its porphyrin with four ammonium groups to small negatively charged substrates bound to the artificial binding site formed [168,169].

2.3.4 TUPS

A new photolabel, thiouredopyrenetrisulphonate or TUPS, has been developed over the past 10 years as an alternative to the ruthenium labels that are available. Single photon excitation of the dye yields its very low potential triplet state [170]. Initial work utilised the triplet state of TUPS free in solution to react with proteins [171], however further derivitization of the compound first allowed its attachment to a range of soluble amino acids [172], then more specifically to the protein via surface lysines [173,174] and cysteines [175,176]. Recently, the label has been found to form a powerful reductant in the presence of suitable electron donors [177]. In general this label has the advantage of being commercially available and very soluble, simplifying its attachment to proteins. The labelled and unlabelled proteins are easily separated on an ion exchange column due to the additional negative charges of the label, and its absorption in the visible region allows for easy quantification of the efficiency of labelling.

2.3.5 Other methods

Several other methods are currently available for the rapid excitation of samples and initiation of electron transfer in proteins. These include pulse radiolysis, where a short pulse of high-energy electrons is applied to an aqueous solution, forming the radiolytic radicals e^-_{aq}, $H^{\cdot}$ and $HO^{\cdot}$. A range of compounds can be added to the solution that will scavenge these radicals, themselves forming strongly reducing agents that can go on to react with the proteins under study. Using ^{32}P-enriched phosphate as an internal radiation source and combining the pulse radiolysis with absorption spectroscopy allowed the trapping and identification of the cytochrome P450 catalytic cycle [178].

Another, more specialised, technique involves the binding of carbon monoxide (CO) to the ferrous haem in proteins. Pulsed illumination induces the dissociation of CO with high efficiency and lowers the redox potential of the haem, thus yielding a very local and powerful reductant in the heart of the protein. This approach was taken to compare a series of mutants of the iron ligand of yeast iso-1-cytochrome *c* spectrally and photochemically for binding to its native redox partner, cytochrome *c* oxidase [179].

2.4 Conclusions

In summary, a wide range of experimental methods have been and continue to be developed for the study of electron transfer in biological systems, to continually test and refine our understanding of the underlying theory as initially laid out by Marcus. The results obtained from the application of these techniques also demonstrate the importance of the macromolecular phenomena of protein-protein association and dissociation in these reactions. Needless to say, the approaches are not mutually exclusive. *De novo* designed 4-helix bundles have not only had haem groups incorporated for the creation of new haem proteins [180], but also both flavin [181] and ruthenium [182] attached to their surface to make them photoactive. Similarly, a zinc myoglobin was chemically cross-linked to cytochrome b_5, creating a photoactive heterodimer [124]. The modular approach in

combining different elements of photoactivation and protein engineering provides ever expanding potential for new approaches to probing biological electron transfer.

Chapter 3

A Crystallographic Study of Cys69Ala Flavodoxin II of *Azotobacter vinelandii*: Structural Determinants of Redox Potential

Sharmini Alagaratnam, Gertie van Pouderoyen, Tjaard Pijning, Bauke W. Dijkstra, Davide Cavazzini, Gian Luigi Rossi and Gerard W. Canters

---

Abstract

Flavodoxin II from *Azotobacter vinelandii* is a 'long-chain' flavodoxin, and has one of the lowest E_1 midpoint potentials found within the flavodoxin family. To better understand the relationship between structural features and redox potentials, the oxidised form of the C69A mutant of this flavodoxin was crystallised and its three-dimensional structure determined to a resolution of 2.25 Å by molecular replacement. Its overall fold is similar to that of other flavodoxins, with a central five-stranded parallel β-sheet flanked on either side by α-helices. An 8-residue insertion compared to other long-chain flavodoxins forms a short 3_{10} helix preceding the start of the α_3 helix. The FMN cofactor is flanked by a leucine on its *re* face instead of the more conserved tryptophan, resulting in a more solvent accessible FMN-binding site and stabilisation of the hydroquinone (hq) state. In particular the absence of a hydrogen bond to the N5 atom of the oxidized FMN was identified which destabilizes the ox form, as well as an exceptionally large patch of acidic residues in the vicinity of the FMN N1 atom, which destabilizes the hq form. It is also argued that the presence of a Gly at position 58 in the sequence stabilizes the semiquinone form (sq), as a result, raising the E_2 value in particular.

Introduction

The redox potential of an electron transfer protein is of prime importance in relation to its function, where the correlation between protein structure and redox potential helps explain how nature has adapted proteins to their specific functions. In the past this has been studied for a range of flavodoxins, small (14 - 23 kDa) acidic α/β proteins that contain a single non-covalently bound flavin mononucleotide (FMN) cofactor, from different organisms. *In vivo* they act as remarkably versatile low potential one-electron donors in a range of reactions [1] in mainly prokaryotic organisms, including obligate and facultative anaerobes, microaerophiles and photosynthetic cyanobacteria, as well as in both red and green eukaryotic algae. In the photosynthetic bacteria *Anabaena* for example it replaces ferredoxin as an electron shuttle from photosystem I to ferredoxin-$NADP^+$ reductase under iron-deficient conditions [183].

Flavodoxin II from *Azotobacter vinelandii* ATCC 478, the subject of this paper, has been implicated in electron transfer to nitrogenase, where its synthesis was co-induced with nitrogenase upon introduction of *A. vinelandii* cells to nitrogen-fixing conditions after growth on NH_4Cl [12]. This flavodoxin is a so-called 'long-chain' flavodoxin, and has one of the lowest E_1 midpoint potentials found within the flavodoxin family [26] (see also below).

Two subgroups have been identified within the flavodoxin family, the short-chain and the long-chain flavodoxins. The long-chain flavodoxins are up to 38 residues longer than the short-chain flavodoxins, mainly due to a long inserted loop of 22 residues in the final strand of the central β-sheet, towards the end of the protein. Flavodoxin II from *A. vinelandii* contains this insertion and is therefore considered to be a member of this subgroup. The distinction between long- and short-chain flavodoxins appears to parallel a difference in redox potentials for these proteins. FMN, both when free in solution and bound to apoflavodoxin, can exist in three redox states, namely oxidised (ox), one-electron reduced semiquinone (sq) and two-electron reduced hydroquinone (hq). For FMN free in solution, the midpoint potential for the ox/sq redox couple, E_2, is lower than that of the sq/hq potential, E_1. However, complex formation with apoflavodoxin alters these

potentials dramatically, inducing an inversion as well as a substantial separation between them. As a result, flavodoxin can transfer electrons in two discrete one-electron steps [40].

Three-dimensional structures are known of oxidised flavodoxins from both subgroups, namely from *Clostridium beijerinckii* [184] and *Desulfovibrio vulgaris* [28] for the short-chain and from *Anabaena variabilis* [30], *Chondrus crispus* [185], *Escherichia coli* [34], *Helicobacter pylori* [186], *Megasphaera elsdenii* [187], and *Anacystis nidulans* [188] for the long-chain flavodoxins. Additionally, structures of the sq and/or hq forms of the flavodoxins from *A. nidulans*, *C. beijerinckii* and *D. vulgaris* are also available [28,29,41,189,190]. The combination of structural data with mutagenesis of identified key residues has resulted in a general picture where it appears that the separation of the midpoint potentials in flavodoxin is effected by the differential stabilisation by the apoflavodoxin of the three oxidation states of FMN. In all three structures of flavodoxin semiquinones listed above, a striking difference in the flip of the 58-59 backbone peptide (*A. vinelandii* numbering) upon reduction to the sq form was observed [28,41]. The hydrogen bond then formed between the carbonyl of residue 58 and N5 of the FMN stabilises the neutral semiquinone in the protein, and is purported to be the basis of the positive shift of the ox/sq potential compared to FMN free in solution [27,29,190]. The identity of one of the residues within this 58-59 peptide is also known to be a crucial determinant of E_2 [27,31]. The exceptionally low sq/hq E_1 potentials in flavodoxins, on the other hand, are thought to be brought about by specific destabilising electrostatic interactions between the anionic hq and the FMN binding site, which contains patches of uncompensated negatively charged residues [38,191]. In addition, sandwiching of the FMN between two aromatic residues is not only unfavourable for the charged hq, but also actively excludes solvent from the FMN binding pocket, thus maintaining an apolar environment [39,40,192].

E_2 in particular appears to be higher in general for the short-chain compared to the long-chain flavodoxins (see Fig. 3.1). The 22-residue insertion that differentiates the long- and short-chain subgroups does not however contact the FMN cofactor, and as such is unlikely to be the source of the differences in potentials, as has previously been noted [193]. In fact, a recent study of shortened variants of the long-chain flavodoxin from *Anabaena* indicated that the loop was only indirectly responsible for stabilising the protein

complex with FMN, and was more likely to be involved in the recognition of partner proteins [14,16].

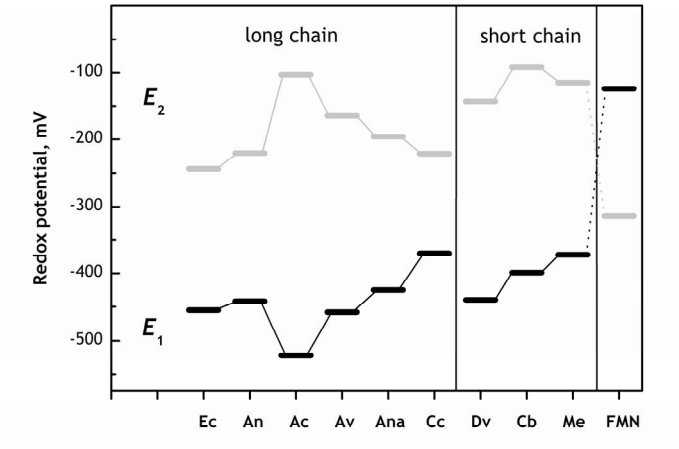

Fig. 3.1. The E_1, sq/hq and E_2, q/sq midpoint potentials for long and short chain flavodoxins from different sources at pH 7.0, in mV. The species from which the flavodoxins were isolated are (from left to right) *E. coli*, *A. nidulans*, *A. chroococcum*, *A. vinelandii*, *Anabaena* 7120, *C. crispus*, *D. vulgaris*, *C. beijerinckii*, *M. elsdenii* and finally FMN free in solution, with E_1 and E_2 inverted with respect to the flavodoxins. In particular the E_2s of *A. vinelandii* and *A. chroococcum* approach those of short rather than long chain flavodoxins.

While research has continued into the details of the physiological role of flavodoxins, such as its role in the kinetic regulation of nitrogenase [194], its ease of expression and purification as well as stability has made it a popular model for a number of more general biochemical studies, in addition to the redox potential studies described above. For flavodoxin II from *A. vinelandii* these include functional studies of electron transfer to other (non-physiological) partner proteins [45,50], kinetics of flavin binding to apoflavodoxin [195,196], electrochemical studies [26] as well as protein folding and unfolding studies [197,198]. Despite the wealth of information available on the characteristics and reactivity of this particular flavodoxin, only the secondary structure content of the protein is known from NMR spectroscopic studies [193], as well as a predicted three-dimensional structure obtained by alignment and modelling using the structure of the *A. nidulans* flavodoxin [199].

Here we report the structure of the oxidised form of the Cys69Ala (C69A) mutant of flavodoxin II from *A. vinelandii* as solved by X-ray diffraction to a resolution of 2.25 Å using molecular replacement. While the basic fold of the flavodoxin resembles that of other known flavodoxins, several unique features stand out. An 8-residue loop purported by analogy to be involved in partner protein complex formation is identified at the surface of the protein. Focussing on the local structure around the FMN-binding pocket, a striking difference was noted in the absence of a hydrogen bond to the N5 of FMN, contrary to all other structures of oxidised long-chain flavodoxins known. The presence of a leucine instead of a conserved tryptophan on the *re* face of the FMN results in a more polar FMN binding site, while a significantly larger cluster of negatively charged residues is found around the N1 of the FMN than in other flavodoxins. Both these factors are known determinants of E_1, the sq/hq potential. Despite the fact that only the E_1 redox couple is biologically relevant, close study of the structure of flavodoxins in the various redox states has been instrumental in furthering understanding of how variations in composition and structure modulate both E_1 and E_2 redox potentials of this protein family in particular, with implications for redox proteins in general. In this *A. vinelandii* flavodoxin, the structure suggests destabilization of the ox and hq forms of the protein, while stabilization of the sq form moves the ox/sq E_2 redox potential to a relatively high value. The discussion affords new insights into how variations in protein composition and structure can modulate their redox potentials.

Materials and Methods

Expression and purification of recombinant A. vinelandii flavodoxin II

C69A flavodoxin II from *A. vinelandii* ATCC 478 was expressed heterologously in *E. coli* strain TG2 from a pUC19 plasmid containing the mutated Cys69Ala flavodoxin gene [200]. The large-scale culture was induced with 1 mM IPTG upon inoculation, and grown for 24 hours before harvesting. The protein was purified according to described protocols and was considered to be pure when the absorption peaks showed a ratio A_{274}/A_{452} of 4.7 [201]. The molar absorption coefficient at 452 nm of 11.3 mM^{-1} cm^{-1} [12] was used to determine the concentration of flavodoxin.

Crystallization and X-ray data collection

Crystals were grown at room temperature using the sitting drop vapour diffusion method. The reservoir contained 2.8 M ammonium sulphate and 0.1 M Tris buffer, pH 7.0. The drops were made by mixing 2 µl of protein solution (15 mg/ml in 0.1 M Tris buffer, pH 8.0) and 2 µl of the reservoir solution. Plates and clusters of plate-like crystals grew over a period of between one to two weeks. The crystal used for data collection was transferred to a 4:1 solution of reservoir solution and water. The crystal was subsequently dipped in Al's oil (1:1 paraffin oil and silicon oil) and flash frozen in a stream of evaporating nitrogen gas of 100K. The crystal belongs to space group $P2_12_12_1$ with cell dimensions a = 39.01 Å, b = 70.54 Å, and c = 132.64 Å. It diffracted to 2.25 Å resolution. Data were collected in house with a MAR CCD detector with CuKα X-rays from a NONIUS FR591 rotating anode generator (Table 3.1). Data were processed with DENZO and SCALEPACK [202]. Reduction to structure factor amplitudes was performed with TRUNCATE [203].

Model building and crystallographic refinement

The structure of flavodoxin II C69A was solved by molecular replacement. The search model was based on the structure of the 47% sequence identical *Anabaena* flavodoxin (PDB-code 1RCF [204]) using the 3D-PSSM server [205]. This resulted in a model in which the side chains had been modelled by placement with a rotamer library [206]. Two molecules were located in the asymmetric unit using the molecular replacement program EPMR [207] yielding a solvent content of 50%. Using data between 10 and 4 Å resolution the correlation coefficient and R-factor of EPMR became 0.227 and 57.0% for the first molecule only and improved to 0.387 and 50.4% when both molecules in the asymmetric unit were included. The two molecules were rigid body refined with CNS [208] resulting in an R-factor of 48% (10 - 3Å). After a first round of simulated annealing (30 - 2.25Å, R-factor of 37.0%, R-free of 42.7%), the electron density map was clear and showed the FMN group that had been omitted from the molecular replacement model. Side chains pointing in the wrong direction and main chain at insertion points were manually rebuilt using the programs O [209] and QUANTA (Accelrys). The improved model was further refined with

REFMAC5 [210]. No NCS constraints were used. Water molecules were added and electron density for 6 sulphate ions was also present. The final R-factor is 22.3% and the free R-factor 27.8%. The refinement statistics and information about the final model are listed in Table 3.1. The geometry of the final model was analyzed using PROCHECK [211]. Figures were prepared using PyMOL (http://pymol.sourceforge.net). The co-ordinates have been deposited in the Protein Data Bank [212] under accession number 1YOB.

Calculation of surface accessibility of FMN in flavodoxins

The programme NACCESS [213] was used to calculate the surface accessibility of the FMN cofactor in $Å^2$ for a number of both long- and short-chain flavodoxins, using the PDB files of each of the proteins as input, and the default probe size of 1.4 Å.

Results and Discussion

The crystal structure determination of A. vinelandii *C69A flavodoxin II*

The crystal structure of *A. vinelandii* C69A flavodoxin II was solved at 2.25 Å resolution using molecular replacement with a homology model based on the *Anabaena* flavodoxin structure [30,204]. The protein crystallized with two monomeric molecules in the asymmetric unit, called A and B, which are related by a 133° rotation. The refinement statistics and contents of the final model are given in Table 3.1. Except for some solvent exposed side chains, the molecules are clearly defined in density. Superposition of the Cα atoms of the two molecules gives a root mean square (RMS) difference of 0.7 Å. Excluding residues that differ by more than 3 σ (residues 1, 59, 178 and 179), the RMS difference decreases to 0.38 Å. Taking into account only the non-glycine and non-proline residues and discounting the first and last residues of each molecule, 268 residues (88.2%) are in the most favoured region of the Ramachandran plot, 36 residues (11.8%) in the additional allowed regions, and none of the residues are in the generously allowed regions or in the disallowed regions.

Table 3.1. Data collection, refinement and model statistics.

Resolution (Å)	30 - 2.25		
Total observations	156381		
Unique observations	17468		
Completeness (%)	92.0		
Completeness last shell (2.33-2.25Å) (%)	85.4		
R_{merge} (%)	7.2		
R_{merge} last shell (2.33-2.25Å) (%)	49.2		
I/sigma	16.1		
I/sigma last shell (2.33-2.25Å)	2.4		
Refinement statistics			
R-factor (%)	22.2		
Free R-factor (%)	27.9		
R.m.s. deviation from ideality			
Bond lengths (Å)	0.0068		
Bond angles (°)	1.32		
Model statistics			
Polypeptide chain	A	B	Total
Number of amino acid residues	179	179	358
Number of FMN groups	1	1	2
Number of water molecules			221
Number of sulphate ions			6

The polypeptide fold of A. vinelandii C69A flavodoxin II

C69A flavodoxin II from *A. vinelandii* is the longest flavodoxin to date for which a structure has been determined. Its three-dimensional fold is shown in Fig. 3.2, and consists of the α/β fold common to all flavodoxin structures presently known. The main secondary structure elements of the protein were defined from the PDB co-ordinates using the DSSP programme by Kabsch and Sander [214]. The central core of the protein is made up of a highly conserved five-stranded parallel β-sheet, the final strand of which is interrupted by a 22-amino acid insertion between β_{5a} and β_{5b}, characteristic of long-chain flavodoxins. There is however more variability between different flavodoxins in the number and length of the α-helices that pack against the central β-sheet core. Here, a total of 5 α-helices were

identified, with helices 1 and 5 found together on one face of the sheet, while helices 2, 3, and 4 are clustered on the other face. A short helical region of 1.5 turns, α_2, was found after a 3_{10} helix in between strands β_2 and β_3.

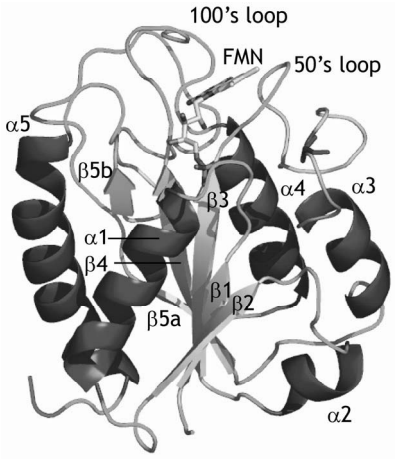

Fig. 3.2. The three-dimensional fold of *A. vinelandii* flavodoxin II, showing the α-helices, β-sheets and random coil structural elements. The inserted loop of residues 61-71 follows the end of the α_3 helix, and the mutation Cys69Ala is shown in sticks in the middle of that loop. The FMN cofactor is also represented in stick form at the top of the protein.

Structural comparisons to other flavodoxins

The α-carbon backbone of molecule A of the *A. vinelandii* flavodoxin was superposed onto all other known structures of long-chain flavodoxins, and the RMS difference was calculated for each pair of proteins (Table 3.2). The structures of flavodoxins from five other sources superpose well onto the *A. vinelandii* flavodoxin, with RMS differences below 1 Å for all structures, except for that from *C. crispus*, the only eukaryotic flavodoxin in the group. Interestingly, flavodoxin from *A. vinelandii* appears to resemble that from *H. pylori* most closely in structure with an RMS difference of 0.89 Å, while the amino acid sequence identity between the two proteins of 39% is comparatively low. The two structures only deviate significantly at the points where the longer *A. vinelandii* contains insertions, namely in turns Lys23-Thr29, which connects α_1 and β_2, and Asp119-Gly121, which connects α_4 and β_5. Similarly a single residue insertion in the *H. pylori* flavodoxin of Gly69 leads to a slightly different position of the Gly83-Ser87 loop in the *A. vinelandii* flavodoxin. The stretch between strands β_2 and β_3 typically shows more diversity in fold between the various flavodoxins. Although the flavodoxin from *A. vinelandii* is most

identical to that from *Anabaena*, the former has a 3_{10} helix followed by a short α-helix at this point, while the latter does not exhibit any helical structure in this region. The flavodoxins from *A. nidulans* and *C. crispus* have a 3_{10} helix and a short single-turn α-helix here respectively. Additionally, α_3 of *A. vinelandii* is relatively long, more similar to the flavodoxin from *Anabaena* than to those from *A. nidulans* or *C. crispus*.

Table 3.2. RMS differences in Å between superpositions of the α-carbon atoms of all long-chain flavodoxin structures. The amino acid sequences were compared using the local alignment programme BLAST [215], and the identity between them is indicated in brackets.

	A. vinelandii	*H. pylori*	*E. coli*	*A. nidulans*	*Anabaena* 7120
A. vinelandii	–	–	–	–	–
H. pylori	0.89 (39%)	–	–	–	–
E. coli	0.93 (44%)	0.83 (43%)	–	–	–
A. nidulans	0.97 (41%)	0.96 (38%)	0.83 (45%)	–	–
Anabaena 7120	0.99 (47%)	0.95 (42%)	0.84 (46%)	0.54 (70%)	–
C. crispus	1.17 (39%)	1.22 (34%)	1.25 (37%)	1.14 (36%)	1.20 (41%)

Structure-based alignment of the flavodoxin sequences in Fig. 3.3 also reveals that, compared to other long-chain flavodoxins, the *A. vinelandii* flavodoxin has an additional inserted loop of residues 64-71. These eight amino acids map onto a stretch following strand β_3, coloured cyan in Fig. 3.2, at the FMN-binding end of the protein. The insertion takes on the conformation of a short 3_{10} helix, followed by a turn and a loop that precede the start of α_3. An analogous loop has previously also been identified by sequence analysis in the 94% identical *A. chroococcum* flavodoxin [15], the 3D-structure of which has never been released [216]. However from two-dimensional NMR data the loop was inferred to be at the protein surface, and was shown to be involved in complex formation with the Fe protein of nitrogenase [15]. Our structure of the *A. vinelandii* flavodoxin corroborates the former result, clearly showing this loop to be solvent exposed.

The protein used for this study is the Cys69Ala (C69A) mutant, which has widely been used for functional studies, as it does not dimerize via the cysteine thiol group like

Table 3.3. Hydrogen bond interactions between FMN and apoflavodoxin or water atoms in *A. vinelandii* flavodoxin II for molecule A.

FMN atom	Protein/ water atom	Distance (Å)
N1	O 56 Thr	3.52
	N 98 Asp	3.00
O2	N 98 Asp	3.37
	O 105 Asn	3.29
	N 107 Leu	2.78
N3	O 105 Asn	2.71
O4	N 60 Gly	3.32
	W22	2.64
N5	W22	3.17
O2*	O 56 Thr	2.68
	N 56 Thr	3.27
O3*	NZ 13 Lys	3.67
	OD1 154 Asp	2.62
O4*	W2	2.90
OP1	OG 9 Ser	2.57
	N 13 Lys	3.54
	N 14 Thr	2.86
	OG1 14 Thr	2.63
OP2	N 10 Asn	2.95
	N 11 Thr	3.06
	OG1 11 Thr	3.32
	W 28	2.56
OP3	N 11 Thr	3.38
	OG1 11 Thr	2.45
	N 12 Gly	3.12

wild type does [217], while retaining the redox properties of the wild type protein [26]. The Cys69Ala mutation sits in the middle of the above loop on the surface, towards one side of the protein with no direct contacts with the FMN cofactor (Fig. 3.2). This is consistent with the unchanged redox potentials of this mutant. Additionally, as the Cβ carbon of Ala69 is solvent exposed, assuming that the mutation does not cause conformational changes, by analogy the thiol group of the cysteine residue in the wt protein may also be expected to be solvent accessible. This may explain the tendency of the wt protein to dimerize over time [217].

A single phosphate group is present in the structure as part of the FMN cofactor. The gene for flavodoxin II used for this study is identical to that cloned from *A. vinelandii* strain OP Berkeley [11], that has also been expressed heterologously in *E. coli* [218]. This crystal structure confirms an earlier notion that this flavodoxin form does not contain a covalently bound phosphate [12], as was also found for the recombinant flavodoxin from *A. vinelandii* strain OP Berkeley [218].

A total of seven solvent molecules were found buried in the interior of the protein, occupying comparable positions in both molecules in the asymmetric unit. The positions of these water molecules with respect to the three-dimensional fold of the flavodoxin molecule are illustrated in Fig. 3.4a. Two of them were found to interact with residues at the top ends of strands β_3 and β_4, and β_4 and β_5. Two others bridge the loop connecting the end of α_2 to the start of β_3, and to the ^{152}D-L-D-N^{155} loop between the end of β_5 and the start of α_5 respectively. A structurally conserved solvent molecule was also found between Leu93 on β_4 and the end of β_{5a}, just at the start of the inserted loop common to long-chain flavodoxins; it is visible as the dark sphere towards the back of the molecule in Fig. 3.4a. Finally, two more water molecules were identified in the cavity adjacent to the more buried *re* face of the FMN. These latter two will be discussed in more detail below. However all mentioned solvent molecules appear to play a structural role in the packing of the protein. This is confirmed by the fact that they mostly occupy positions similar to those of water molecules found in other long-chain flavodoxins [34,204,219].

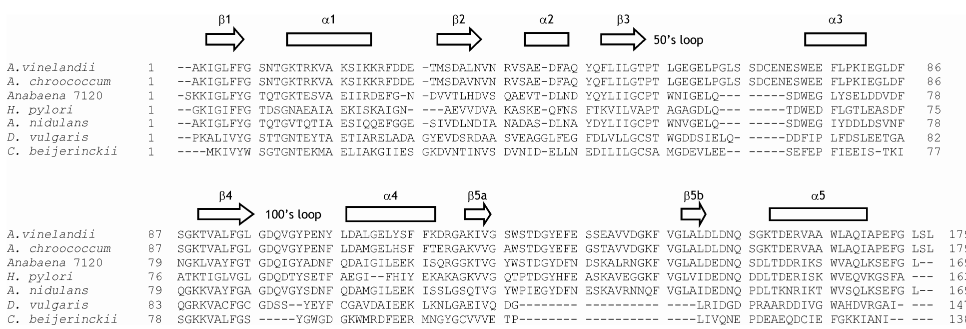

Fig. 3.3. Structure-based sequence alignment using SEQUOIA v 0.9.7 [220] of the oxidised long chain flavodoxins from *A. vinelandii*, *Anabaena* 7120 (PDB-entry 1RCF [204]), *H. pylori* (PDB-entry 1FUE [186]), *A. nidulans* (PDB-entry 1CZU [219]), and the oxidised short chain flavodoxins from *D. vulgaris* (PDB-entry 1J8Q [221]) and *C. beijerinckii* (PDB-entry 5NLL [27]). The 22-residue loop that differentiates short and long chain flavodoxins is clearly visible inserted between strands β_{5a} and β_{5b}. The primary sequence of *A. chroococcum* flavodoxin was aligned with that of *A. vinelandii* using CLUSTALW Version 1.81 [17]. The main secondary structure elements of the *A. vinelandii* protein were defined from the PDB co-ordinates using the DSSP programme [214], and are indicated above the amino acid sequence alignment.

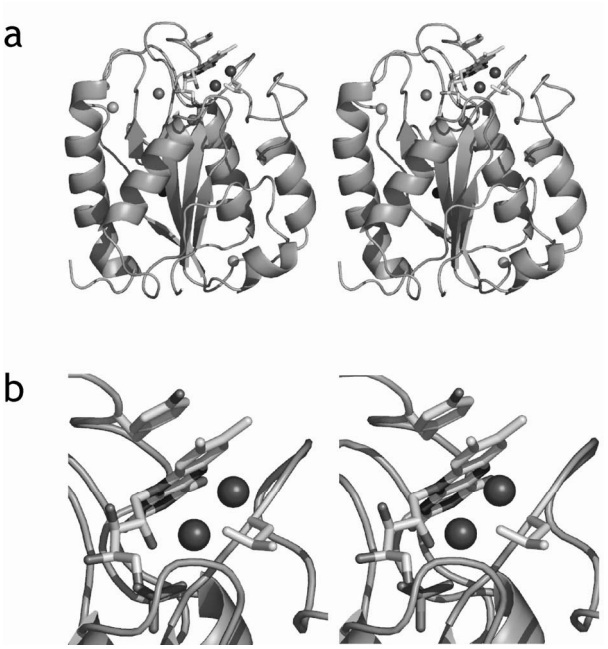

Fig. 3.4. (a) Stereo views showing the positions of the structured solvent molecules, represented as spheres, with respect to the whole flavodoxin molecule where the two waters bridge α-helices and β-strands, while two more waters bridge the ends of two β-strands. A single black water molecule is found towards the back of the flavodoxin, at the start of the 22-residue insertion in β5 strand of the sheet. (b) Zoom in on the FMN-binding site flanked by Tyr102 and Leu57 at the top of the molecule in (a) where two red waters can be seen to lead from the cavity on the re face of the FMN created by the smaller leucine 57 side chain to the surface of the protein.

The FMN-binding pocket

As with other flavodoxins, the FMN cofactor binds non-covalently at one end of the central β-sheet, with the pyrimidine part of the molecule buried in the interior of the protein, and with the dimethyl benzene edge that has been proposed to mediate electron transfer, solvent exposed [7]. The FMN molecule is bound in a very flat conformation compared to other flavodoxins. Superposition of the α-carbon atoms of different flavodoxins as described above shows that the FMN sits at a very similar angle with respect to the protein fold, except for the three flavodoxins that have a non-tryptophan substitution at position 57 (*A. vinelandii* numbering). The FMN in these proteins is more tilted. For example the FMN in the *C. beijerinckii* flavodoxin is tilted by some 25° compared to that from *Anabaena*. This angle is closer to 15° in both *H. pylori* and *A. vinelandii*. The isoalloxazine ring in both these flavodoxins is also completely planar, as opposed to a slight butterfly-like bend that has been observed for other flavodoxins, which is approximately 8° for the *Anabaena* flavodoxin.

The different parts of the FMN cofactor associate with the flavodoxin polypeptide chain through a variety of interactions including hydrogen bonds and hydrophobic stacking. Three main regions of apoflavodoxin implicated in the non-covalent binding of FMN in other flavodoxins are also closely associated with the flavin in *A. vinelandii* flavodoxin, as detailed below.

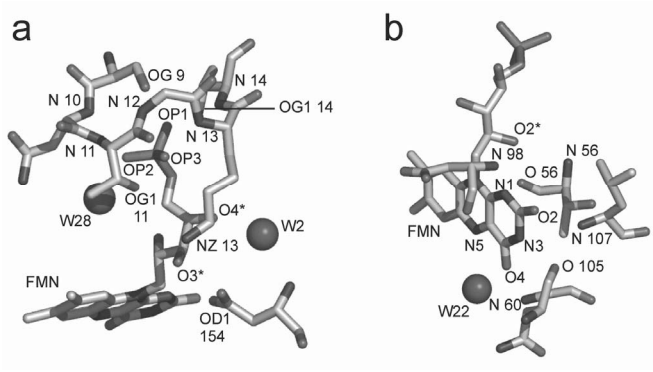

Fig. 3.5. The FMN-binding site in oxidised *A. vinelandii* flavodoxin II showing the hydrogen bonding partners from both main chain and side chain atoms (denoted by atom name, followed by the residue number) of the flavodoxin as well as waters (denoted W) to (a) the phosphoribityl side chain of the FMN (including the phosphate-binding loop consisting of residues 9-14 including the crucial Gly12), and (b) the isoalloxazine part of the FMN.

First, the extended phosphoribityl side chain acts to anchor the cofactor to the protein via an extensive network of hydrogen bonds, as summarised in Table 3.3 and shown in Fig. 3.5a. The hydroxyl groups of the ribityl chain as well as the phosphate oxygen atoms form hydrogen bonds mainly to backbone amide and carbonyl groups of the protein, and to two solvent molecules. In particular, numerous interactions are present between the phosphate oxygen atoms and backbone amides as well as side chain hydroxyl groups of the ^{9}S-N-T-G-K-T^{14} loop, as deduced from the H-bonding distances between the atoms. This loop, crucially requiring Gly at position 12, has been identified as a consensus sequence for phosphate binding in flavodoxins [41]. It has a conformation very similar to that observed in other flavodoxins.

Second, the so-called '50's loop' following β_3 identified in other flavodoxins is also closely involved in FMN binding in the *A. vinelandii* flavodoxin, in particular residues ^{56}T-L-

G-E-G[60]. Despite considerable variation in sequence in this region between species, the conformation and interaction of these residues with respect to the FMN is conserved. Fig. 3.6 shows how this 4-residue loop adopts almost identical positions in *Anabaena*, *C. beijerinckii* and *A. vinelandii*, with many backbone carbonyl and amide groups within hydrogen bonding distance of the FMN. Unique to the *A. vinelandii* flavodoxin is an interaction between Thr56 and N1 of FMN as well as O2* of the ribityl side chain (see Table 3.3, and Fig. 3.5b). The two-residue peptide that undergoes a backbone flip upon reduction of the ox to the sq and hq forms is the 58-59 peptide also located in this loop. In all structures of oxidised flavodoxins, the backbone carbonyl of residue 58 points away from the N5 atom of FMN in an 'O-down' conformation, whereas in the semiquinone state, determined for the flavodoxins from *C. beijerinckii*, *D. vulgaris* and *A. nidulans*, the carbonyl group assumes an 'O-up' conformation and points to the N5 [28,29,41]. Our structure shows that in *A. vinelandii* flavodoxin in the oxidised state, the carbonyl group of Gly58 is also in the 'O-down' conformation, and points away from the N5, towards the *re* face of the FMN cofactor (Fig. 3.6c). This is similar to the carbonyl groups of the analogous residues in the long-chain *Anabaena* and the short-chain *C. beijerinckii* flavodoxins (Fig. 3.6a and b respectively).

Finally, numerous hydrogen-bonding interactions between FMN and the apoprotein were identified in the '100's loop', from residues 98 to 107. A number of backbone amide and carbonyl groups are present within hydrogen bonding distance of the isoalloxazine ring of FMN, in particular from residues 98, 105 and 107 to N1, O2 and N3 of FMN (see Table 3.3). Fig. 3.5b shows the main hydrogen bonding partners of the flavodoxin polypeptide to the isoalloxazine part of the FMN, both from the 50's and 100's loop. The 100's loop also contains Tyr102, which flanks the FMN cofactor shielding its *si* face from the solvent, and which has been shown to play an important role in the energetics of FMN binding through coplanar aromatic stacking interactions [118,191].

Distinctive features of FMN binding in A. vinelandii *flavodoxin and consequences for its midpoint potentials*

H-bonding to N5 of FMN destabilizes the ox form. The hydrogen bonding state of the N5 of FMN in the oxidised flavodoxin is also known to affect the E_2 redox potential by stabilising the oxidised form of the protein [29,30]. In all structures of oxidised long-chain flavodoxins known to date, a hydrogen bond is found from a residue within the 50's loop to the unprotonated FMN N5. In *Anabaena* (Fig. 3.6a), *A. nidulans* and *E. coli* the donor is the backbone amide of residue 59, while in *C. crispus* it is the side chain hydroxyl group of the adjacent Thr58. Although these hydrogen-bond donors are at between 3.1 and 3.6 Å from N5 in the different flavodoxins, their geometry is favourable, pointing directly towards the N5 [34,204,219]. Additionally, the apolar environment of the FMN binding site may increase the strength of the interaction [30], and, more compellingly, direct NMR evidence for hydrogen bonding to N5 exists [31,32]. Although the hydrogen bond is broken upon reduction of the flavodoxin to the semiquinone, N5 subsequently makes a hydrogen bond with the carbonyl oxygen atom as described above, which requires the backbone peptide plane to flip (see above). However, in the oxidised *A. vinelandii* flavodoxin, no candidate for a hydrogen-bonding interaction with N5 could be found (Fig. 3.6c). The closest backbone amide group is that of Glu59, at a distance of 4.0 Å from N5, but it is in an unfavourable position for hydrogen bonding. In this sense, the oxidised *A. vinelandii* protein resembles the short-chain flavodoxins from *D. vulgaris* [189] and *C. beijerinckii* [31] (Fig. 3.6b) more closely, where no potential hydrogen bond donor is near the N5 atom either. It is likely that the absence of a hydrogen bond to N5 in the oxidised form of the protein destabilises the ox form of the FMN making reduction comparatively easier, yielding a higher E_2 value.

Gly58 stabilizes the sq form. From sequence alignments, the residue at position 58 is most commonly a glycine in short-chain and an asparagine in long-chain flavodoxins. Uncommonly for a long-chain flavodoxin, the one from *A. vinelandii* has a glycine at this position. While the glycine can optimally accommodate the O-up conformation at that position of the type II' turn found in flavodoxin semiquinones [33], the Cβ of the asparagine found in the long-chain *A. nidulans* flavodoxin makes very close contact with the

following amide group, raising the energy of the O-up conformation [29]. That this residue affects the stabilization of the semiquinone bound to flavodoxin and thus the redox potentials was confirmed by the Asn58Gly mutant of the long-chain *A. nidulans* flavodoxin, which had an ox/sq potential 46 mV more positive than wild type, while its sq/hq potential was lowered by 26 mV [29]. On the other hand, mutants of the short-chain *C. beijerinckii* flavodoxin where the homologous Gly57 residue was replaced by alanine, asparagine, aspartate and proline all had ox/sq potentials that were reduced by approximately 60 mV, while the Gly57Thr mutant with its bulkier β-branched side chain had an E_2 that was even lower, by 180 mV [27]. Direct measurement of the strength of the N5H···O57 hydrogen bond in this series of mutants by NMR definitively proved this effect, with a strong correlation between the temperature coefficients of the N5H and both E_2 and binding energy of the FMN semiquinone to the flavodoxin [31]. Thus it is conceivable that the atypical glycine at this position in the flavodoxin from *A. vinelandii* may be a factor in shifting the ox/sq potential to a more positive value. The analogous residue in the *H. pylori* flavodoxin is also a glycine, however its redox potentials are not known. The long-chain flavodoxin from *E. coli* may provide further support for the proposed correlation between E_2 and the nature of the residue at position 58: the ox/sq potential for this flavodoxin is among the lowest of all those known, where the protein has a bulky tyrosine residue here [34].

Additional charges close to the N1 of FMN further destabilize the hq form. Up to 11 acidic amino acids were found within 15 Å of N1 of FMN in the *A. vinelandii* flavodoxin, namely the aspartates 68, 98, 108, 152 and 154, and the glutamates 59, 61, 104, 134, 136 and 139. Several of these residues are situated in the 100's loop, including the closest charged group at a distance of 3.0 Å, the carboxylic moiety of Asp98. Conversely, only three basic residues are present, and then only at the very periphery of the 15 Å radius from the FMN N1, with the positively charged side chains solvent exposed at the surface of the protein instead of pointing towards the FMN-binding pocket. This acidic character of the binding pocket around the N1 is known to be a major determinant of the sq/hq potential E_1. The FMN hydroquinone in flavodoxins from both *M. elsdenii* [35] and *D. vulgaris* [222] have been found to exist as anions, while evidence for steric hindrance preventing protonation at N1 was

found for the *C. beijerinckii* flavodoxin [36]. The negative charges of the side chains destabilise the anionic hydroquinone, creating an unfavourable electrostatic environment that makes the reduction of the semiquinone more difficult. A patch of uncompensated negatively charged residues is commonly found grouped around the N1 of FMN in flavodoxins, and totals 6-7 residues in both the *D. vulgaris* [38] and *A. nidulans* [29] flavodoxins. Zhou and Swenson systematically mutated all six acidic residues in the *D. vulgaris* flavodoxin, with the effect that E_1 was raised by about 15 mV on average per neutralised amino acid [37]. If by analogy the hq of the *A. vinelandii* flavodoxin is also negatively charged [32], by this gauge, the five additional negative charges observed in this protein could potentially result in a negative shift in E_1 in the order of 75 mV.

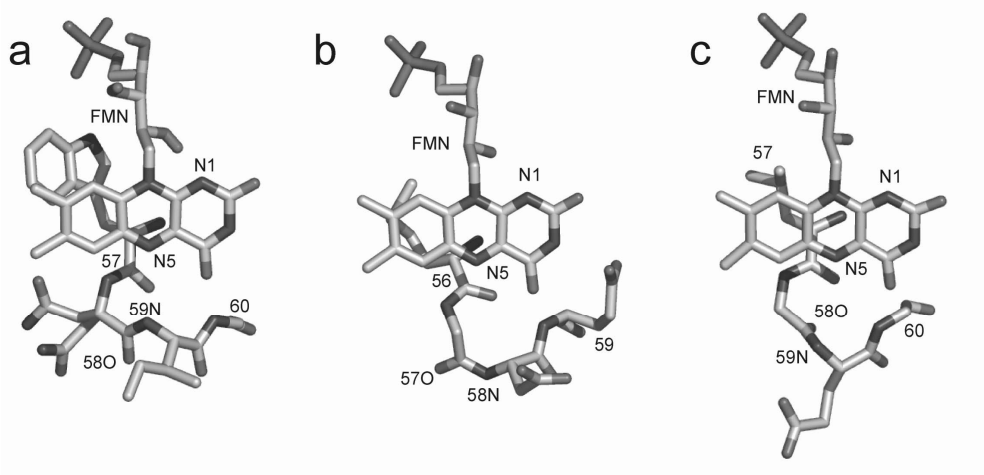

Fig. 3.6. Conformation of the four-residue turn in the 50's loop that contacts the FMN, in the same orientation from (a) *Anabaena* (b) *C. beijerinckii* and (c) *A. vinelandii*. The residue numbers are shown next to the backbone amides of the corresponding amino acids, where the backbone amide of residue 59 in (a) can clearly be seen to point towards the N5 of FMN, while in (b) and (c) the corresponding amide groups of residues 58 and 59 respectively have geometries which are unsuitable for hydrogen bonding to the N5.

Leu at the re *face of FMN results in a more polar FMN binding site, and stabilizes the hq form.* While in most flavodoxins the FMN is stacked against a tyrosine on its *si* or outer face, more variability has been found in the amino acid present on its *re* or inner face. This is

most commonly a tryptophan, however non-aromatic residues have also been found. In *A. vinelandii* flavodoxin a leucine residue is present. As a result, an open cavity is created at the re face of the co-factor, making it much more accessible to solvent. In fact, in both molecules of the asymmetric unit, two water molecules with low B-factors occupy this cavity in identical positions. They connect the innermost ring of the FMN to the surface of the flavodoxin (Fig. 3.4b). The FMN in the *A. vinelandii* flavodoxin is the most solvent exposed one in the long-chain flavodoxins of known structure, where values as calculated by NACCESS [213] for the surface accessibility for FMN in the five long-chain flavodoxins of known structure and potentials are: *A. vinelandii* (averaged for molecule A and B), 114.8 Å; *Anabaena*, 93.9 Å; *A. nidulans*, 100.1 Å; *C. crispus*, 98.7 Å; and *E. coli*, 99.7 Å.

The presence of smaller and/or polar residues stabilises the anionic FMN hq in the protein, thus shifting the sq/hq potential to more positive levels. This was corroborated by the mutation of the analogous Trp60 in the *D. vulgaris* flavodoxin to alanine which raised E_1 by 83 mV [223], while the Trp57Leu *Anabaena* flavodoxin mutant had an E_1 that was higher by 30 mV [40]. A methionine flanks the *re* face of the *C. beijerinckii* flavodoxin FMN, and a similar FMN-to-surface water channel is present. This flavodoxin has one of the highest E_1 potentials known [36]. Intriguingly however, despite the small leucine residue and the presence of two water molecules within close proximity of the FMN, at −458 mV the *A. vinelandii* flavodoxin appears to have one of the lowest E_1 values of all flavodoxins [26] (Fig. 3.1). It is possible that the additional negative charges clustered around the N1 compensate for the increased polarity of the FMN-binding site in this protein.

Comparisons between the two Azotobacter *flavodoxins*

The *A. chroococcum* flavodoxin has a sq/hq potential which, at −522 mV, is even more negative than that of the *A. vinelandii* flavodoxin. Aligning the two protein sequences shows that the *A. chroococcum* flavodoxin also contains the additional negatively charged residues, as well as a phenylalanine instead of a tyrosine at position 106 (Fig. 3.3). In the *A. vinelandii* structure, this residue was found within 5 Å of the most buried ring of the FMN, in an almost coplanar conformation. No other differences could be mapped to locations

close to the FMN that could account for the extremely low E_1 of the *A. chroococcum* flavodoxin, which reinforces the overriding influence of the acidic nature of the FMN-binding site.

We report here the first crystal structure of flavodoxin II from *A. vinelandii*, of the monomeric C69A mutant. In general the structure closely resembles that of other long-chain flavodoxins, with the exception of an 8-residue insertion between β_3 and α_3, which is found as a short 3_{10} helix followed by a turn at the surface of the protein. The C69A mutation is solvent exposed, as was previously proposed due to the propensity of the wt protein to form disulphide-bridged dimers.

On the whole the interactions between the FMN cofactor and the apoflavodoxin are similar to those previously identified in other long- and short-chain flavodoxins, although variations in the amino acid sequence have resulted in several novel hydrogen bonds. More noteworthy however is the absence of a hydrogen bond to the N5 atom of the isoalloxazine ring, observed in all structures of oxidised long-chain flavodoxins determined to date. This is expected to destabilise the oxidised FMN, and may in part explain the relatively high ox/sq E_2 potential of this flavodoxin. In addition, a glycine is present in the two-residue peptide which flips upon reduction of the protein, instead of the asparagine typical of long-chain flavodoxins. In both these characteristics the *A. vinelandii* flavodoxin resembles the short-chain flavodoxins from *C. beijerinckii* and *D. vulgaris* more closely, where this is mirrored in their comparable E_2 values.

A cavity is found on the *re* face of the FMN, due to a leucine residue flanking the cofactor instead of the more common tryptophan. A short channel consisting of two water molecules leads from this cavity to the surface of the protein. As a result, the FMN in this flavodoxin is much more solvent exposed, an effect which is known to stabilise the anionic hq form and raise the sq/hq E_1 potential. On the other hand, destabilization of the hq form is promoted by an exceptionally large cluster of 11 uncompensated negatively charged residues around the anionic FMN N1 atom, almost twice the number found in both short- and long-chain flavodoxins. The more polar FMN binding site counteracts the

destabilisation of the hq, and the net effect leads to the E_1 value of −458 mV observed. However, differential stabilization of the sq form by the formation of a hydrogen bond to the N5 effectively raises E_2 to a value closer to that of short-chain flavodoxins.

In summary, this structure of the oxidised flavodoxin II of *A. vinelandii* is an important starting point for a deeper understanding of the factors that modulate the redox potential of flavodoxins in general, and this protein in particular. Comparing this structure with other long and short chain flavodoxins has allowed us to identify particular features (a more polar FMN binding site due to the Leu-Trp replacement, a large cluster of acidic residues close to the N1) and residues (Gly58 that does not hydrogen bond to N5 in the oxidised state) that may be key to fine-tuning the E_1 and E_2 potentials. Further mutational, biochemical and structural studies involving these residues will be required to correlate the observed structural and functional differences. Modulations by the interactions of these residues with the FMN result in what may more usefully be considered as a continuous range of E_1 and E_2 values for the different flavodoxins, as opposed to stricter definitions of class and redox potential based on chain length. Finally, while NMR techniques can identify residues important for complex formation between flavodoxin and its redox partners, mapping these onto the three-dimensional structure of the protein may give new insights not only into the nature of the complex but also into the particular pathways that may be involved in the electron transfer reaction.

Chapter 4

Probing the reactivity of different forms of azurin by flavin photoreduction

Sharmini Alagaratnam, Pieter van Vliet, Nico J. Meeuwenoord, José A. Navarro, Manuel Hervás, Miguel Angel De la Rosa, Marcellus Ubbink and Gerard W. Canters

---

Abstract

A mutant of the copper protein azurin which has had a cavity introduced in its co-ordination sphere can exist in different forms depending on the ligands reconstituting the copper site. The imidazole-bound and the more solvent exposed water-bound forms of copper azurin were tested and compared to wild type for reactivity to reduction by two different flavin compounds in laser flash photolysis experiments. Differences were observed both for reduction by the flavins with different reduction potentials, as well as between the three different forms of azurin. Interestingly, the solvent-exposed copper site of the azurin mutant was less reactive than the buried imidazole-bound and wt copper sites; factors contributing to these differences are discussed.

Introduction

There is growing interest in the effect of modifications of proteins on their reactivity, especially when the modification affects the active site of proteins. The interest arises not only from a fundamental point of view, but also because of possible applications in industrial processes and nano-biotechnology. A particularly relevant type of modification changes the active site either by replacing the prosthetic group or by creating a gap or channel that connects to the active site. By modifying the prosthetic group, for instance by adding substituents and reinserting it, or by filling the gap with a group that slightly differs from the original, the mechanistic or enzymatic properties of the protein may be manipulated. It is therefore of interest to explore to what extent this strategy can be applied more generally.

Examples include the incorporation of new or alternative metals into an active site [122,162,165], as well as the replacement of prosthetic haem [113,150,224,225] and flavin [36,50,114] groups by their modified equivalents. When the group is non-covalently attached in the native enzyme, the question of the extent to which non-covalent substitution may result in viable proteins becomes relevant, as well as how the mechanistic properties are affected. A particularly interesting case is provided by Cu- and Fe-containing active sites in which the metal is held in place by side chains of amino acids. By replacing one of the ligand residues, for instance by a glycine or an alanine, a gap is created that may be filled by an external ligand, as was done for a haem ligand in cytochrome *c* [179]. When the ligand is attached to a linker, in principle easy and direct access is obtained to the mechanistic or catalytic heart of the protein or enzyme. This approach has successfully been employed to create a photoexcitable myoglobin that has a ruthenium group covalently attached to the protein's haem cofactor [149].

The His117Gly (H117G) mutant of the redox protein azurin from *P. aeruginosa* shows remarkable adaptability in its copper co-ordinating site. In the wild type (wt) protein, the copper ion is held in place by three strongly co-ordinating co-planar ligands, cysteine (Cys) 112 and histidines (His) 46 and 117, as well as a weaker distal ligand, methionine (Met) 121. A low-lying π-π^* transition gives rise to the bright blue colour of

azurin (ε_{628} = 5 mM^{-1} cm^{-1}) when oxidised, typical of the so-called type-1 copper sites [226], while in the reduced form the protein is colourless. Exchanging the more surface-exposed histidine 117 ligand for a non-co-ordinating glycine by site-directed mutagenesis creates a cavity on the surface of the protein, making the copper site accessible to external ligands [75]. In the absence of any additional ligands, two water molecules were shown to be in close proximity to the copper ion of copper-reconstituted H117G (Cu-H117G) azurin [227]. The two other strong ligands, His46 and Cys112, were also detected by X-ray absorption fine structure (EXAFS) experiments [73], together resulting in a geometry more typical of a type-2 copper site [228], albeit a fairly exposed one. By contrast, binding of imidazole to Cu-H117G azurin was found to restore the spectroscopic features of the copper site back to those of the wt species [75]. Further EXAFS experiments on this Im-Cu-H117G species showed that the copper ion has three main ligands that are indistinguishable in character from those in wt azurin [74]. As such, imidazole must occupy a position similar to histidine 117 in wt azurin, very closely reconstituting the original environment of the copper site.

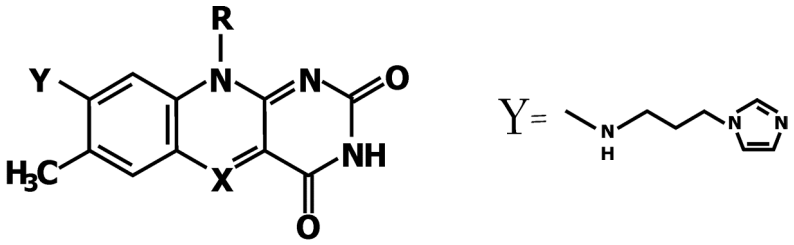

Fig. 4.1. General structure of flavins where R = ribityl chain. In (a) 5-deazariboflavin X = C, Y = CH_3 and in (b) IPAR X = N and Y is shown below.

In this paper we have used flavin-mediated laser flash photolysis to probe the reactivity of these different azurin species, and compared them to wt azurin. Excitation of a flavin-containing sample at 337 nm in the presence of a sacrificial electron donor such as EDTA forms the semiquinone radical $FlH^{\cdot}$, a strong reductant [132]. Two different flavins were used in this study as illustrated in Fig. 4.1. The midpoint potential of the quinone/semiquinone couple of 5-deazariboflavin, or 5-dRf, is –650mV [130], and as such

the semiquinone can act as a very powerful electron donor. In addition, a new substituted flavin has been synthesized with an imidazole group attached via a propyl linker to the 8α position of the flavin ring. This molecule, 8α-imidazolyl-N-propylyl-amino-riboflavin, or IPAR, can be used not only for insertion into H117G azurin but also for combining with other proteins, to be reported elsewhere. In the context of this work however, it provided us with an alternative flavin electron donor but also with one that is directly attached to the copper in the case of Cu-H117G, by the association of the imidazole moiety of IPAR to the Cu site. The reactivity of wt, Im-Cu H117G and Cu-H117G azurin towards reduction by 5-dRf and IPAR was compared, and reasons for the significant differences observed discussed.

Materials and Methods

General procedures

Optical absorption was measured with a PerkinElmer Lambda 800 UV-Vis spectrometer. ^{1}H NMR spectra were recorded on Bruker AC200 (200 MHz) or Bruker DMX-600 (600 MHz) spectrometers. Mass spectra were measured on a Finnegan MAT TSQ-70 spectrometer with an electrospray interface.

Materials

All reagents for synthesis were obtained from commercial sources and used as received. 5-dRf was a kind gift from Dr. Carlo van Mierlo at Wageningen University, the Netherlands. Wt and H117G azurin from *Pseudomonas aeruginosa* were expressed heterologously in *Escherichia coli* strain JM109, and purified according to previously described protocols [75,229]. H117G azurin was isolated in its apo form, and reconstituted just before use with copper and, when applicable, imidazole, by a 30 minute incubation on ice with 1.1 equivalents each of $Cu(NO_3)_2$ and imidazole. Extinction coefficients used were as follows [74]: apo-H117G azurin ε_{280} = 9.1 mM^{-1} cm^{-1}; Cu-H117G azurin ε_{420} = 2.35 mM^{-1} cm^{-1}, ε_{628} =

1.25 mM^{-1} cm^{-1}; Im-Cu-H117G azurin ε_{628} = 5.3 mM^{-1} cm^{-1}. All experiments with performed in 20 mM MES buffer pH 6.0.

IPAR Synthesis

The synthesis of 8α-imidazolyl-(N-propylyl)-amino riboflavin (IPAR) is schematically represented in Fig. 4.2, and is based on the synthesis of 8α-N-imidazolyl-riboflavin [230] but with significant modifications of steps (iii) and (iv).

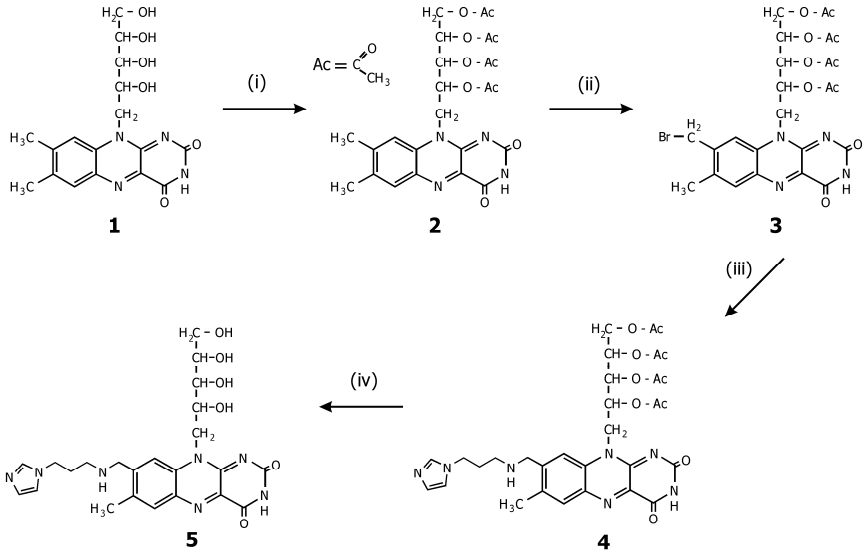

Fig. 4.2. Synthetic route for IPAR: (i) Flavin peracetylation, (ii) 8α-monobromination, (iii) Substitution of bromine with 1-(3-aminopropyl)-imidazole, (iv) Deacetylation of ribityl sidechain.

(i) Peracetylation of riboflavin

Riboflavin (5 g, 13.3 mmol) was dissolved in acetic acid (150 ml) and acetic anhydride (150 ml) followed by the addition of perchloric acid (4 ml, 70%). After the addition of water (1 l), the flavin was extracted with dicholoromethane (3 x 50 ml). The organic phase was dried over $MgSO_4$, filtered and reduced to a volume of 30 ml by rotary evaporation. The flavin was then precipitated by adding cold dry diethyl ether (3 x 200 ml) and dried

protected from light in a dessicator over P_2O_5. Yield 80% (10.5 g), M = 544. ^{1}H NMR (200 MHz, $CDCl_3$): δ (ppm) 1.67 (2'-$OCOCH_3$); 2.08 (5'-$OCOCH_3$); 2.22 (3'-$OCOCH_3$); 2.28 (4'-$OCOCH_3$); 2.44 (8α-CH_3); 2.57 (8α-CH_3); 4.21, 4.23, 4.27, 4.29, 4.40, 4.42, 4.47, 4.48 (5'-CH_2); 4.93, 5.12 (1'-CH_2); 5.44 (3'-CH_2, 4'-CH_2); 5.66 (2'-CH_2); 7.56 (9-CH); 8.03 (6-CH); 8.57 (3-NH).

(ii) 8α-monobromination of tetraacetyl riboflavin

Tetraacetyl riboflavin (7 g, 13 mmol) was dissolved in boiling dioxane (70 ml), and to which dibenzoperoxide (60 mg) was added. Bromine (2.9 g) diluted in dichloromethane (10 ml) was then added dropwise to the mixture, followed by 30 minutes refluxing. The mixture was concentrated to dryness *in vacuo*. The oily residue was redissolved in dichloromethane (70 ml), washed with 100 mM phosphate buffer pH 7.0 (2 x 50 ml) and once with Milli-Q water (50 ml). The organic layer was dried over $MgSO_4$, filtered and reduced to 30 ml by evaporation. The flavin was precipitated by addition to dry cold diethyl ether (2 x 200 ml) and dried protected from light in a dessicator over P_2O_5. Yield 80% (10.3 g), M = 623. ^{1}H NMR (200 MHz in $CDCl_3$): as tetraacetyl-riboflavin but with the following differences: δ (ppm) 2.44 (8α-CH_3) absent; 4.68 (8α-CH_2); 7.82 (9-CH); 8.09 (6-CH); 8.84 (3-NH).

(iii) Substitution of 8α- bromo-tetraacetyl-riboflavin with 1-(3-aminopropyl)-imidazole

8α-bromo-tetraacetyl-riboflavin (2 g, 3.0 mmol) was dissolved in dimethyl formamide (4 ml) and cooled on ice. Aminopropyl imidazole (0.4g, 3.2 mmol) diluted in dimethyl formamide (4 ml) was slowly added at 4°C to the flavin mixture over 45 minutes, followed by 1 further hour of incubation on ice while light protected. The flavin was precipitated with cold dry diethyl ether (100 ml), and dried protected from light *in vacuo*. The product was then purified by silica gel column chromatography (eluent: dicholoromethane/methanol 90/10 to 85/15, v/v). The appropriate fractions were pooled, concentrated, dried over $MgSO_4$, filtered and precipitated again with diethyl ether as above. Yield 10% (0.23g), M = 667. ^{1}H NMR (600 MHz): δ (ppm) 1.802, 2.081, 2.145, 2.281 (2', 3', 4', 5'-$OCOCH_3$); 2.120 (8δ-CH_2); 2.469 (7α-CH_3); 2.770, 2.781, 2.789, 2.800, 2.812,

2.822, 2.831, 2.842, 2.851 (8γ-CH_2); 3.908, 3.934, 3.990, 4.016 (8α-CH_2); 4.124, 4.135, 4.146 (8ε-CH_2); 4.237, 4.246, 4.258, 4.266, 4.426, 4.442, 4.463, 4.467 (5'-CH_2); 4.860 (1'-CH_2); 5.410 (3',4'-CH); 5.545, 5.618, 5.675 (2'-CH_2); 6.952 (5-CH imidazole); 7.070 (4-CH imidazole); 7.533 (2-CH imidazole); 7.808 (9-CH); 8.035 (6-CH). ^{1}H-NMR and ^{13}C-NMR spectra were recorded in D_2O using 2D-GS COSY, HMQC-GS ^{13}C H COSY, ^{13}C HMBC nodec (long-range CH COSY). The resulting assignment is as follows. ^{13}C NMR (600 MHz) δ (ppm): 18.4 (7α-CH_3); 20.3, 20.6, 20.8, 21.0 (2', 3', 4', 5'-$OCOCH_3$); 31.0 (8δ-CH_2); 44.7 (8ε-CH_2); 46.5 (8γ-CH_2); 51.4 (8α-CH_2); 61.8 (5'-CH_2); 68.7 (3'-CH_2); 70.6 (4'-CH_2), (1', 2'-CH_2 are not detected); 113.0 (9-CH); 118.7 (5-CH imidazole); 130.9 (4-CH imidazole); 133.1 (6-CH); 138 (2-CH imidazole); 134.5, 135.7, 136.0, 155.0, 170.2, 170.7 (carbons and carbonyls from the riboflavin ring).

(iv) Deacetylation of the ribityl side chain

The product (30 mg) was dissolved in 0.9 ml dry methanol. 60 mM potassium butanolate (0.3 ml) was added dropwise to the flavin in the dark. After stirring for 2½ hours, the reaction was stopped by adjusting the pH to 6.0 by the addition of 15% acetic acid. Milli-Q water was added to give a final volume of 15 ml. This mixture was purified by preparative reverse phase HPLC using a Biocad control system with an Alltima RP18-5μ 10×250mm column (eluent: 1% trifluoroacetate, 5 - 10% acetonitrile). Yield 30% (10mg), M = 499.

Extinction coefficient of IPAR

The extinction coefficient of IPAR at 445 nm, ε_{445}, was determined using a ^{1}H NMR spectrum of a stock of IPAR in D_2O containing 100 μM trimethylsilylpropionate (TSP). Peaks corresponding to known protons in IPAR were integrated and calibrated against the integrated area of the TSP peak to obtain the IPAR concentration. Visible absorption spectra of several dilutions of the IPAR sample were measured, and the ε_{445} derived by correlating the absorption at 445 nm with the concentration of IPAR.

Affinity of IPAR for Cu-H117G Azurin

A concentrated stock of H117G azurin was first reconstituted by incubation with 0.8 equivalents of $Cu(NO_3)_2$ at 4°C for 1 h. This protein stock was diluted by addition to an anaerobic cuvette containing 2 ml deoxygenated 20 mM MES pH6.0, to a final concentration of approximately 50 μM. Aliquots from a 10 mM stock of IPAR were then added to the protein and allowed to equilibrate before recording optical spectra in the range 520 to 800 nm, where the recovery of the blue colour of the imidazole-reconstituted Type-I site is observed. As only IPAR with a deprotonated imidazolyl moiety can bind Cu-H117G azurin, the binding reaction Cu-H117G + IPAR ⇆ IPAR-Cu-H117G with the dissociation constant K_d is in competition with the protonation/deprotonation equilibrium IPAR + H^+ ⇆ IPAR-H^+ with the dissociation constant K_a, analogous to binding of imidazole to Cu-H117G azurin [74]. Similarly, the increase in absorption at 628 nm upon addition of IPAR is dependent on K_d^{app}, the apparent dissociation constant, and is given by the following two equations:

$$[\text{IPAR-Cu-H117G}]^2 - \{([\text{Cu-H117G}]_t + [\text{IPAR}]_t + K_d^{app}) \cdot [\text{IPAR-Cu-H117G}]\} + \{[\text{CuH117G}]_t \cdot [\text{IPAR}]_t\} = 0 \quad (4.1)$$

$$A_{628} = \varepsilon_{628}^{nl} [\text{Cu-H117G}] + \varepsilon_{628}^{IPAR} [\text{IPAR-Cu-H117G}] \quad (4.2)$$

$[\text{Cu-H117G}]_t$ and $[\text{IPAR}]_t$ represent the total concentrations of IPAR and Cu-H117G azurin in the solution respectively, [Cu-H117G] and [IPAR-Cu-H117G] the concentrations of Cu-H117G and IPAR-bound Cu-H117G azurin, A_{628} the absorption of the sample at 628 nm, ε_{628}^{nl} and ε_{628}^{IPAR} the extinction coefficients at 628 nm for the Cu-H117G and IPAR-Cu-H117G species respectively.

The value K_d^{app} obtained by fitting the data to equations (1) and (2) can then be corrected by the pK_a of the IPAR imidazolyl group (7.0 at 25°C, Chapter 5) to obtain the true dissociation constant, K_d [74] using:

$$K_d^{app} = K_d \cdot (1+\alpha) \qquad (4.3)$$

$$\log \alpha = pK_a - pH \qquad (4.4)$$

Redox potentiometry of IPAR

Spectropotentiometric titrations were performed at 25°C in a 10 ml anaerobic cuvette [231]. A solution of 20mM of MES at pH 6.0 was first bubbled with argon for 1 h, before adding IPAR with a Hamilton syringe via the rubber septum to give a final concentration of approximately 30μM. The solution was flushed on its surface with argon throughout the titration, and stirred continuously. Sodium dithionite was used as reductant, and potassium ferricyanide as oxidant. Enough oxidant or reductant was added to the solution so as to change the potential by between 20 and 40 mV each time, and the solution was allowed to stabilise for 2 min before recording of the optical absorbance spectrum. Solution potentials were measured by using a gold electrode connected to a Schott CG 825 potentiometer, with a saturated calomel electrode as the reference electrode. All potentials reported here are with reference to the NHE electrode. E_1 and E_2 could be determined by fitting the absorbance changes to the Nernst equations for the two redox couples sq/hq and ox/sq simultaneously, as follows:

For the two redox couples: $ox + e^- \leftrightarrows sq$ and $sq + e^- \leftrightarrows hq$

with $K_1 = [sq]/[ox]$

$K_2 = [hq]/[sq]$

and $[ox] + [sq] + [hq] = [\text{total IPAR}]$

the solution potential E is dependent on the redox potentials for the two couples:

$$E = E_2 + RT/F \ln(1/K_1) \qquad (4.5)$$

$$= E_1 + RT/F \ln(1/K_2) \qquad (4.6)$$

The absorption at 445 nm, A_{445}, changes with solution potential *E* according to:

$$A_{445}(E) = [ox](E)\cdot\varepsilon_{445}^{ox} + [sq](E)\cdot\varepsilon_{445}^{sq} + [hq](E)\cdot\varepsilon_{445}^{hq} \quad (4.7)$$

where ε_{445}ox, sq and hq represent the extinction coefficients of the ox, sq and hq forms of IPAR at 445 nm respectively. Both ε_{445}^{ox} (determined as described) and ε_{445}^{hq} (which could be estimated from the end point of the titration) were fixed, leaving only ε_{445}^{sq} to be varied in the fitting procedure.

Laser flash photolysis

Details of the laser flash photolysis apparatus, data collection and analysis were as previously described [57,232]. The system was based around a relatively low energy nitrogen laser that excited the sample at 337 nm. 1 ml of the sample buffer containing 100 μM of either 5-dRf or IPAR in 20mM MES pH 6 was sealed into 3 ml cuvettes with a tapered neck using rubber septa, and made anaerobic by vigorous bubbling with argon for 2 h. Aliquots of concentrated solutions of azurin were then added by means of a gas tight Hamilton syringe, and the sample was further degassed by flushing argon at its surface. All experiments were performed under pseudo-first order conditions, where the concentration of protein acceptor (>10 μM) exceeded that of 5-dRfH$^{\cdot}$ produced per flash (<1 μM) [131].

Results

IPAR synthesis and characterisation

Synthesis. The synthetic route for IPAR is shown in Fig. 4.2. The four hydroxyl groups on the ribityl side chain of riboflavin (**1**) were first protected by acetylation giving tetra-acetyl riboflavin (**2**). The 8α position of this molecule was then functionalized by bromination to give **3**, 8α-bromo-tetra-acetyl-riboflavin. The compound was then substituted with 1-(3-aminopropyl)-imidazole before deacetylation to give the final product 8α-imidazolyl-N-

propylyl-amino-riboflavin, IPAR (**4**). ^{1}H NMR and mass spectrometry confirmed the identity of the molecule.

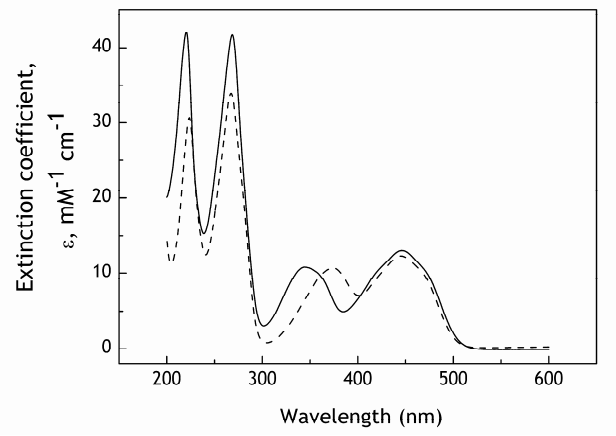

Fig. 4.3. Normalized UV-visible spectra of oxidised solutions of IPAR (solid line) and riboflavin (dashed line), in water at 25°C.

ε_{445} of IPAR. The electronic absorption spectrum of IPAR was found to be very similar to that of its precursor riboflavin (Fig. 4.3) with one significant difference, namely a blue shift of approximately 20 nm of the near ultraviolet flavin absorption band to 350 nm. The extinction coefficient of IPAR at 445 nm was also determined, as described in the Materials and Methods section. The value for ε_{445} for IPAR was thus determined to be 13.0 ± 0.3 mM^{-1} cm^{-1}.

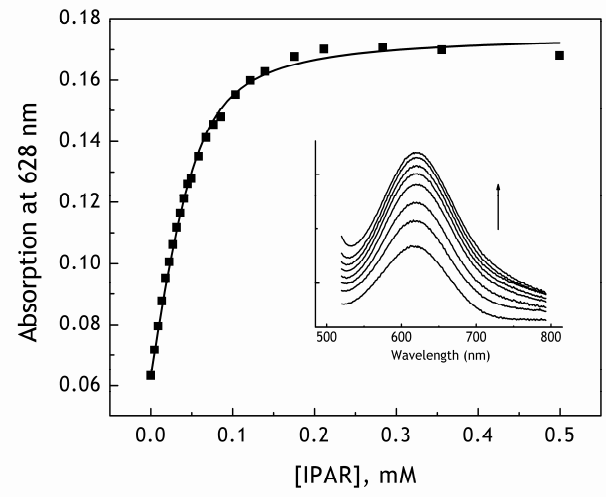

Fig. 4.4. The absorption at 628 nm (black squares) of a 45 μM solution of Cu-H117G azurin (in 20 mM MES, pH 6.0, 25°C) with increasing IPAR concentration, was fitted (solid line) as described, yielding a $K_{d\ app}$ of 12 ± 1 μM. Inset: Visible spectra of Cu-H117G azurin with increasing concentrations of IPAR (0, 18, 37, 59, 95, 124 and 220 μM). The arrow indicates the direction of the changes observed with increasing concentrations of IPAR.

K_d of IPAR-Cu-H117G. Fig. 4.4 shows the increase in absorption at 628 nm upon addition of IPAR to Cu-H117G azurin, from which the apparent dissociation constant, K_d^{app}, for IPAR binding to Cu-H11G azurin could be determined using the fitting procedure described in [74]. The K_d^{app} thus obtained was 12 ± 1 μM, and correcting for imidazolyl protonation (pK_a = 7.0, see Chapter 5) gave K_d = 1.1 ± 0.1 μM.

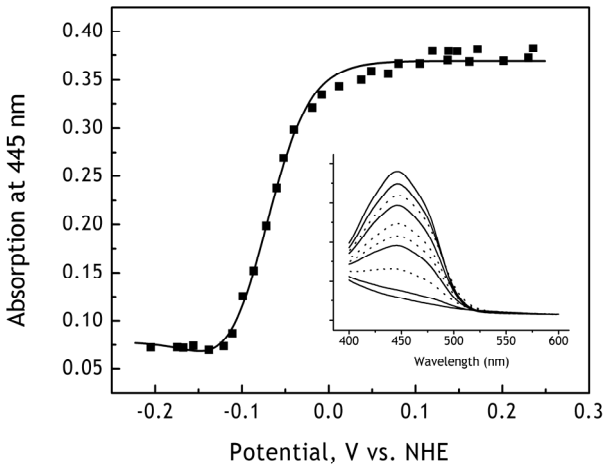

Fig. 4.5. Potentiometric titration of 30 μM of IPAR in 20mM MES, pH 6.0, 25°C, fitting the absorbance changes upon oxidation and reduction at 445 nm as described in Materials and Methods. Inset: Absorbance spectra showing the changes in going from the quinone to the hydroquinone and back to the quinone form of IPAR, solid lines are curves from the reductive titration, and dotted lines from the oxidative titration.

E_m of IPAR. Addition of aliquots of dithionite to the IPAR solution led to the gradual loss of absorption at 445 nm, with no other absorption changes between 400 and 800 nm. Reoxidation of the solution by addition of ferricyanide resulted in recovery of the 445 nm peak. These changes, shown in Fig. 4.5, indicate that IPAR undergoes two-electron reduction to its hydroquinone form, as has previously been observed for other flavins free in solution [230,233]. Fitting of changes in absorbance at 445 nm (Fig. 4.5) as described in Materials and Methods showed that the fit was rather insensitive to ε_{445}^{sq}, leading to a large uncertainty in this value. As a result, only approximate values for the redox potentials could be determined, with E_m = −71 ± 7 mV, and E_1 and E_2 within 40 mV on either side of this value.

Laser flash photolysis

Laser flash photolysis of a mixture of 5-dRf and Im-Cu-H117G azurin in 20mM MES buffer at pH 6.0 gave rise to kinetic transients shown in Fig. 4.6. At 520 nm, where the 5-dRf semiquinone radical absorbs maximally, an initial rise in absorbance is followed by a decay. This decay is concurrent with the decay in absorbance observed at 630 nm, where the reduction of copper in azurin is followed.

This behaviour was observed for both the flavins used in this study, 5-dRf and IPAR, as well as for the three different azurin species tested, namely wt azurin, Im-Cu-H117G, and Cu-H117G. The rate of flavin semiquinone decay, concurrent with copper reduction, increased linearly with the concentration of all species of oxidised copper azurin tested. Plotting the observed rates against oxidised protein concentration (Fig. 4.7) allowed the determination of the second-order rate constant, k_2, for the three copper azurin species described. k_2s for the reduction of these azurin species by 5-dRf and IPAR semiquinone radical are summarised in Table 4.1.

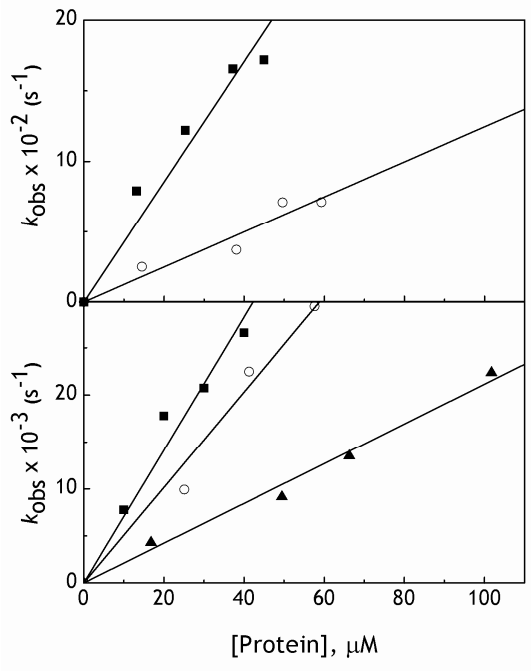

Fig. 4.7. Dependence of observed rates (k_{obs}) for reduction of different azurin species by 5-dRf (lower plot) and IPAR (upper plot) semiquinone radicals on concentration of wt (open circles), Im-Cu H117G azurin (solid squares) and Cu-H117G (solid triangles) azurin.

In trying to determine k_{et}^{intra}, or the electron transfer rate along the IPAR linker to Cu-H117G azurin, increasing and equimolar amounts of IPAR and Cu-H117G were subjected to laser flash photolysis characterization, maintaining 20 mM MES pH 6.0 as the working buffer and

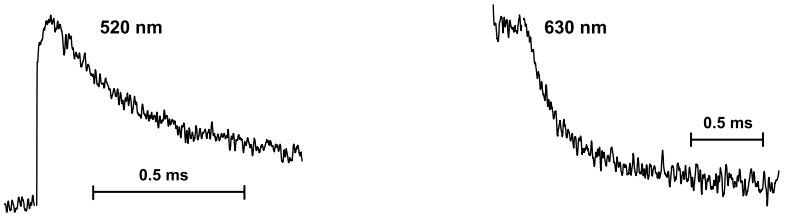

Fig. 4.6. Transient absorbance changes showing the rapid formation and futher slower decay of 5-dRf semiquinone radical measured at 520 nm (upper trace), and reduction of Cu(II) azurin measured at 630nm (lower trace). The concentration of Im-Cu-H117G azurin was 25 μM, in 20 mM MES pH 6 and 100 μM 5-dRf at room temperature.

with IPAR as the sole electron donor. Again, rates of azurin reduction varied linearly with protein concentration (Fig. 4.8a). As a consequence of the dissociation equilibrium between IPAR and Cu-H117G azurin, the concentrations of IPAR-bound and free Cu-H117G azurin varied over the range of concentrations used (summarized in Fig. 4.8b). Despite the ratio between the azurin species shifting from an excess of Cu-H117G to an excess IPAR-Cu-H117G, the change in k_{obs} remained linear, such that second-order rate constants for electron transfer from excited IPAR to both azurin species had to be very similar, and could be estimated at $1.8 \pm 0.3 \times 10^7$ M^{-1} s^{-1}.

Discussion

Optical spectra. The new flavin derivative IPAR was found to have characteristics comparable to other similarly substituted riboflavins. The shift of the near ultraviolet absorption band of IPAR due to the presence of the 1-(3-aminopropyl)-imidazole group, is similar in character and magnitude to shifts that have been observed upon substitution at the 8α-position of riboflavin and FMN with histidine [234] as well as imidazole groups [117,235]. The ε_{445} for IPAR is a little higher than for the parent compound, but not significantly different from other flavins, both substituted and non [235].

Following the increase of the blue absorption band at 628 nm with addition of IPAR to Cu-H117G azurin was a suitable method for estimation of the K_d for IPAR binding

Cu-H117G azurin, 12 μM at pH 6.0. An expected concurrent decrease in the absorption of the band at 420 nm could not be observed as the intense IPAR absorption peaks obscure the azurin spectrum in this region. Crucially, restoration of Cu-H117G to the spectroscopic features of the wt protein points strongly to the structural restoration of the mutated site by the addition of the IPAR ligand. The dissociation constant of 1.1 ± 0.1 μM for the binding of IPAR to Cu-H117G is slightly lower than that for the binding of imidazole, 2.4 μM at the same pH [74]. This indicates that neither the linker not the flavin parts of IPAR

a

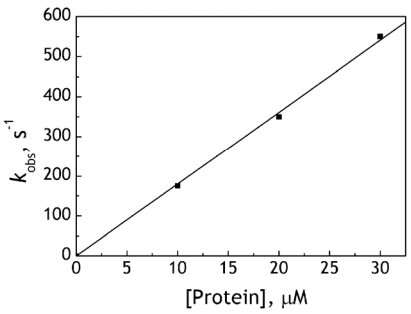

Fig. 4.8. a) Change of k_{obs} at 630 nm with increasing IPAR and Cu-H117G azurin concentration. b) Distribution of species as calculated using K_d = 12 μM for the dissociation of the IPAR-Cu-H117G azurin complex equilibrium.

b

$[IPAR]_o$, μM & $[Cu\text{-}Azu]_o$, μM	[IPAR-Cu-Azu], μM	[Cu-Azu], μM	[Free IPAR], μM
10	3.3	6.5	6.5
20	9.4	10.6	10.6
30	16.1	13.9	13.9

adversely affect the binding of the imidazole moiety to the mutated copper site, in fact the burying of a part of the alkyl IPAR linker within the protein may lead to an overall positive entropic effect.

Redox characteristics of IPAR. Redox titration curves for flavins have long been known to deviate from that predicted by the Nernst equation for the transfer of two electrons, due to the presence of the semiquinone intermediate [236]. A modified equation taking this into account fits the redox potentiometric data much better. At −71 mV, the E_m obtained for

IPAR was 90 mV higher than that of riboflavin (–161 mV [233]), but closer to that of 8α-N-imidazole substituted riboflavin (–104.5 mV [230]), comparing all values at pH 6.0. In this series of experiments, the redox potential of interest is that of the flavins' ox/sq couple, as it is the sq which acts as the electron donor to azurin. Comparing these values, it is immediately obvious that the E_2 of IPAR is substantially higher than that of 5-dRf by more than 500 mV, as might be expected because it resembles its riboflavin precursor more than the deaza analogue.

Table 4.1. Second-order rate constants, k_2, obtained for the reduction of different azurin species with 5-dRf and IPAR as electron donors.

	k_2, x 10^7 M^{-1} s^{-1}	
Azurin species	dRf	IPAR
wt	51 ± 2	1.1 ± 0.1
Im-Cu-H117G	71 ± 4	4.3 ± 0.3
Cu-H117G	21 ± 1	1.8 ± 0.2
IPAR-Cu-H117G	–	1.8 ± 0.2

Laser flash photolysis of 5-dRf vs. IPAR. The transient absorbance changes observed in Fig. 4.6 are consistent with the rapid formation of flavin semiquinone radical. As such it is likely that the MES buffer plays an additional role as a sacrificial electron donor in this experiment, in a manner analogous to EDTA [22,131]. The second-order rate constants obtained also compare well with those obtained using riboflavin/EDTA to reduce plastocyanin (1.5 x 10^9 M^{-1} s^{-1} [135]), indicating that oxidation of MES by triplet flavin occurs efficiently.

IPAR also proved to be viable as an electron donor, albeit with second-order rate constants that were approximately an order of magnitude lower than with 5-dRf (Table 4.1). This may be as expected due to E_2 for 5-dRf at –650 mV being approximately 500 mV lower than that of IPAR at –71 mV, leading to a larger driving force in the reaction with 5-dRfH$^{\cdot}$. A semi-empirical equation (Equation 4.8) for the exponential decay of the electron tunnelling rate k_{et} for non-adiabatic electron transfer,

$$\log k_{et} = 15 - 0.6R - 3.1(\Delta G+\lambda)^2/\lambda \qquad (4.8)$$

where R is the edge-to-edge distance between the redox centres, λ the reorganisation energy, and ΔG the driving force for the reaction, predicts higher rates of electron transfer with larger ΔG, provided that $|\Delta G| < \lambda$. The difference of 0.5 eV between IPAR and 5-dRf could conceivably lead to the difference of an order of magnitude in the rate constants observed.

For both the electron donors, Im-Cu-H117G azurin was reduced with higher second-order rate constants than wt azurin. This is contrary to what has previously been observed for reduction of these two azurin species by the enzyme 4-ethylphenol methylenehydroxylase (4-EPMH), where Im-Cu-H117G was reduced at a rate of one order of magnitude lower than wt azurin [76]. The contrasting behaviour may reflect differences in the efficiency of productive complex formation between the large 4-EPMH enzyme and the much smaller 5-dRf molecule. Non-imidazole reconstituted Cu-H117G gave a lower k_2 than either wt or Im-Cu-H117G azurin, again for both 5-dRf and IPAR. A space-fill representation of a model of Cu-H117G is shown in Fig. 4.9, with wt azurin in a similar orientation for comparison. The copper atom is completely shielded from the solvent in the wt structure, in particular by its histidine 117 ligand. This is very different for Cu-H117G azurin, where the model shows the copper atom to be clearly exposed to the solvent, as the bulky imidazole side chain of histidine 117 has been replaced by the single hydrogen atom of the glycine side chain. Despite this, higher reduction rates were observed in all cases for the wt than for Cu-H117G azurin. Mechanistically, thus, it is interesting to see that when the active site is opened up by the replacement of His117 by a glycine in the absence of external ligands that mimic the histidine side chain, the electron transfer activity in fact drops markedly. When an imidazole group is in place however, the activity is restored to above the level of the wt enzyme. This counters the concept that redox centres need to be buried in proteins to prevent unwanted reactions from occurring, and is in contrast to what has been observed for cytochrome *c*-550 where opening up of the cavity leads to enhanced enzymatic activity instead [237].

The electronic interaction between the (flavin) electron donor and the (azurin) acceptor is crucial in determining k_{et}, where the histidine side chain, missing in Cu-H117G azurin, may play a vital role in ensuring good coupling between the partners. The fact that Im-Cu-H117G azurin is more readily reduced than wt azurin may point to additional flexibility and/or mobility in the free imidazole group as opposed to the amino acid side chain histidine that may improve the coupling. In the absence of any imidazole-like ligand, as for the Cu-H117G species, k_{et} is expected to be orders of magnitude lower were the cavity to be a vacuum. The co-ordination sphere of the copper site of this species has been found to differ markedly from wt azurin, with two water molecules co-ordinating the copper atom [227]. The waters clearly act as conductors for electron transfer bridging the approximately 7 Å gap between the copper and the surface of the protein, and lead to observed rates which are lower than but still within the same order of magnitude as both wt and Im-Cu-H117G azurin. It is likely that the changed ligand arrangement of the Cu-H117G species also affects the rearrangement energy for the reaction, which may explain its lower reduction rate when compared to wt and Im-Cu-H117G azurin.

The concentration dependence of the Cu-H117G and IPAR-Cu-H117G azurin reduction by IPAR in Fig. 4.8a is again indicative of inter- and not intra-molecular reactions. The second-order rate constants for reduction of the two species were similar in magnitude to k_2s for the reduction of other azurin species by IPAR (Table 4.1). The bimolecular reaction between IPAR and the various azurin species is however apparently the rate determining step that, given the short distance along the linker and the k_2s of the bimolecular reactions, suggests that k_{et}^{intra} for electron transfer along the linker to the Cu-H117G azurin is $\gg 3 \times 10^4\ s^{-1}$.

Conclusions

The combination of two different flavins with MES buffer as studied by laser flash photolysis allowed us to probe the reactivity of wt, and imidazole bound and water bound forms of the azurin mutant H117G. IPAR was between 10 and 100 times less efficient as an

electron donor to the various azurin species compared to 5-dRf. The imidazole-reconstituted form of H117G azurin behaved much like wt azurin in reduction by flavins, while the Cu-H117G azurin that has a more exposed copper site was surprisingly less reactive than the two other forms. In reality it is likely that the histidine side chain plays a vital role both in ensuring good electronic coupling to the copper site as well as influencing the reorganizational energy associated with the reduction of copper in azurin.

Acknowledgements

Dr. B. Aguilera and Dr. W. Tepper are gratefully acknowledged for their assistance with the synthesis and purification of IPAR and fitting of the redox potentiometric data respectively.

Chapter 5

Electron transfer behaviour of a non-covalent heterodimer of azurin and flavodoxin

Sharmini Alagaratnam, Pieter van Vliet, Marcellus Ubbink, José A. Navarro, Manuel Hervás, Miguel A. De la Rosa, and Gerard W. Canters

---

Abstract

A non-covalent heterodimer of azurin and flavodoxin was created by means of cofactor reconstitution at the active sites of each of the monomers using a bifunctional linker known as IPAR. The complex was found to be active for electron transfer as initiated by the flavin sensitizer 5-deazariboflavin. On a shorter timescale, direct reduction at both redox centres was observed, but on a longer timescale rather slower electron transfer was found to occur from the flavodoxin semiquinone to azurin. The latter reaction was however dominated by second order processes as a result of the particular distribution of monomeric species, due to the dissociation equilibria.

Introduction

While proteins have long been known to be the mediators in the electron transfer (ET) chains of metabolism of the cell, our understanding of the various and subtle ways in which this mediation is achieved is fragmented and often empirical. Through their three-dimensional structure, proteins determine factors crucial to the occurrence and rate of ET, as formalised in Marcus theory [78]. Whether ET occurs intermolecularly once a protein-protein complex has been formed, or intramolecularly between redox centres within a single protein, there remains much discussion about the influence of the intervening medium in coupling the redox centres electronically for efficient ET [84,238]. Various attempts have been made to unravel these influences, by the construction of a range of synthetic donor-acceptor systems [239,240], multi-site labelling of proteins with electron donors [153,174], as well as semisynthetic redox proteins [241]. In this article we have created a maquette of two different redox proteins, connecting their redox centres by a linker of defined length and identity. The aim is to study the electron transfer reaction between the two redox centres along the linker, which may in future be modified to test its effect.

The two proteins chosen as building blocks for the heterodimer, azurin from *P. aeruginosa* and flavodoxin II from *A. vinelandii*, are stable in solution, easy to overexpress and purify, and well characterised structurally and biochemically [1,18,242,243]. Their different redox states have been extensively studied, along with the corresponding spectroscopic features that can be used to follow electron transfer within the complex. Although the two proteins are not physiological partners, ET has been shown to occur from the flavodoxin semiquinone to oxidised azurin free in solution [70].

ET to and from the Type 1 copper site in azurin has been shown to occur via the hydrophobic patch at the 'north' end of the protein [244,245], and more specifically the ligand His 117 that shields the copper from the solvent [76]. Upon reduction, the intense blue colour of azurin bleaches, providing a local spectroscopic probe of its redox state. Mutation of this histidine to a glycine created a cavity in the protein and led to a mixed Type 1/2 copper site with the copper being more solvent exposed [72,75]. Addition of a

range of external imidazole-type ligands to copper-reconstituted H117G (Cu-H117G) azurin however restored the copper site back to its wild type state as determined by visible and EPR spectroscopy [75], and as demonstrated in Chapter 4 is active for electron transfer.

The FMN cofactor of flavodoxin can also be removed and replaced by riboflavin, or a range of other substituted flavins [1]. Flavodoxins reconstituted with external flavins have been shown to display the same redox and spectroscopic behaviour as native flavodoxins upon reduction [117]. As such, we conceived of a bifunctional linker with an imidazole moiety on one end and with a flavin group on the other, separated in the first instance by a simple alkyl chain. The imidazole group can bind and reconstitute the copper site, while the flavin group of the linker can reconstitute apoflavodoxin. The synthesis of such a molecule, 8α-imidazolyl-(N-propylyl)-amino riboflavin, or IPAR, has been described in the previous chapter. This chapter investigates its binding to both Cu-H117G azurin and apoflavodoxin.

This represents a very gentle, non-covalent method for directly linking the two redox centres of the two proteins into a ternary complex with the linker, avoiding any unnatural strain on the sensitive ET sites. The electron transfer properties of the system were tested in a laser flash photolysis set-up with 5-deazariboflavin (5-dRf), where the laser flash initiates ET by forming 5-dRf semiquinone (sq), an efficient electron donor [132]. The progression of electrons through the system under study was followed by transient absorption spectroscopy, and allowed the elucidation of the ET behaviour of the heterodimeric complex.

Materials and Methods

Materials

The riboflavin derivative 8α-imidazolyl-(N-propylyl)-amino riboflavin, or IPAR, was synthesised as previously described (Chapter 4). 5-dRf was a gift from Dr. Carlo van

Mierlo at Wageningen University, the Netherlands. All other compounds used were used as received and of the purest grade available. All experiments with performed in 20 mM MES buffer pH 6.0.

Spectrometry and pK_a determination

Optical absorption was measured with a Shimadzu UV-2101PC spectrophotometer. Flavin fluorescence was measured on a Perkin-Elmar Luminescence Spectrometer LS50B. NMR spectra were recorded on a Bruker-AC200 (200MHz) or Bruker-DMX-600 (600MHz) spectrometer and mass spectra on a Finnegan MAT TSQ-70 equipped with an electrospray interface. For determination of the pK_a values of IPAR, between 2 and 10 μM of the compound was dissolved in a buffer containing 25 mM each of Tris, phosphate and acetate. The buffer was first brought to pH 11 using 5 M NaOH, after which the pH was lowered in 0.5 pH unit increments, using 5 M acetic acid. For the ultraviolet-visible titration the position of the near ultraviolet (UV) flavin peak was followed. For the fluorescence titration the samples were excited at 445 nm and emission followed at 525 nm. All pH titration data were fitted to the Henderson–Hasselbach equation using the programme Origin 7.5 (OriginLab Corporation, Northampton, MA).

Protein expression and purification, cofactor removal and reconstitution

The monomeric C69A mutant of flavodoxin II was used in this study, as disulphide bridged homodimers have been observed for the cysteine containing wild type (wt) protein [217]. For all structural and functional purposes, the C69A mutant has been shown to behave identically to wt flavodoxin but exists as a monomer in solution [26]. C69A flavodoxin II from *Azotobacter vinelandii* was expressed from a pUC19 plasmid containing the mutated flavodoxin gene, again kindly provided by Dr. van Mierlo. The protein was expressed heterologously in *Escherichia coli* (*E. coli*) strain TG2, and induced with 1 mM IPTG upon inoculation of the large-scale culture. The protein was purified according to described protocols and was considered to be pure when the absorption peaks showed a ratio A_{274}/A_{452} of 4.7 [12]. The extinction coefficient at 452 nm of 11.3 mM^{-1} cm^{-1} [12] was used to determine the concentration of flavodoxin. Apoflavodoxin was prepared from the

holoprotein by the trichloroacetic acid precipitation method [18], with one modification, namely that the apoflavodoxin pellet was first redissolved in 0.3 M CHES buffer at pH 9.0 before dialysis into 20 mM MES pH 6.0 for storage and later use. Recombinant H117G azurin from *Pseudomonas aeruginosa* was expressed in *E. coli* strain JM109, and purified according to previously described protocols [75,229]. H117G azurin was isolated in its apo form, and reconstituted just before use with copper by a 30 minute incubation on ice with 1.1 equivalents of $Cu(NO_3)_2$. Extinction coefficients used were as follows [74]: apo-H117G azurin ε_{280} = 9.1 mM^{-1} cm^{-1}; Cu-H117G azurin ε_{280} = 9.8 mM^{-1} cm^{-1}, ε_{420} = 2.35 mM^{-1} cm^{-1}, ε_{628} = 1.25 mM^{-1} cm^{-1}.

Affinity of IPAR for apoflavodoxin

The quenching of flavins, close to complete upon binding to apoflavodoxin, provides a sensitive monitor for the association and dissociation of IPAR and apoflavodoxin [19,196]. The dissociation constant for this reaction, K_d, was obtained by titrating a 2 μM IPAR solution in 20 mM MES buffer pH 6.0 at 25 °C with increasing amounts of apoflavodoxin. The sample was excited at 445 nm and IPAR fluorescence was detected at its maximum emission wavelength of 530 nm. The data was fitted to Equation 5.1, where I is the observed fluorescence emission after each addition, I_n the remaining fluorescence that is unquenched at the end of the titration, F_t the total IPAR concentration, and P_t the total flavodoxin concentration, from [196]:

$$I = I_n + I_d\left[\left(F_t - P_t - K_d\right) + \sqrt{\left(F_t + P_t + K_d\right)^2 - 4F_tP_t}\right] \qquad (5.1)$$

Electrochemistry

Staircase cyclic voltammetry (SCV) of IPAR and IPAR-reconstituted flavodoxin was performed using an μAutolab potentiostat controlled by Eco Chemie GPES software version 4.3 (Eco Chemie, Utrecht, The Netherlands) according to a previously described method using a flame–treated glassy carbon electrode, and 3 mM neomycin as a promoter

[21]. 75 μM of apoflavodoxin was reconstituted with 25 μM IPAR before use in the electrochemical set-up. Redox potentiometric titrations were carried out under argon at 25°C in an anaerobic 10 ml cuvette containing the gold measuring electrode and a saturated calomel reference electrode. Solution potentials were measured using a Schott CG 825 potentiometer. Sodium dithionite was used as the reductant and potassium ferricyanide as the oxidant, and the solution was allowed to stabilise for 2 mins before recording of the optical absorbance spectra. The following compounds were added at 5 μM concentration as mediators: 1,4-benzoquinone, phenazine methosulphate, phenazine ethosulphate, tetramethyl-p-benzoquinone, 2,5-dihydroxy-p-benzoquinone and methyl viologen. The electrodes were calibrated by immersion in a saturated solution of quinhydrone in 50 mM phosphate buffer at pH 7.0, giving a redox potential vs. NHE of 286 mV. All potentials reported here are with respect to the NHE electrode. The changes in absorption were fitted to the standard Nernst equation as in [26].

Laser flash photolysis

The laser flash photolysis apparatus has been previously described [57,232]. Samples were prepared in 2 ml glass cuvettes with tapered necks, and 20 mM MES buffer containing 100 μM 5-dRf was first bubbled vigorously for 2 hours with argon. The components of the heterodimeric complex, apoflavodoxin, IPAR, copper and apo-H117G azurin, were added to the cuvettes in the ratio of 7 : 1 : 1 : 20, to promote ternary complex formation. Upon addition of the other protein and/or IPAR components of the complex with gas–tight Hamilton syringes, the samples were flushed at the surface under gentle stirring to eliminate all remaining traces of oxygen. The samples were excited at 337 nm, and redox processes were followed at 480 nm (for flavodoxin) and 670 nm (for azurin). Between 5 and 8 traces were averaged for each point, and the traces fitted to either single or double exponential decay functions to obtain the observed rate constant, k_{obs}.

Results

pK_a determination of IPAR

IPAR exhibited changes both in fluorescence yield as well as the position of its near UV absorption band in the pH range between 3 and 11. The fluorescence of oxidised IPAR was almost completely (>95%) quenched between pH 3 and 8 (Fig. 5.1a). Fitting this data to the Henderson-Hasselbach equation gave a pK_{a1} of 6.5 ± 0.2. The pH dependence of the visible absorption spectrum was more complex, reflecting two pK_a transitions. The near UV peak of the flavin shifted first by 21 nm from 345 to 366 nm between pH 3 and 7, before shifting back again to 351 nm at pH 11 (Fig. 5.1b). Fitting this data to a similar expression but for a doubly ionising system gave pK_{a1} = 7.0 ± 0.4 and pK_{a2} = 9.6 ± 0.3.

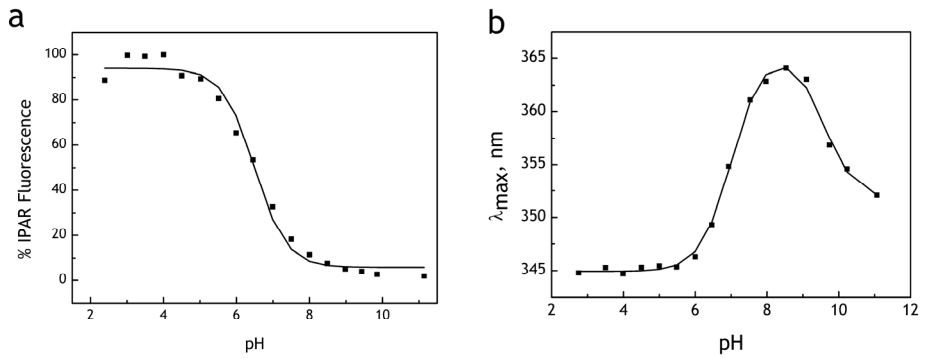

Fig. 5.1. Changes in (a) the fluorescence intensity of 1.8 μM IPAR and (b) the position of near UV peak in nm of 10 μM IPAR, both in 25 mM each of Tris, sodium acetate and sodium phosphate buffer. The pH was changed incrementally with 5 M acetic acid and 5 M sodium hydroxide. The fluorescence sample was excited at 445 nm and emission detected at 525 nm. The data was fitted to the Henderson-Hasselbach equation for a singly and a doubly ionising system for the fluorescence and visible absorption data respectively.

Binding of IPAR to apoflavodoxin

Addition of apoflavodoxin to a 2 μM solution of IPAR led to a decrease in the intensity of fluorescence of the flavin at 530 nm, as reported for other flavins and

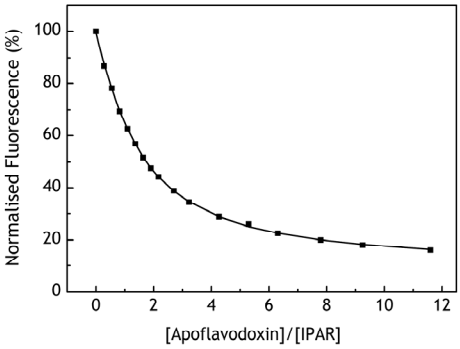

Fig. 5.2. Normalised changes in fluorescence with increasing adding amounts of apoflavodoxin to 2 μM IPAR in 20 mM MES pH 6.0, at 25 °C. The line represents the least squares fit obtained using Equation 5.1, and gave K_d = 2.04 ± 0.04 μM.

apoflavodoxins from various organisms [19,118,196]. Fitting the observed decrease with increasing concentrations of apoflavodoxin to Equation 5.1 allowed the determination of K_d for the dissociation of IPAR from apoflavodoxin (Fig. 5.2), which was found to be 2.04 ± 0.04 μM in 20 mM MES at pH 6.0.

Electrochemistry of IPAR-apoflavodoxin

SCV was performed on samples of both IPAR and apoflavodoxin reconstituted with IPAR. The data for IPAR alone show a single redox couple, with a midpoint potential of −80 mV, similar to the value that was determined by redox potentiometry in Chapter 4. For IPAR-reconstituted apoflavodoxin however, an additional couple was observed with a more negative midpoint potential, with an average of −197 mV (Fig. 5.3). This additional couple was assigned to the semiquinone/hydroquinone (sq/hq) redox couple, or E_1 of protein-bound IPAR. As will be discussed later, the E_2 ox/sq redox couple of flavodoxin is not usually observed by this method. Using the alternative method of redox potentiometric titrations however, two major changes were observed in the spectrum of the apoflavodoxin-IPAR

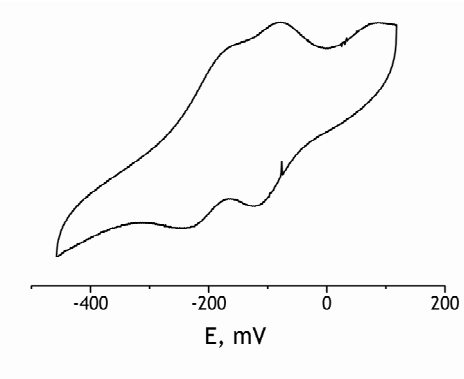

Fig. 5.3. Cyclic voltammogram of IPAR-reconstituted apoflavodoxin in 20 mM MES pH 6.0, with 3 mM neomycin. Scan rates of 4 mV/s were used.

complex. Absorption at 445 nm was found to decrease due to reduction of the ox form, and a broad absorption band peaking at 580 nm first appeared then subsequently disappeared. The behaviour of the latter peak is due to the formation of the sq followed by its further reduction to hq. The changes in absorption at both 445 nm and 580 nm were plotted against potential and iteratively fitted in combination with the value of E_1 from the cyclic voltammetry result to the Nernst equation for a one-electron redox couple (Fig. 5.4). This allowed the determination of E_2, the redox potential for the oxidised/semiquinone (ox/sq) redox couple for the IPAR-apoflavodoxin complex, at −20 mV.

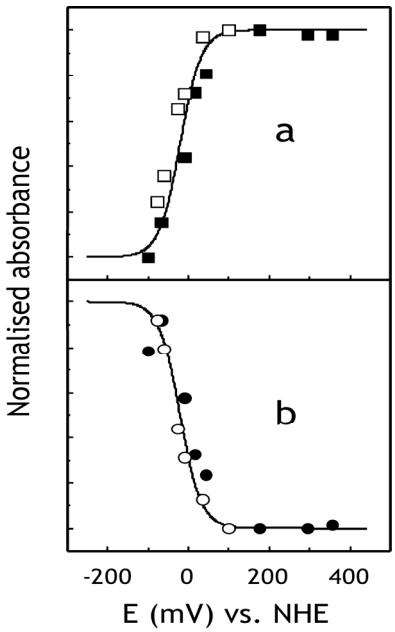

Fig. 5.4. Absorbance changes at (a) 445 nm and (b) 580 nm during the redox potentiometric titration of IPAR-reconstituted apo-flavodoxin in 20 mM MES, pH 6.0 plotted against potential vs. NHE. Open symbols denote values from the reductive titration, and closed symbols the oxidative. The lines represent the least squared fit of the data to the Nernst equation as detailed in Materials and Methods.

Binding of IPAR-apoflavodoxin to Cu-H117G

IPAR has previously been shown to bind Cu-H117G azurin with a 1.1 ± 0.1 μM (Chapter 4). Absorption spectroscopy was used to investigate the association of flavodoxin-bound IPAR to Cu-H117G azurin. Addition of 50 μM IPAR-reconstituted flavodoxin to 50 μM Cu-H117G azurin gave rise to an increase in absorption at 630 nm, a change that is qualitatively identical to that observed after the addition of IPAR alone. The expected corresponding decrease in the absorption at 420 nm [75] was however obscured by the intense absorption of IPAR in this region. The absorption deriving from IPAR was

accurately removed from the spectrum as follows. After addition of either IPAR or IPAR-reconstituted apoflavodoxin and recording of the absorption spectrum, the sample was illuminated with an agfatronic flash lamp. This resulted in the reduction and full bleaching of the copper centre by photochemically reduced flavin. As such, after the illumination only the IPAR absorption contributed to the spectrum. Subtracting the flavin spectrum recorded after the flash from the pre-flash spectrum resulted in a dark-minus-light spectrum (dashed and dotted spectra in Fig. 5.5). From these spectral changes a K_d of 180 μM was determined for the binding of IPAR-reconstituted flavodoxin to Cu-H117G azurin.

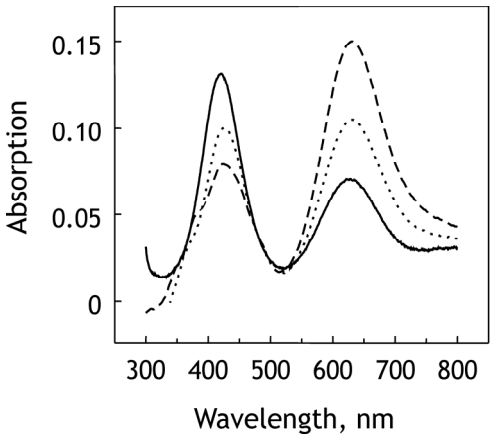

Fig. 5.5. Absorption spectra of 50 μM Cu-H117G azurin (solid line) and the IPAR-subtracted spectra after the addition of 50 μM IPAR (dashed line) and 50 μM IPAR-reconstituted flavodoxin (dotted line).

A summary of the different equilibria investigated and the corresponding dissociation constants is show in Fig. 5.6. No experimental method could be found to probe complex formation between IPAR-reconstituted H117G and apoflavodoxin directly, however from equilibrium thermodynamics a K_d of 360 μM was calculated for this equilibrium.

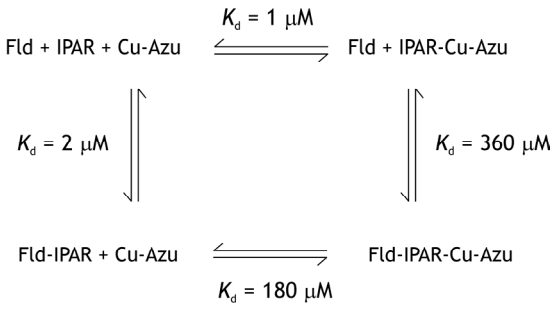

Fig. 5.6. Equilibria and the corresponding dissociation constants (K_d) of the complexes formed between flavodoxin (denoted Fld), IPAR and Cu-H117G azurin (Cu-Azu).

A computer model of the heterodimeric protein complex linked by IPAR was generated using the programme XPLOR 3.8 to get an indication of the degree of steric hindrance between the two proteins when brought in close contact with each other, as would be the case when linked by IPAR. This was done by first editing the Protein Data Bank (PDB) structure files of C69A flavodoxin, 1YOB [246], and azurin, 1AZU [247]. The FMN cofactor of flavodoxin was edited to create IPAR lacking the imidazole ring, while the imidazole ring of the His117 residue was detached from the protein backbone in the wild type azurin structure. The modified azurin with the free imidazole ring was brought close to the IPAR in flavodoxin with restrained body energy minimisation before attaching the imidazole ring to the IPAR propylyl chain by non-restrained rigid body energy minimisation. Finally the linked region of IPAR and azurin was energy minimised to remove van der Waals collisions. This resulted in the model shown in Fig. 5.7, where the two proteins can be seen to be positioned relatively snugly against each other when linked by IPAR.

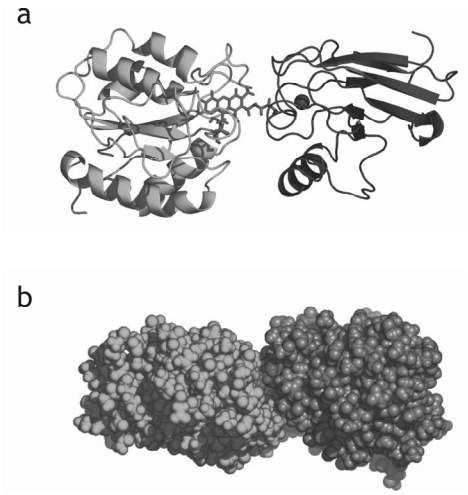

Fig. 5.7. (a) Cartoon and (b) spacefill representation of a model of the ternary complex of flavodoxin-IPAR-Cu-H117G azurin generated using XPLOR (see Materials and Methods). Flavodoxin is coloured in cyan, azurin in blue and IPAR is shown in red. The copper atom of azurin in (a) is shown as a sphere.

Laser flash photolysis

Excitation of a sample containing the three components of the IPAR-apoflavodoxin-azurin complex gave rise to a sequence of transient changes in absorbance that could be distinguished from each other on different timescales. Within the first 0.5 ms, the absorption at both 480 nm and 670 nm was found to decrease monoexponentially (Fig. 5.8a).

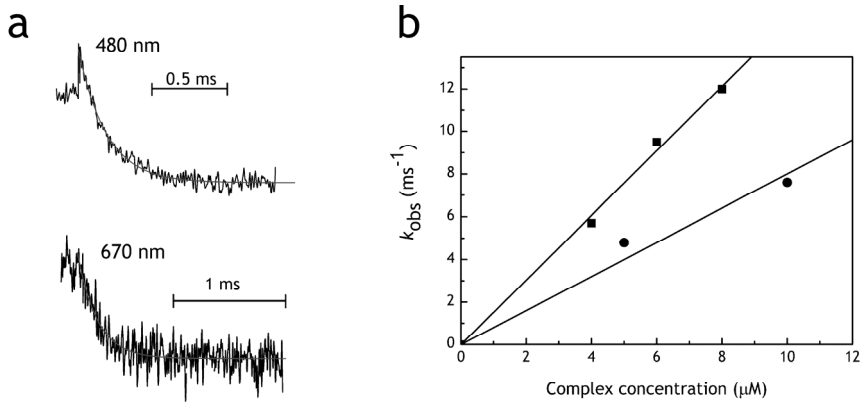

Fig. 5.8. (a) Transient absorption changes over 2 ms, showing the direct reduction of IPAR-flavodoxin (480 nm) and the blue copper centre of H117G azurin (670 nm) by 5-dRf semiquinone, at 10 μM IPAR concentration in 20mM MES pH 6.0. The traces (black lines) have been fitted to a single exponential decay function(red lines). (b) Rate constants (k_{obs}) for the reduction at 670 nm of Cu(II) in azurin (squares) and at 480 nm of IPAR-flavodoxin (circles) as a function of IPAR concentration.

On a timescale of 500 ms however, absorption at 480 nm was found to recover, while that at 670 nm decayed further (Fig. 5.9a). On the contrary, in the absence of Cu-H117G azurin, no recovery of the absorption at 480 nm was observed. These two processes were found to occur concurrently, indicating that the events are most likely linked. k_{obs} was studied as a function of concentration of protein complex, the results of which are shown for the redox reactions both on the short, 0.5 ms timescale (Fig. 5.8b) and the longer 500 ms timescale (Fig. 5.9b). From this, the second-order rate constants k_2 could be derived for the different reactions.

Discussion

*p*K$_a$ *determination of IPAR*

The pH dependent changes in the fluorescence yield and the position of the near UV maximum absorption band of IPAR were similar to those observed with 8α-histidyl and -imidazolyl substituted flavins [230,234,248]. The changes were ascribed to the presence of two different ionizable groups within the molecule, namely the nitrogen in the

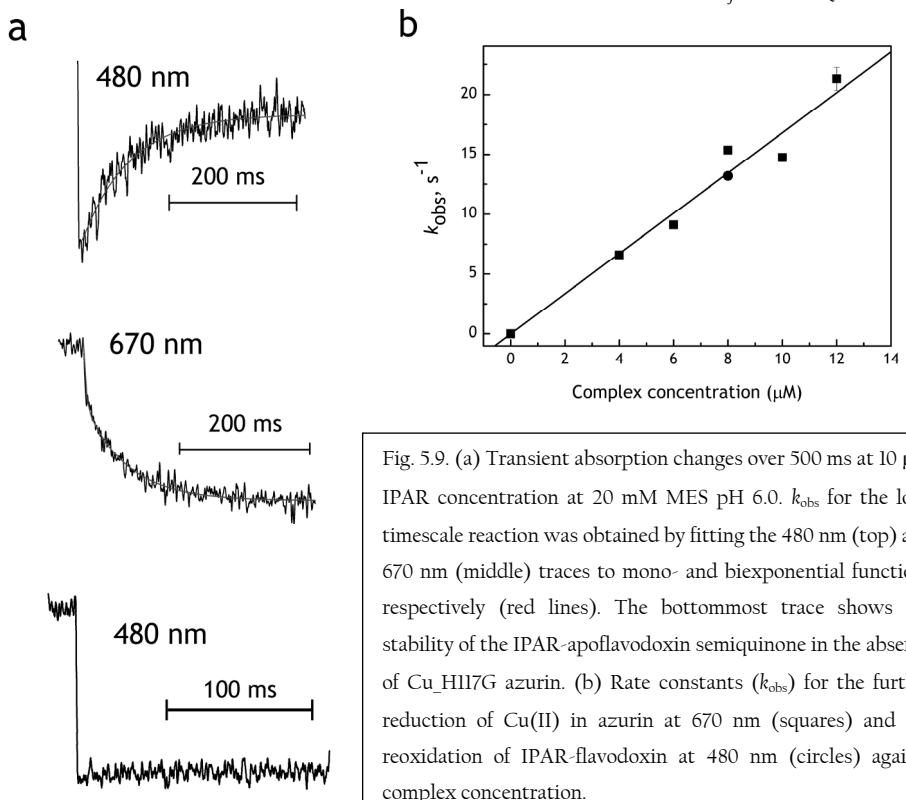

Fig. 5.9. (a) Transient absorption changes over 500 ms at 10 μM IPAR concentration at 20 mM MES pH 6.0. k_{obs} for the long timescale reaction was obtained by fitting the 480 nm (top) and 670 nm (middle) traces to mono- and biexponential functions respectively (red lines). The bottommost trace shows the stability of the IPAR-apoflavodoxin semiquinone in the absence of Cu_H117G azurin. (b) Rate constants (k_{obs}) for the further reduction of Cu(II) in azurin at 670 nm (squares) and the reoxidation of IPAR-flavodoxin at 480 nm (circles) against complex concentration.

imidazole group (pK_{a1}) and the N3 position of the flavin group (pK_{a2}). Fluorescence quenching of imidazole-substituted flavins has been shown to be due the deprotonation of the imidazole group [230]. The extent by which the position of the near UV absorption band of IPAR shifted was markedly larger than that for other 8α-imidazolyl flavins, which shift by 10 to 12 nm. However pK_{a2} for IPAR compared relatively well to that for 8α-N-imidazolylriboflavin where pK_{a2} = 9.7 [230] , which may be expected as the two molecules are identical in their flavin moieties. The two values for pK_{a1} from the fluorescence and visible absorption titrations the same within the error margin but taking the average of the two of 6.75 still gave a value higher than that for 8α-N-imidazolylriboflavin (pK_{a2} = 6.0). The reason for the larger shift in λ_{max} and the difference of 0.7 pH units in pK_a is unclear, but may indicate a different mode of interaction between the isoalloxazine and imidazole rings, especially in view of the longer and more flexible linker connecting the two parts of the molecule.

Binding studies of IPAR to apoflavodoxin

The value of K_d = 2 μM for the dissociation of IPAR from apoflavodoxin at pH 6.0 is comparable to values for the binding of riboflavin to apoflavodoxin, K_d = 1 μM at pH 7.0 in 50 mM phosphate buffer [196], and is an indication that the additional imidazolyl linker substituted at position 8 on the flavin ring does not affect binding of the IPAR to apoflavodoxin adversely. From the crystal structure of this protein [246], the methyl group at position 8 and indeed much of the peripheral dimethyl ring of FMN appears to be solvent exposed. The same is true for other flavodoxins for which structures have been determined [27,30], and led to the hypothesis that electron transfer to and from flavodoxin is mediated by this part of the flavin cofactor [7].

Electrochemistry

Modification at the 8α position of riboflavin is known to influence the redox properties of the flavin [230]. As such, electrochemical studies were carried out to determine the midpoint potentials of IPAR, both in solution and when bound to apoflavodoxin. The single redox couple observed in the cyclic voltammogram (CV) of IPAR in 20 mM MES pH 6.0 represents E_m, the two-electron reduction of IPAR ox to hq, as previously observed by redox potentiometry (Chapter 4). It has previously been noted that E_2, or the ox/sq couple of a flavodoxin, whether with its native cofactor or reconstituted with an alternative flavin, is not detectable by CV [21,26]. As such, the additional more negative redox couple observed in CV of apoflavodoxin-bound IPAR was assigned to the sq/hq or E_1 couple of apoflavodoxin-bound IPAR. The negative shift in redox potential is consistent with apoflavodoxin binding IPAR, and reflects the thermodynamic stabilisation of the sq of the flavin by the apoprotein [249]. E_2 for the IPAR-apoflavodoxin complex could be determined by redox potentiometry, and at −20 mV was very similar to that for the native C69A flavodoxin, −45 mV at pH 6.0 [26]. A positive shift of a similar order (40 mV) has been reported for the same flavodoxin reconstituted with a different substituted flavin, 8α-N-imidazolyl-FMN [50].

Interactions of the N5H of the flavin ring with the peptide backbone are known to be vital for the stabilisation of the sq [27], in the case of *A. vinelandii* raising the value of E_2 by 150 mV as compared to free FMN [218,246]. Since this position of the flavin ring is unchanged and fairly distant from the imidazolyl linker substitution site at position 8, it is not unexpected that E_2 is only slightly shifted between the native FMN and IPAR-reconstituted forms. There was however a substantial difference between E_1 for these two forms of flavodoxin: E_1 for IPAR-reconstituted flavodoxin was approximately 260 mV more positive than for native flavodoxin. A similarly large positive shift of 186 mV was determined for the sq/hq couple of the complex of riboflavin with the apoflavodoxin of *D. vulgaris* [38,250] compared to the native protein. It is thought that the absence of the phosphate group in the riboflavin-apoflavodoxin complex destabilises the sq state of the complex in particular, due to disruption of the hydrogen-bonding network that exists in the native complex with FMN [38]. This was borne out by a 63 000-fold higher K_d for the binding of riboflavin sq to apoflavodoxin, compared to 2100- and 54-fold increases in K_d for the ox and hq forms [196]. The absence of the terminal phosphate group in IPAR is as such likely to account for the observed increase in E_1. Crucially, the fact that E_1 and E_2 could be measured for the IPAR-apoflavodoxin complex confirmed that the IPAR-reconstituted flavodoxin was fully functional with respect to electron transfer.

Binding of IPAR-reconstituted flavodoxin to Cu-H117G azurin

The nature of the changes in the UV-visible spectrum of Cu-H117G azurin, with increasing absorbance at 630 nm and decreasing absorbance at 420 nm, indicate that the imidazole moiety of the IPAR-flavodoxin complex reconstitutes the copper site in a similar way to imidazole [75] and free IPAR (Chapter 4). The dissociation constant K_d, for the binding of IPAR-flavodoxin to Cu-H117G azurin, is at 180 μM much higher than that for IPAR along binding Cu-H117G azurin (1 μM). The model of azurin linked to flavodoxin by IPAR generated using the programme XPLOR (Fig. 5.7) shows that although a non-covalent complex can indeed be formed between the two proteins, the proteins are fairly close together. In particular, the model shows that the complex is very close fitting on one side, with a more solvent exposed interface on the other where the extended alkyl chain of

IPAR is also visible. The model also predicts a low degree of rotational freedom between the two monomers of the complex. The relatively high K_d between IPAR-reconstituted flavodoxin and Cu-H117G azurin compared to free IPAR binding azurin may reflect the rather compact fit between the two proteins when linked by IPAR.

Laser flash photolysis

By monitoring changes in absorption at two different wavelengths in the visible spectrum, it was possible to discriminate between changes at the different redox centres in the system under study. At 480 nm, absorption is due mainly to IPAR-flavodoxin, with a small contribution immediately after the flash from the sq of 5-dRf. The latter is clearly visible in the short timescale trace (Fig. 5.8a, top trace), as an initial spike of increased absorption at the point of the flash. In all these experiments, MES acted as the sacrificial electron donor to the 5-dRf triplet state formed by the laser flash, in a manner analogous to EDTA in other flavin-sensitized reduction reactions [132]. This reaction with MES giving 5-dRf sq has been shown to be equally efficient and productive in initiating electron transfer reactions in redox proteins (Chapter 4).

The increased absorption at 480 nm was then found to decay to below the baseline, corresponding to reduction of the IPAR-flavodoxin by the free flavin reductant. Similar behaviour was observed at 670 nm, where the absorption derives from the oxidised copper site of azurin. The bleaching observed at this wavelength indicates reduction of copper (II) to copper (I), again by 5-dRf sq. This was confirmed by the dependence of the reaction rate on protein concentration (Fig. 5.8b), where the k_2 values for the Cu and flavin reduction derived from this plot were 8.0×10^8 M^{-1} s^{-1} and 1.5×10^9 M^{-1} s^{-1} respectively. The reduction rate for the blue copper site by flavin semiquinones appears somewhat higher than that for similar proteins, where plastocyanin was reduced at a rate of 2.4×10^7 M^{-1} s^{-1} by lumiflavin sq [135]. However, using 5-dRf sq (which has a lower reduction potential) with wild type azurin gave a k_2 of 5×10^8 M^{-1} s^{-1} (Chapter 4). k_2 for the flavin redox centre was also comparable to that for the reaction of IPAR-reconstituted apoflavodoxin with 5-dRf sq, at 2.2×10^9 M^{-1} s^{-1} (S. Alagaratnam, unpublished results), as well as for other flavodoxins [61].

At longer timescales of up to 500 ms, the copper site of azurin was observed to further reduce, from an additional decrease in absorption that was again monoexponential in nature. Taking the short timescale direct reduction into account, the kinetic traces at 670 nm could be well described by a biexponential decay function (Fig. 5.9a, middle trace). Conversely, at 480 nm, a recovery in absorption was noted (Fig. 5.9a, top trace), indicating reoxidation of the flavin centre of IPAR in flavodoxin. As this monoexponential growth rate correlated well with the rate of reduction at the copper site, it was assumed that electron transfer is occurring from the flavin to the copper site of the complex. This was confirmed by the stable loss in absorbance at 480 nm in the absence of Cu-H117G azurin (Fig. 5.9a, bottom trace). The observed rate for such an intramolecular reaction would be expected to be independent of complex concentration, however from the plot shown in Fig. 5.9b the dependence of the rate on complex concentration is clear, with a k_2 of 1.7 x 10^6 M^{-1} s^{-1}.

The comparative amounts of the different components of the complex added were determined by calculating the distribution of the various species present in solution, using the dissociation constants from this study. As the complex is non-covalent, an equilibrium is established where the following components are also present with the flavodoxin-IPAR-Cu-H117G azurin complex: IPAR-bound Cu-H117G azurin, Cu-H117G azurin; and because apoflavodoxin can also bind the flavin 5-dRf sensitizer, both IPAR- and 5-dRf-bound apoflavodoxin. Because they are colourless, both apoflavodoxin and apoazurin can be disregarded when considering the kinetic absorption changes.

Various ratios of the complex components were tested in the laser flash photolysis set-up, among them increased concentrations of Cu-H117G azurin and of IPAR. The ratio used in the experiment described above gave the highest proportion of ternary complex of all the conditions tested, relative to the other components. An example of the distribution of the various species is illustrated in Fig. 5.10, where despite the optimized ratios the ternary complex represented a very small proportion of all reactive species present. This distribution of the different components was ultimately found to be the source of the concentration dependence of the slow timescale reaction observed. In an effort to drive the equilibrium towards IPAR being fully bound by the two proteins, higher concentrations of

apoflavodoxin and Cu-H117G azurin had to be added to the sample. The reactions of these components eventually dominated the spectral changes seen, leading to the concentration-dependent behaviour of the long timescale reactions. The kinetic traces observed arise thus principally from the reaction of IPAR- or 5-dRf-bound flavodoxin with Cu-H117G azurin, with a smaller contribution from the intramolecular electron transfer within the flavodoxin-IPAR-Cu-H117G azurin complex. Due to the dominance of the competing reactions, it was not possible to separate this component out of the measured rates.

The second-order reaction rate of reaction determined from Fig. 5.9b is approximately three times lower but within the same order of magnitude for a comparable experiment performed using wild type flavodoxin and wild type azurin with 5-dRf, the k_2 of which was 5 x 10^6 M^{-1} s^{-1} (S. Alagaratnam, unpublished results). From structural comparisons of flavodoxins from various sources in its three different oxidation states [27,28,187], reduction to the sq form is found to be associated with protonation at the N5 of the flavin ring. The peptide backbone adopts a different conformation in the sq form, so that the carbonyl oxygen of a glycine residue (57 in *C. beijerinckii*) forms a hydrogen bond with N5H. Conversely, reoxidation of the sq entails deprotonation at this position, and reversal of the conformational change. It has recently been shown that the reoxidation of flavodoxin sq rather than the reduction of oxidised flavodoxin is rate limiting [4]. In the context of this work however, this limit was not reached as the reoxidation rate increased with higher azurin concentrations.

Conclusions

A flexible heterodimeric complex of flavodoxin and azurin was successfully constructed by reconstitution of the individual proteins and direct connection of the redox centres by means of the bifunctional linker IPAR. Cofactor reconstitution as a method for linking the proteins allowed for a very gentle process of tethering the proteins together, avoiding any unnatural strain on the proteins. The individual redox centres were initially reduced by the electron donor 5-dRf, however on a longer timescale the 'banked' electrons from the stabilised IPAR sq bound to apoflavodoxin could react further with the azurin copper site. The slow intramolecular reoxidation of IPAR-flavodoxin could in principle

also occur, as well as through intermolecular reactions, with individual components of the non-covalent complex also present in the sample mixture. The latter reactions dominate the kinetics observed. A photosensitizer that is directly attached to IPAR-flavodoxin will be used for the initiation and subsequent measurement of electron transfer rate within the complex, while avoiding secondary reactions with azurin. Efforts to this end are being undertaken in our laboratory, the results of which will be reported elsewhere. Ultimately, the length of the IPAR linker may be too short to allow the efficient formation of a ternary complex with azurin and flavodoxin, where extending this linker region even by one or two carbons may improve the association of the complex significantly.

Acknowledgements

Dr. Walter van Dongen and Dr. Willem van Berkel are gratefully acknowledged for sharing their expertise in flavodoxin expression and purification.

Chapter 6

Peptide-linked heterodimers of flavodoxin and azurin: Construction, expression, purification and characterisation

Sharmini Alagaratnam, José A. Navarro, Manuel Hervás, Miguel Angel De la Rosa and Gerard W. Canters

---

Abstract

A C-to-N terminal peptide-linked heterodimer of the redox proteins flavodoxin and azurin was conceived of as a model system for studying electron transfer between redox partners within close proximity of each other. Three peptide linkers of 13, 23 and 27 amino acids were designed, based on glycine repeats interspersed with serine and threonine residues, and molecular modelling used to test their ability to bridge the distance between the termini of flavodoxin and azurin while still allowing the redox patches of the two proteins to meet for productive electron transfer. The genes for flavodoxin and azurin were cloned into the same plasmid, and the three linkers genetically introduced in between them such that the flavodoxin C-terminal was linked to the azurin N-terminal. The three constructs were expressed in *E. coli* and a purification protocol combining steps from flavodoxin and azurin purifications developed. The purified proteins were spectroscopically characterized for both flavin and copper occupancy, where both the length of the linkers and age of the proteins were found to affect in particular the efficiency of the copper site reconstitution. Laser flash photolysis using 5-deazariboflavin as the external electron donor revealed that electron transfer occurred from the flavin to the copper redox centres, and that intermolecular electron transfer between heterodimer molecules dominated over the intramolecular reaction within a single heterodimer.

Introduction

In an alternative approach to creating redox-active heterodimers of proteins, a project was initiated to link flavodoxin from *Azotobacter vinelandii* and azurin from *Pseudomonas aeruginosa* by a peptide chain via their C- and N-termini respectively. The two proteins have previously been shown to form transient complexes productive for electron transfer, despite not being physiological redox partners [70]. A flexible peptide linker attached at the termini would in principle bring the two proteins in close proximity of each other, greatly increasing their local concentration to allow for electron transfer between them, while not affecting their overall structure. An example of a triple fusion of three redox proteins exists, which forms a self-sufficient catalytic system for camphor oxidation [251]. Based on their relative redox potentials, electron transfer in a chimeric fusion protein of flavodoxin and azurin as initiated by laser flash photolysis would be expected to occur from reduced flavodoxin to oxidised azurin. Changes in redox states of the bound flavin in flavodoxin and the Type-1 copper site in azurin can be monitored by transient absorption spectroscopy to give information on the sequence and rates of electron transfer within the system. Important concerns for creating such a system with flavodoxin and azurin would be the length and the identity of the connecting polypeptide linker; these issues are addressed below.

A number of alternative designs for C-to-N terminal linking of two polypeptide chains are described in the literature, but all have in common that the linking amino acids are hydrophilic in character, as the linker will be highly exposed to the solvent. In addition, the amino acid glycine is frequently employed due to its flexibility and small size (see [252] and [253] for examples). Homodimers of a number of DNA binding proteins have also been created in this way, which mimic the proteins' dimeric *in vivo* state and display enhanced DNA binding compared to the monomeric forms of the same proteins found *in vitro* [254,255]. The peptide linkers introduced in these systems consisted of glycine, serine and threonine residues arranged in repeats of GGGS and GGGT, and successfully bridged distances of up to 80 Å from the C-terminus of one protein to the N-terminus of the other [256]. Linker length was found to be a crucial factor for efficient dimerization [257,258], underlining the importance of good estimates of bridging distances.

Using a previously constructed of model of flavodoxin and azurin which have their redox centres oriented towards each other (see Chapter 5), a distance of 55 Å was measured *in silico* between the C-terminal of flavodoxin and the N-terminal of azurin. The non-dimerizing Cys69Ala mutant of flavodoxin was used for this construct, to prevent complications in the study of the heterodimers, where this mutant has otherwise been shown to be both functionally and spectroscopically identical to the wild type [26]. It is referred to from here onwards simply as flavodoxin. A mutant of azurin, His117Gly, was also employed, which has a cavity at the copper site which can be reconstituted with imidazole-like ligands to give the wild-type spectroscopic features of a Type-1 copper site [75]. This mutant thus allowed for additional linking capabilities at the active site if later desired. Three polypeptide linkers based on repeats of GGGS and GGGT varying between 13 and 27 amino acids in length were designed and tested by molecular modelling to ascertain if they would be able to bridge the gap between the two termini. DNA sequences encoding for the three linkers were then introduced between the genes for flavodoxin and azurin, and the three linked fusion proteins successfully expressed and purified. Finally the fusion proteins were characterised in terms of redox centre occupancy by spectroscopic means, and electron transfer by laser flash photolysis using 5-deazariboflavin (5-dRf) as the external electron donor [132].

Materials and Methods

Standard molecular biology methods were used for *in vitro* DNA manipulation, agarose gel electrophoresis, polymerase chain reaction (PCR), transformation into *Escherichia coli* strain JM109 and subsequent plasmid preparation [259]. Restriction enzymes, *Taq* polymerase, T4 polynucleotide kinase and T4 DNA ligase were from New England Biolabs (Beverly, MA). Primers were synthesized by Eurogentec (Belgium). Sequencing of the resulting plasmids was performed by Baseclear (the Netherlands).

Prior to hybridization, the complementary primers used to extend the polypeptide linkers were phosphorylated by incubation at 37°C for 30 min with 20 units T4 polynucleotide kinase, 1 mM working concentration of adenosine triphosphate (ATP) in the kinase buffer for every 400 pmol of primer. The kinase was then inactivated by incubation at 70°C for 10

min. The complementary primers were then mixed in equal ratios, heated to 94°C for 2 min to denature any secondary structure that may be present before allowing the mixture to slowly cool to room temperature, and hybridizing. This mixture was then added immediately to the ligation mixture or stored at −20°C for future use.

The plasmids encoding for the fusion proteins connected by polypeptide linkers of three different lengths were individually transformed into *E. coli* JM109 for expression of the proteins. The cultures were grown in LB medium with 100 μg/ml of ampicillin to maintain the plasmids, and induced with 1 mM IPTG when the OD_{600} had reached approximately 1. The cells were grown for a minimum of a further 5 hours before harvesting.

All materials used during the protein purification were of the purest possible grade, and standard protein handling procedures applied for column chromatographic separation, protein concentration and subsequent detection by SDS polyacrylamide gel electrophoresis (SDS-PAGE) and Western blotting using polyclonal antibodies raised in rabbit against flavodoxin and azurin. Optical absorption of the pure proteins was measured with a PerkinElmer Lambda 800 UV-Vis spectrometer.

Molecular modelling was performed using the programmes Swiss PDB Viewer and XPLOR 3.1. The PDB files initially used for the heterodimer model are 1AZU for azurin [247] and 1YOB for flavodoxin ([246], Chapter 3), where the creation of the model has previously been described (see Chapter 5). The three linkers were first created as individual PDB files in the programme Swiss PDB Viewer. Then, using the available model of the flavodoxin-azurin heterodimer as the framework, the linkers were attached to the C- and N- termini of flavodoxin and azurin respectively, in the orientation indicated above. In the programme XPLOR, all atoms of the azurin and flavodoxin were fixed, except for the backbone atoms of the last residue of flavodoxin and the first of azurin. The energy of the system was then minimised, and resulting coordinates of the atoms written to output PDB files.

The laser flash photolysis apparatus has been previously described [57,232]. Samples were prepared in 2 ml glass cuvettes with tapered necks, and 20 mM MES buffer containing 100 μM 5-dRf was first bubbled vigorously for 2 hours with argon. The reconstituted fusion proteins were added in steps to the degassed cuvettes with gas–tight Hamilton syringes, systematically increasing their concentration. Upon addition of the protein, the samples were flushed at the surface under gentle stirring to eliminate all remaining traces of oxygen. The samples were excited at 337 nm, and redox processes were followed at 480 nm for flavodoxin and 670 nm for azurin. Between 5 and 8 traces were averaged for each point, and the traces fit to either single or double exponential decay functions to obtain the observed rate constant, k_{obs}. k_2, or the second-order rate constant, was then determined by plotting k_{obs} against the protein concentration.

Results

Design and molecular modelling of peptide length

Based on the 55 Å distance between the flavodoxin C-terminus and the azurin N-terminus, three different linkers were conceived of with the lengths of 13, 23 and 27 residues, consisting of glycine-rich repeats, and with the sequences:

13 residue linker end Fld – GGGS SGGT SGGG G – start Azu
23 residue linker end Fld – GGGS SGGG TGGG SGGG GTSG GGG – start Azu
27 residue linker end Fld – GGGS SGGG TGGG SGGG TGGG GTSG GGG – start Azu

The shortest linker is not expected to allow the electron transfer patches of flavodoxin and azurin to interact, while the two others are, based on their extended lengths. This hypothesis was tested by molecular modelling, as described in Materials and Methods, and the resulting output structures are shown in Fig. 6.1. The 13-residue linker in Fig. 6.1a was found broken, indicating that it is too short to bridge the distance between the flavodoxin and azurin termini. The 23-residue linker was found to successfully connect the termini although in a more stretched, taut conformation (Fig. 6.1b), with the redox centres of the

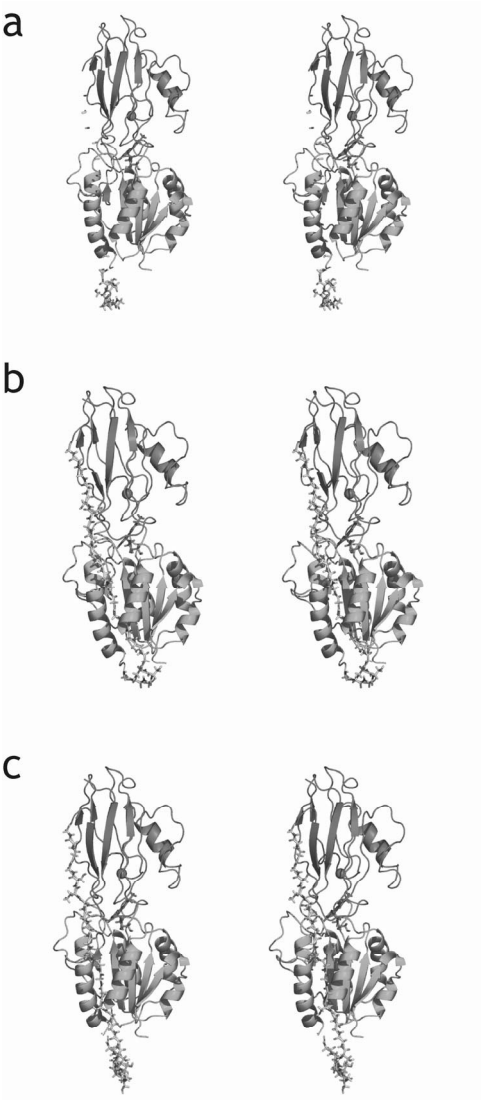

Fig. 6.1. Stereo view of PDB output files of energy minimisation step of the model of flavodoxin and azurin, attached by the 13, 23 and 27-residue linkers in a, b and c respectively. The upper protein azurin and the lower flavodoxin are both represented as cartoons of their secondary structure, the copper atom of azurin as a sphere and the FMN cofactor of flavodoxin in stick form, as are the linkers.

two proteins facing each other. By comparison, the 27-residue linker gives more leeway for the formation of a productive electron transfer complex (Fig. 6.1c).

Based on the molecular modelling results, it was decided to introduce the three linkers between flavodoxin and azurin. The approach taken was to first to clone the azurin gene in after that of flavodoxin on the same plasmid, then inserting DNA fragments coding for the linkers in between them. The three resulting constructs corresponding to the three heterodimers with linkers of different lengths could then be used to express the fusion proteins in *E. coli*. The genes for C69A flavodoxin and H117G azurin were present on the pUC-based plasmids pC69Afld and pGKH117G respectively. These were the starting points for the creation of the flavodoxin C-terminal to azurin N-terminal fusion proteins in the four steps described below. Fig. 6.2 illustrates the steps diagrammatically where the thick black and grey arrows denote the genes for flavodoxin and azurin respectively, as well as the direction of their open reading frames. A series of five primers,

FA2 – 7, were used to create the linkers for the three constructs, where the amino acids coded for by the primers are indicated by single-letter code above the sequence of the primers (see below). Lower case letters correspond to the original sequence deriving from the flavodoxin and azurin genes, while upper case letters indicate introduced bases coding for the polypeptide linkers. Restriction enzyme recognition sites are underlined and the enzyme noted under the line. FA2 and 3 were used as PCR primers to remove the stop codon of flavodoxin and the signal peptide of azurin respectively, while FA4-5 and FA6-7 were designed to hybridize to form short double-stranded fragments which could be ligated in directly between the genes for flavodoxin and azurin.

Linker sequences

```
                                                  L1                  fld C-term
                    stop S   T   G   G   S   S   G   G   G   l   s   l   g   f
FA2       5' GG CCG TTA ACT AGT ACC GCC ACT CGA GCC GCC CCC cag gga cag ccc gaa ct 3'
                      Spe I           Xho I

                                                 L2             azu N-term
                              T  S   G   G   G    G   a   e   c   s
FA3       5' GCA CCG GAA TTC CGA ACT AGT GGT GGC GGC GGG gcc gag tgc tcg 3'
                   EcoR I      Spe I
```

FA4 and FA5 hybridize to form the 14-residue extending linker L3:

```
                                                L3
           S    S   G   G   G  T    G   G   G  S   G   G   G   T   G   G   G   G
FA4       5' TCG AGT GGC GGT GGC ACA GGG GGT GGC TCA GGC GGT GGC ACG GGT GGC GGT GGC A      3'
        3'      CA CCG CCA CCG TGT CCC CCA CCG AGT CCG CCA CCG TGC CCA CCG CCA CCG TGA TC  5'    FA5
             Xho I                                                                 Spe I
```

FA6 and FA7 hybridize to form the 10-residue extending linker L4:

```
                                          L4
              S   S   G   G   G   T   G   G   G   S   G   G   G   G
FA6       5'  TCG AGT GGC GGT GGC ACA GGG GGT GGA TCC GGC GGT GGC GGC A  3'
          3'      CA CCG CCA CCG TGT CCC CCA CCT AGG CCG CCA CCG CCG TGA TC 5'  FA7
              Xho I                                                 Spe I
```

Step 1. Replacement flavodoxin stop codon by 9-residue linker L1

The primer FA2 is complementary to the last five residues of the flavodoxin gene, but instead of the flavodoxin stop codon codes for nine residues of Linker 1, or L1, followed by a new stop codon. PCR on pC69Afld with the standard Reverse Primer for pUC plasmids in conjunction with the primer FA2 thus results in the removal of the stop codon of flavodoxin, instead extending it by the 9 residues of Linker 1 indicated. The fragment obtained was digested with the enzymes *Spe* I in the linker sequence, and *Sty* I within the flavodoxin gene.

Step 2. Removal of azurin signal peptide and N-terminal extension by 6-residue linker L2

The first section of primer FA3 codes for 6 residues of the linker region (Linker 2, or L2), and ends with 12 bases complementary to the first four residues of the azurin gene, but not the signal peptide that precede these (indicated by the white box at the start of the azurin gene). PCR of the pGKH117G plasmid with an internal non-mutagenic azurin primer and primer FA3 thus resulted in a fragment which codes for L2, followed immediately by the start of the azurin gene, but with its signal peptide removed. By digestion and ligation of this fragment and the original pGKH117G plasmid with *Eco*R I and *Sal* I, the plasmid pFA2 was generated.

Step 3. Fusion of flavodoxin and azurin with a 13-residue linker

A three-way ligation with the *Sty* I-*Nde* I digested pC69Afld, the *Sty* I-*Spe* I fragment from Step 1 and the *Spe* I-*Nde* I fragment of pFA2 from Step 2 created the fusion heterodimer of flavodoxin and azurin, connected by the 13-residue linker consisting of L1 and L2, in the plasmid pFA3.

Step 4. Extension of the linker region to 23 and 27 residues

The introduced *Xho* I and *Spe* I restriction sites on L1 allowed replacement of the small fragment between the two sites by ligating in the extending linkers L3 and L4, resulting in

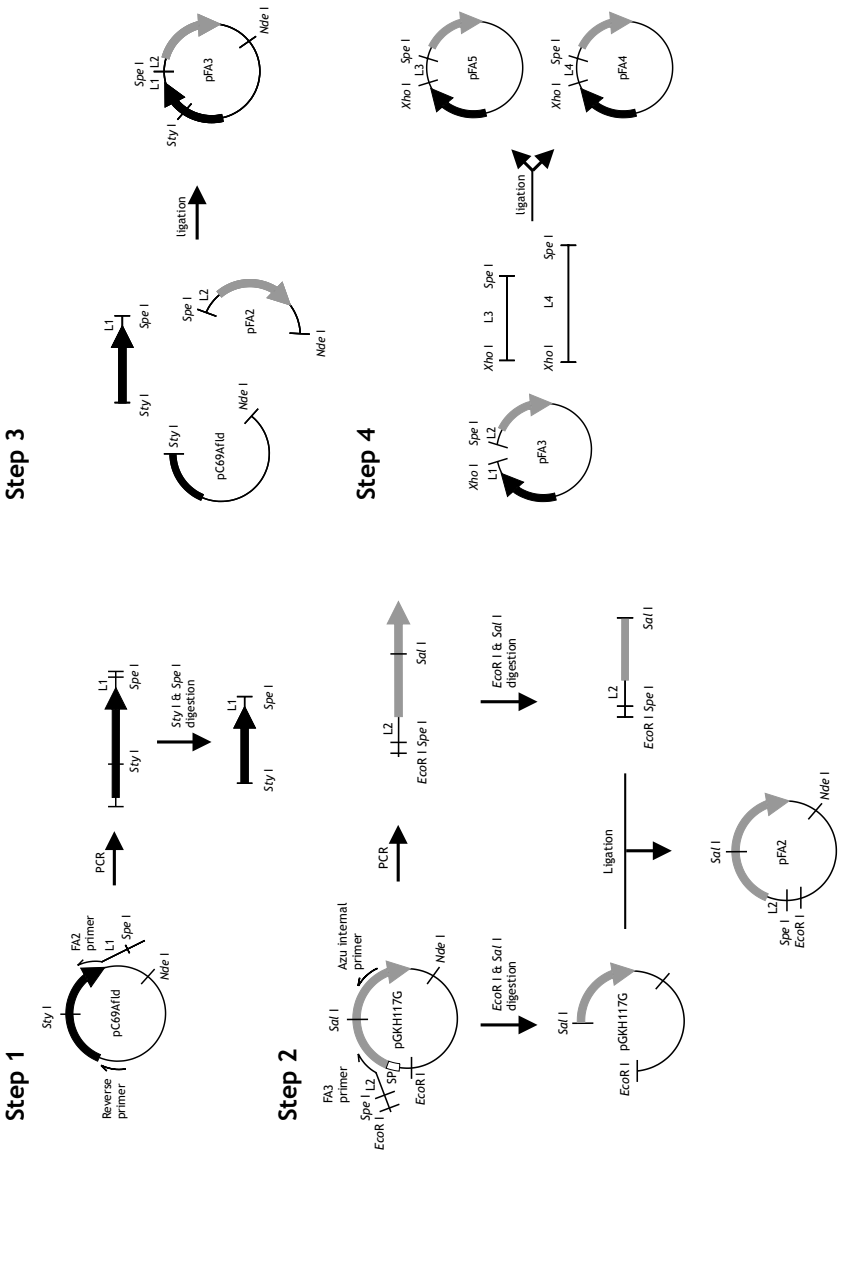

Fig. 6.2. Steps 1 – 4 of the cloning strategy for creation of the fusion protein of flavodoxin and azurin, linked by polypeptide chains of three different lengths.

the 23 amino acid-linked flavodoxin-azurin fusion on pFA5 and the 27 amino acid-linked fusion on pFA4. The linkers L3 and L4 were synthesized as four individual primers, where primers FA6 and FA7 were complementary to each other and formed the 10-residue extension by simple hybridization, and similarly FA4 and FA5 the 14-residue extension. As can be seen from their sequences, the *Xho* I and *Spe* I sites were included in the primers, thereby circumventing the need to digest them prior to ligation.

Results and Discussion

Confirmation of clones, expression testing

For each of the three plasmids, a total of eight colonies resulting from the final ligation step were picked and tested first by restriction mapping before being sent for sequencing. Of the clones which were confirmed to have the correct sequence, at least four for each linker length were subjected to expression testing. The level of expression for these clones was compared before selection of a single clone for subsequent use in growth and purification of the fusion proteins.

Protein purification

A new protocol for the purification of the fusion proteins was developed, combining elements of the protocols used for the individual proteins flavodoxin and azurin, as outlined below.

a) Breaking of cells

The cell pellet after growth and harvesting was resuspended in a buffer of 100 mM Tris, pH 8.0, with 0.5 mM EDTA and 1.5 mM $MgCl_2$. As the fusion protein is cytoplasmically expressed, the cells were disrupted by passing the cell suspension twice through the French press at 1000 bar to free the protein, prior to which DNase and the protease inhibitor PMSF were added. The cell-free extract was collected after pelleting of the cell walls and other large macromolecular complexes by centrifugation at 15 000 rpm for 15 min.

b) pH precipitation

The pH precipitation step in the purification of azurin [75] was successfully incorporated into the protocol for fusion protein purification. The pH of the cell free extract was slowly adjusted to 4.0 with 20% acetic acid, followed by a 15 min incubation, both under continuous stirring and on ice. No significant loss of the fusion protein was noted, while many other proteins precipitated. The latter were removed by centrifugation for 20 min at 8000 rpm.

c) CM column

The first chromatographic step also originated from the azurin purification protocol. The supernatant from the pH precipitation step above was applied to a CM column equilibrated with 50 mM ammonium acetate buffer, and subjected to a gradient between pH 4.0 and 7.0 in the same buffer. The fusion protein eluted towards the end of the gradient, where fractions containing the fusion protein as determined from the yellow colour originating from the flavodoxin and by SDS-PAGE were pooled, concentrated and exchanged into a buffer of 100 mM Tris pH 8.0 with 0.5 mM EDTA for the final purification step.

d) Q-Sepharose column

The final Q-Sepharose column step was taken from the protocol for flavodoxin purification [201]. The fusion protein was applied to the column equilibrated with 100 mM Tris pH 8.0 with 100 mM potassium chloride, and subjected to a salt gradient from 100 to 700 mM potassium chloride. The fusion protein eluted at approximately 550 mM of salt. The yellow fractions were pooled, concentrated and after checking for purity by SDS-PAGE exchanged into 20 mM MES pH 6.0 for storage at −20°C.

Both the 13 and 23-amino acid linked heterodimers yielded approximately 8.5 mg pure protein per litre of culture, while the 27-amino acid linked heterodimer had a significantly lower yield of 3 mg per litre of culture.

Fusion protein characterization

In SDS-PAGE, the three fusion proteins could be seen to run at a height corresponding to that expected for the combined molecular weights of azurin (14 kDa) and flavodoxin (20 kDa) (see Fig. 6.3a). The 13-residue linked heterodimer also appeared to run slightly lower than the 23- and 27-residue linked proteins, while no significant difference could be identified between the running patterns of the latter two. Individual Western blotting with azurin- and flavodoxin-specific antibodies confirmed the presence of both azurin and flavodoxin epitopes in the bands corresponding to the fusion proteins (Fig. 6.3b and c).

Fig. 6.3. SDS-PAGE (a) and Western blots using anti-flavodoxin (b) and anti-azurin (c) antibodies where F denotes flavodoxin, A azurin, M the marker, and 13, 23 and 27 the 13, 23- and 27-residue linked heterodimers of flavodoxin and azurin respectively. In the lanes containing the 27-residue linked heterodimer, two major bands corresponding to breakdown products of the protein can also be seen at lower molecular weights.

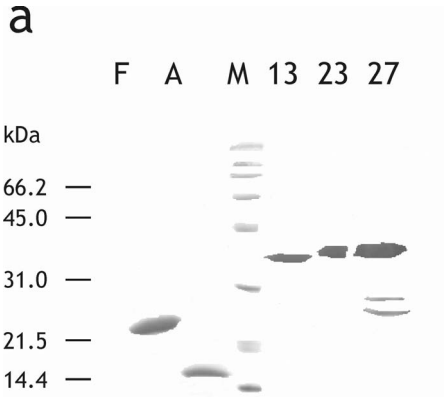

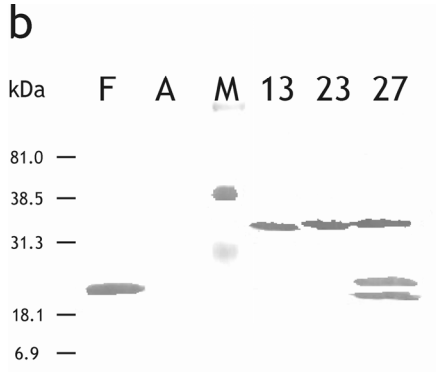

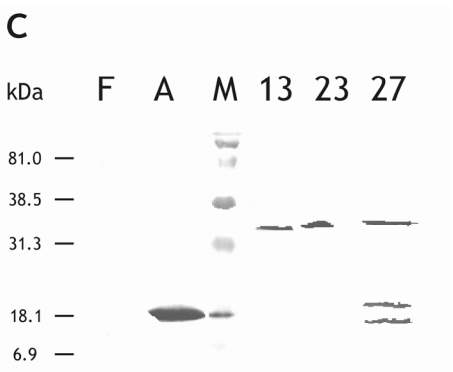

The three fusion proteins made showed marked differences in stability to breakdown, with the 13-residue linked heterodimer the most and the 27-residue heterodimer the least stable. This difference was noted both during purification and storage of the proteins, where the degradation in the case of the 27-residue linked heterodimer was so severe that it led ultimately to extremely low yields and difficulties in further characterisation. For this reason, the spectroscopic characterization that follows only involves the 13- and 23-residue linked fusion proteins.

Upon purification, both the 13- and 23-residue linked fusion proteins displayed the double absoprtion bands with peaks at 365 and 450 nm, and with shoulders typical of flavodoxin-bound FMN cofactor (Fig. 6.4, dashed line). This further confirms that the flavodoxin half of the heterodimer was expressed and folded correctly to accomodate the FMN cofactor in a manner identical to the wild type protein. Apart from the absorption at around 280 nm deriving from the aromatic amino acids, no other absorption bands were detected. This indicates that the H117G azurin part of the heterodimer was present in its apo (non-copper bound) form, as has previously been found for purification of the H117G mutant [75]. In the case of the latter, the copper site could be completely reconstituted spectroscopically by a 30 min incubation at room temperature of the protein with one molar equivalent each of copper nitrite and imidazole [73].

The same procedure was performed with the two fusion proteins, but the extent of reconstitution was strongly dependent on the age of the sample. In both cases incubation of a molar equivalent each of copper and imidazole with the freshly purified fusion proteins led to more than 80% reconstitution of the copper site. This ratio was calculated based on the amplitude of the flavin absorption peak relative to that of the reconstituted copper site, where the extinction coefficients of the flavin group and the copper site in the heterodimer were presumed to be unchanged compared to those in the native protein. This reconstitution is illustrated in Fig. 6.4, where addition of copper brought about an absorption increase in the region corresponding to the copper site and peaking at 625 nm, while the addition of imidazole increased this amplitude approximately four-fold, similar to what has been observed for unlinked H117G azurin [74].

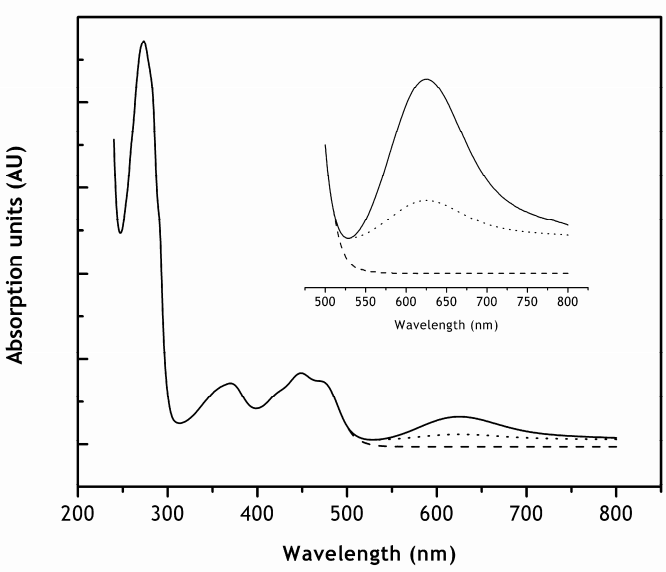

Fig. 6.4. UV-visible spectra of 50 μM of the 13-residue linked flavodoxin-azurin fusion protein in 20mM MES buffer pH 6.0, where the inset shows a zoom in of the changes in the copper absorption band at 630 nm. Dashed line: unreconstituted fusion protein; dotted line: fusion protein after incubation with 1 equivalent of copper; solid line: fusion protein after incubation with one equivalent each of copper and imidazole.

After longer period storage of approximately 3 months at −20°C, it was noted that the fusion proteins could not longer be reconstituted with copper and imidazole to the same extent as freshly prepared protein. Again using the flavin absorption to calculate a lower limit for the fusion protein concentration, the copper sites of the 13- and 23-residue linked heterodimers could be reconstituted to just 30 and 25% occupancy respectively. Neither longer incubation times, addition of ferricyanide as an oxidant nor increasing the amounts of added copper and imidazole increased the amplitude of the blue absorption band of the copper site. Use of even higher levels of added copper and imidazole (above 10 molar equivalents) caused complexes of copper and imidazole to form, which could be separated from the fusion proteins by washing through an Amicon filter with a 10 kDa cut-off.

That the copper site of the fusion proteins could not be fully reconstituted after storage despite incubation with excess copper and imidazole is an indication that a proportion of the sites may be damaged in such a way that no longer allows the binding of copper. While it is known that after purification a certain proportion (<10%) of monomeric H117G azurin is also incapable of reconstitution, contrary to the fusion proteins, long term storage has never been found to exacerbate the problem. The increase in the amount of

fusion protein that cannot have its copper site reconstituted over time may be caused by the presence of the fused flavodoxin, which is also redox active and may somehow led to the damage of the copper site.

Laser flash photolysis

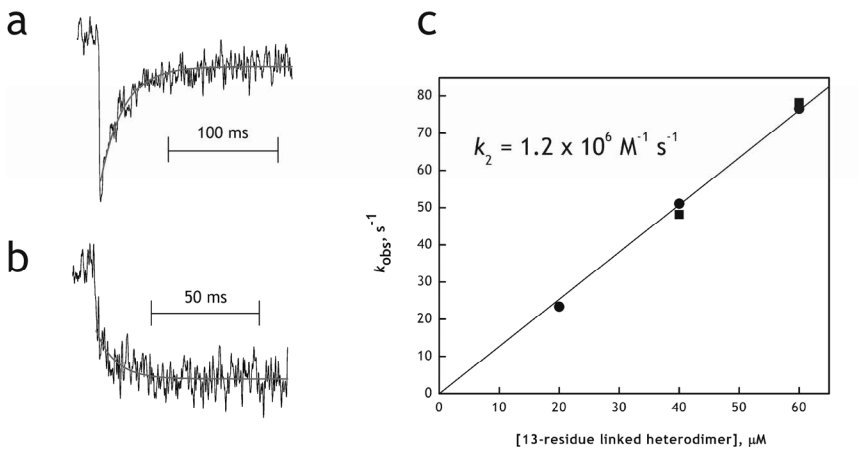

Fig. 6.5. Laser flash photolysis data of the 13-residue linked heterodimer in 20 mM MES pH6.0. a, Change in absorption at 465 nm at 40 μM protein concentration; b, Change in absorption at 640 nm at 60 μM protein concentration; both fitted to a single exponential giving the observed rate, k_{obs}. c, Plot of k_{obs} for reoxidation of the flavin centre (●) and reduction of the copper centre (■) against heterodimer concentration, where the slope of the resulting linear fit gives the second order rate constant, k_2.

The 13- and 23-residue linked heterodimers were tested by laser flash photolysis to investigate their electron transfer behaviour. The external electron donor 5-dRf had previously been shown to reduce both azurin ([56,70], Chapter 4) and flavodoxin ([48], Chapter 5) individually, efficiently interacting with the MES buffer as the sacrificial electron donor (Chapters 4 and 5). Changes in redox state of the flavin and copper centres of the heterodimers could be followed individually by observing at 465 and 640 nm respectively. Similar behaviour was observed for the two redox centres of both the 13- and 23-residue linked heterodimers, and is illustrated in Fig. 6.5. On a short timescale of 2 ms, decreases in absorption were observed at both observation wavelengths, indicating reduction of both the flavin and copper redox centres. On longer timescales of between 100 and 200 ms, the absorption at 465 nm recovered, indicating reoxidation of the flavin group.

Concomitantly, the absorption at 640 nm decayed further, although due to the small amplitude of the signal changes, it was not always possible to estimate the rate of this slower phase copper reduction reaction.

Table 6.1. Second-order rate constants, k_2, for 13- and 23-residue linked heterodimers, determined by plotting k_{obs} against different concentrations of the two constructs as described in Materials and Methods.

Linker length	k_2, $M^{-1} s^{-1}$
13 residues	1.2×10^6
23 residues	3.8×10^6

The rates for flavin reoxidation and copper reduction when available for the same sample were very similar and could be plotted against the concentration of heterodimer. The rate of these reoxidation/reduction reactions were found to increase with increasing heterodimer concentration, indicative of a bimolecular reaction between the two protein-bound redox centres *on separate molecules*. The slopes of these lines give the second-order rate constant for the intermolecular electron transfer reaction for the 13- and 23-residue linked heterodimers, and are summarized in Table 6.1. The values obtained are approximately an order of magnitude higher than that obtained from an early study with the wild type azurin from the same source (*P. aeruginosa*) and the flavodoxin from *C. pasteurianum*, however the latter protein has a somewhat higher redox potential than the flavodoxin used from *A. vinelandii*. Very similar rates have been observed for this combination of flavodoxin and azurin, unlinked, free in solution (see Chapter 5).

Intramolecular electron transfer from the flavin to the copper site of the heterodimer would instead manifest itself as flavin reoxidation/copper reduction rates independent on heterodimer concentration. This phenomenon was however not observed, the kinetics at all times being dominated by the heterodimer concentration-dependent intermolecular reaction. It was concluded that no intra-molecular electron transfer occurs within the heterodimers, linked either with 13 or 23 amino acids. Although flavodoxin and azurin free in solution are known to interact in a head on manner, connecting the two proteins by a peptide linker may restrict their motion in solution such that the formation of a productive electron transfer complex is the limiting factor in allowing for intramolecular electron transfer.

Conclusions

The genes for flavodoxin and azurin were cloned so as to express the two proteins as a single polypeptide chain, separated by three flexible hydrophilic peptide linkers varying in length, consisting of glycine repeats interspersed with serine and threonine residues. The three fusion proteins were successfully expressed and purified from *E. coli*, with the FMN group already incorporated. Reconstitution of the copper site with imidazole and copper proved more challenging, with maximum reconstitution rates of 30%, due to damage at the copper binding site that may have been induced either by co-expression with flavodoxin, or long residence times in the cytoplasm as opposed to the regular periplasmic location of azurin. Both the flavin and the reconstituted copper sites however displayed reduction behaviour that was remarkably similar to the unlinked parent proteins, indicating that the redox sites remained intact and unchanged despite co-expression as a single polypeptide chain. No intramolecular electron transfer from the flavin to the copper site was detected however; an indication that even the 23-residue linker was too short to allow the electron transfer sites of the two proteins of the heterodimer to interact. In this sense, the 27-residue linker which proved to be so sensitive to proteolysis may represent a better candidate for a heterodimer active for intramolecular electron transfer, should a method be found to improve its inherent stability.

Chapter 7

Photoinduced electron transfer in TUPS-labelled flavodoxin derivatives

Sharmini Alagaratnam, Ellen de Waal, José A. Navarro, Manuel Hervás,
Miguel Angel De la Rosa, Katalin Tenger, Petro Khoroshyy,
László Zimányi, Marcellus Ubbink and Gerard Canters

Abstract

To further understanding of the electron transfer properties of flavodoxin, four cysteine mutants of this protein with varying distances of the cysteine to the FMN redox cofactor, have been created, expressed, purified and labeled with the photoinducible redox label 8-thiouredopyrene-1,3,6-trisulphonate (TUPS). A novel labeling strategy has been developed that raises the efficiency of labeling to >80%. Laser flash photolysis characterization of the four TUPS-labelled flavodoxin mutants showed that the FMN cofactor could be reduced to its semiquinone state, with the use of ascorbate to generate the highly reducing negative radical form of TUPS. The kinetics of this reduction step were found to be complex, displaying multi-exponential behaviour. Surprisingly, the rates observed for the intramolecular electron transfer reaction between TUPS and the FMN cofactor were very similar for the four positions of TUPS on flavodoxin, seemingly independent of distance.

Introduction

For the study of electron transfer to and between molecules within a maquette of redox proteins, soluble electron donors such as soluble ruthenium complexes [142] and deazariboflavin [132] have the disadvantage that they are non-discriminatory in their action, in principle reducing any redox centre as long as it is accessible and of a suitable redox potential. Selective reduction by the covalent attachment of a photolabel, such as cysteine- or lysine-reactive ruthenium compounds to one of the redox components affords better control over the initiation of the redox reactions (see [159] for a review). An alternative is the pyrene-based molecule 8-thiouredopyrene-1,3,6-trisulphonate, or TUPS, which when attached to the redox proteins cytochrome *c* [172] and azurin[174] was shown to initiate electron transfer to the haem and copper redox centres of those proteins respectively. The label can be covalently attached to the proteins either via lysines or cysteines on the surface of the protein, and has the additional advantage of being commercially available. This has been applied in for the study of inter-molecular ET between a non-covalent complex of cytochrome *c* and cytochrome *c* oxidase, where TUPS was attached to cytochrome *c* [176]. For the study of the electron transfer properties of a heterodimer of flavodoxin and azurin, selective reduction of the flavodoxin molecule would be very useful.

A range of techniques have been used to study the electron transfer properties of flavodoxins from various sources. Structural studies of the redox protein flavodoxin from three different organisms in its three oxidation states have shown that a backbone peptide flip occurs upon reduction of the oxidized protein to the one-electron reduced semiquinone state [28,29,41]. The hydrogen bond then formed between the carbonyl group of a residue within this peptide and the N5 of the FMN cofactor of flavodoxin persists in the two-electron hydroquinone form, and stabilizes both these states over the oxidized form. A slow protein concentration-independent conversion step from the anionic semiquinone form to the neutral or N5 protonated semiquinone, which has an additional broad absorption band between 550 and 700 nm, has also been observed for other flavodoxins by transient spectroscopy initiated by pulse radiolysis [23] and laser flash

photolysis [61]. Put together, this evidence points to the possibility of the conformational change and its associated protonation step limiting the rate of reduction in flavodoxins.

With this in mind, a series of four cysteine mutants was created and labelled by attachment of TUPS to the thiol group of each cysteine (see Fig. 7.1). Two of the mutations, V100C and N105C, were very close to the FMN cofactor, while the two others, S128C and S178C, were positioned halfway down and at the opposite end of the flavodoxin molecule. The semi-classical Marcus theory of biological electron transfer predicts that the rate of electron transfer is strongly dependent on distance [78], as well as the driving force and reorganization energy of the reaction. In the event that the conformational change and/or protonation event is rate-limiting in flavodoxin, the rate of reduction to the semiquinone form is expected to remain constant despite the short distances for the closest mutations, however for the more distant mutants the reduction reaction is expected to slow or even be abolished. The electron transfer reactions within the TUPS-labelled constructs were initiated by laser flash photolysis, and followed by transient spectroscopy, both by taking transient spectra as well as following changes in absorption at single wavelengths. In combination, this allowed the deduction of the full reaction scheme upon photoexcitation of TUPS-flavodoxin, through its various intermediate states. Flavodoxin was found to be reduced to its semiquinone form by the highly reducing reduced radical of TUPS, generated in the presence of ascorbate as a sacrificial electron donor. Rates for this reduction step could be

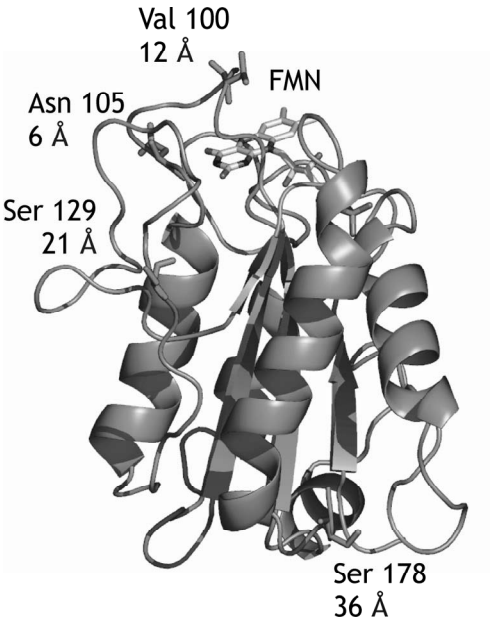

Fig. 7.1. Cartoon representation of C69A flavodoxin (PDB file 1YOB), indicating the four positions that were mutated to cysteines for attachment of the TUPS photolabel in stick form. Distances indicated are through space from the α-carbon of each residue to the N5 position on FMN. The FMN cofactor is also shown as sticks.

determined by multi-exponential fitting of the single wavelength traces, and were found to be independent of TUPS-flavodoxin concentration, indicating the intramolecular nature of the electron transfer reaction. Surprisingly, no distance dependence for the reduction of flavodoxin by the TUPS cofactor was found between the four mutants despite the large difference in distance from the FMN cofactor. Possible explanations for this observation are discussed.

Materials and Methods

Materials and general methods

8-isothiocyanotopyrene-1,3,6-trisulphonate was obtained from Lambda Probes & Diagnostics (Kirchbach, Austria). All other compounds were supplied by Sigma, and were of the purest grade available. Optical absorption was measured using a PerkinElmer Lambda 800 UV-Vis spectrometer. The mass of proteins before and after labelling with TUPS-cystamine was determined using a Q-TOF1 mass spectrometer (MS) (Micromass, Manchester, UK), equipped with an on-line nano-electrospray source. The samples were diluted to a concentration of 3 pmol μl^{-1} in 95:5 water:methanol with 1% acetic acid and introduced into the MS by flow injection analysis. Mass spectra were recorded from *m/z* 50-2500. The protein mass was calculated from the protein envelope by deconvolution with the MaxEnt software.

Mutagenesis of flavodoxin and protein purification

Single cysteines were introduced at positions 100, 105, 129 and 178 in the C69A mutant of flavodoxin II from *A. vinelandii* [200] by site directed mutagenesis using the method of Splicing by Overlap Extension (SOE) by Polymerase Chain Reaction (PCR) [260]. For the sake of simplicity, the mutants will be referred to only by the introduced cysteine mutation, however in all cases the native cysteine at position 69 is no longer present. After the reconstruction PCR, the DNA fragment containing the mutated gene was cloned back into the vector pUC19 with *Hin*dIII and *Kpn*I. Newly introduced restriction enzyme sites

were used to screen for the mutations. Positive clones were sequenced in both directions to ensure no other mutations had inadvertently been introduced, and were then used for expression.

The four flavodoxin mutants were expressed heterologously in *Escherichia coli* strain TG2, and purified according to the established protocols for wild type flavodoxin [200,201], with the exception that 3mM dithiothreitol (DTT) was added to all buffers used during the purification. This was to prevent the formation of flavodoxin dimers, which could complicate the purification. Flavodoxin was pure when the absorption peaks showed a ratio A_{274}/A_{452} of 4.6 – 4.8 [200], at which point the protein was dialysed into 100mM Tris pH 8.0 for long term storage at −20 °C. Finally, to confirm that the mutations were successfully introduced, the proteins were subjected to mass spectrometry. The extinction coefficient at 452 nm of 11.3 mM^{-1} cm^{-1} [12] was used to determine the concentration of flavodoxin.

Preparation of $(TUPS)_2$-cystamine

In an attempt to improve the efficiency of labelling, the original protocol for derivatizing IPTS to give a thiol-specific label [174] was slightly modified. 10 mM of IPTS was incubated with 20 mM cystamine at pH 9.0 for 1 hour at room temperature, in an attempt to label both the amino groups of cystamine with IPTS. This double-TUPS cystamine derivative was separated from unreacted cystamine and IPTS by using a PD-10 column containing Sephadex™ G-25 Medium (Amersham Biosciences). As previously reported [174], the dye-cystamine derivative bound to this column in the presence of 10mM Hepes pH 8.0, and could be eluted with water in fractions of 0.5 ml after washing out the unbound cystamine with 5 ml of buffer. The visible spectra of the fractions were checked individually so as to avoid pooling any unreacted IPTS which eluted after the $(TUPS)_2$-cystamine. Fractions containing $(TUPS)_2$-cystamine were identified by their UV-visible spectrum, distinct from that of IPTS, pooled and then used for thiol-specific labelling of flavodoxin.

Preparation of TUPS-Cys-flavodoxin

The flavodoxin cysteine mutants were first reduced by incubation with a 10-fold excess of DTT for 2 hours at room temperature, to break any intermolecular disulphide flavodoxin dimers that might have formed during storage. The flavodoxin was then separated from DTT by means of a PD-10 desalting column, and immediately added to the reaction mixture which contained a two-fold excess of $(TUPS)_2$-cystamine over flavodoxin (typically 1 mM vs. 0.5 mM), as well as 1 M guanidium hydrochloride and 3 M magnesium chloride, all in 10 mM Hepes pH 8.5. This mixture was left to react overnight at 30 °C.

Before purifying TUPS-labelled from unlabelled flavodoxin, the reaction mixture was first put through a PD-10 column equilibrated in 10 mM Hepes pH 8.0, to remove any unreacted $(TUPS)_2$-cystamine as well as the large amounts of salt. Subsequently, the desalted protein solution was loaded onto a 1 x 10 cm DEAE column, again equilibrated with 10 mM Hepes pH 8.0. The two different forms of the proteins were eluted separately by two step gradients, first to 0.5 M KCl where unlabelled flavodoxin eluted, and then to 1 M KCl, where TUPS-flavodoxin eluted. After pooling and dialysis of the labelled protein peak into 20 mM MES pH 6.0, a small sample of the protein was analysed by mass spectrometry.

Laser flash photolysis

Laser flash photolysis experiments were carried out on two different set-ups, where the details of both systems are as previously described [177,232,261]. The results shown are from the set-up in Szeged, Hungary, where the TUPS-labelled flavodoxin was excited by the third harmonic of a Continuum Surelite-II Nd-YAG laser, with an energy density at 355 nm of a 5 ns laser pulse of 20 mJ/cm^2. A multi-channel diode array and a single wavelength detector were used in combination in the same light path made it possible both to collect time resolved difference spectra as well as follow transient absorption changes at single wavelengths, with the switch of a single mirror. All measurements were conducted in 20 mM MES pH 6.0 at 20°C, with TUPS-flavodoxin concentration varied between 20 and 60 μM. Ascorbate was added to a final concentration of 5 mM with 50 mM NaCl for experiments involving the reduced radical of TUPS. Oxygen was removed from the sample

by the addition of 20 mM glucose, 0.1 mg/ml glucose oxidase and 10 μg/ml catalase. Care was taken not to exhaust the sample with excessive excitation, as the system is non-regenerating.

Results

Creation and labelling of cysteine mutants with TUPS

The four individual cysteine mutations were successfully introduced into the gene for flavodoxin, as confirmed by DNA sequencing of the four plasmids. Both expression and purification of the mutants were comparable to that of wild type protein, yielding up to 15 mg of cysteine-mutated flavodoxin per litre of culture. All mutants gave the exact mass predicted from the amino acid sequence, with the predicted changes in mass due to the mutations. The adapted procedure for generating $(TUPS)_2$-cystamine resulted in an excess of unreacted IPTS. The former was carefully separated from the latter to avoid including IPTS in the reaction with flavodoxin. Upon application of the desalted flavodoxin-$(TUPS)_2$-cystamine reaction mixture to the DEAE column, both labelled and unlabelled flavodoxin bound to the top of the column, but could be completely separated from each other by the application of the two step gradients. The TUPS-labelled flavodoxin carries three additional negative charges compared to unlabelled flavodoxin and as such eluted from the DEAE column at higher salt concentration than unlabelled flavodoxin. The molar ratio of labelled:unlabelled flavodoxin was up to 4:1. Mass spectrometry of each of the four cysteine mutants of flavodoxins with TUPS attached showed a single peak, the mass of which corresponded to the mutant flavodoxin modified by TUPS-

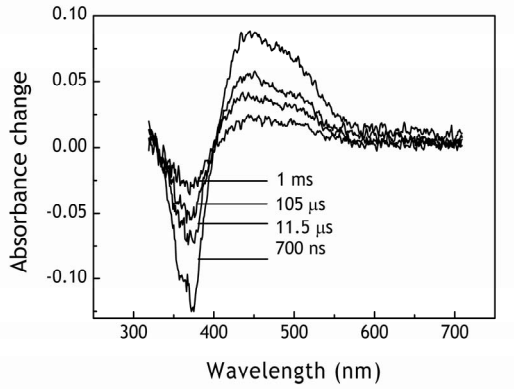

Fig. 7.2. Time-resolved transient spectra of 30 μM TUPS-N105C flavodoxin in 20 mM MES pH 6.0 in the *absence* of ascorbate, at the indicated time points.

cystamine. The mass of each of the proteins was found to increase by 575 Da, consisting of ½ cystamine (76 Da) linker and TUPS (499 Da) molecules.

Transient absorption characterization of TUPS-flavodoxin in the absence of ascorbate

All four TUPS-labelled cysteine mutants were subjected in turn to analysis by flash photolysis, as described in Materials and Methods. The TUPS-labelled mutants all showed the same behaviour upon excitation; the transient spectra of TUPS-N105C flavodoxin are shown in Fig. 7.2 as an example. The transient spectra at the four time points were dominated by the appearance then decay of the TUPS triplet, with no detectable reduction of the FMN cofactor in flavodoxin. Spectra taken at longer timescales (up to 10 ms) did not show any evidence of the presence of flavodoxin semiquinone.

Transient absorption characterization of TUPS-flavodoxin in the presence of ascorbate

Due to the apparent inability of the TUPS triplet to reduce flavodoxin, an alternative approach involving the presence of ascorbate in the sample was taken. The TUPS triplet has been shown to oxidize ascorbate to form the negative radical of TUPS, which is a

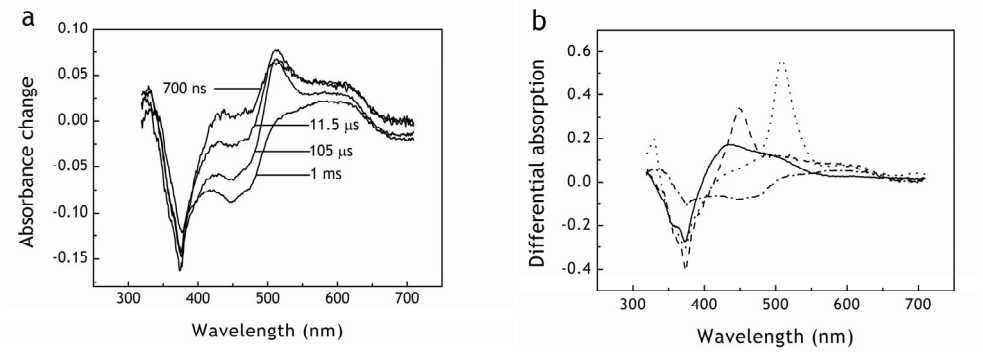

Fig. 7.3. (a) Time-resolved transient spectra of 30 µM TUPS-N105C flavodoxin in 20 mM MES pH 6.0 with 5 mM ascorbate and 50 mM NaCl, at the indicated time points. (b) Base difference spectra used for fitting of the time-resolved transient spectra: Solid line, TUPS triplet (also marked A); dashed line, TUPS positive radical with flavodoxin semiquinone (B); dotted line, TUPS negative radical (C) and dashed and dotted line, flavodoxin semiquinone (D).

strong reductant [177]. Ascorbate was added to a final concentration of 5 mM, as well as sodium chloride to a concentration of 50 mM, to promote the association between the negatively charged ascorbate and TUPS-flavodoxin molecules.

Transient spectra at four time points were again taken of each of the mutants, as illustrated in Fig. 7.3a for TUPS-N105C flavodoxin. Fig. 7.3b shows the spectra of the various intermediate species that are expected, on the basis of the known absorption spectra of the various TUPS and flavodoxin species [177]. Again, the transient spectral changes were qualitatively indistinguishable for the four different TUPS-labelled mutants of flavodoxin. As in the non-ascorbate sample, the first spectrum at 700 ns shows that the TUPS triplet has been formed. However, there is also an additional component to the spectrum arising from the presence of TUPS reduced radical. The latter species can be seen to dominate the spectrum taken at 11.5 μs. At 105 μs, the relative absorption of the reduced radical was found to have decreased slightly, while the spectrum of flavodoxin semiquinone began to be distinguishable. The final spectrum taken at 1 ms consisted purely of the flavodoxin semiquinone, with no triplet or reduced radical species present.

The effects of the concentrations of ascorbate and salt on the observed rates were tested independently. Increasing the ascorbate concentration from 0 to 20 mM increased the rate of TUPS reduced radical formation four-fold (see Fig. 7.4), but the rate of flavodoxin reduction remained constant, as may be expected from an intramolecular reaction. The yield of both reduction steps was unchanged over this range. The addition of up to 200 mM NaCl again accelerated the rate of TUPS reduced radical formation by seven-fold, while the rate of flavodoxin reduction was again unchanged. The yield of flavodoxin semiquinone was improved

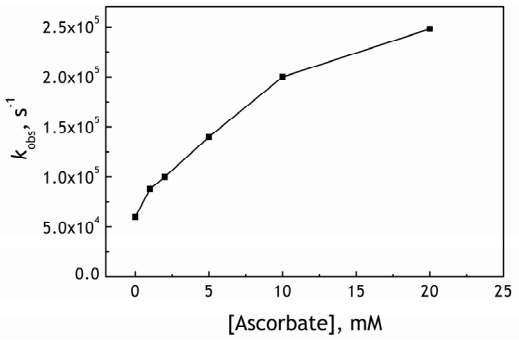

Fig. 7.4. Dependence on ascorbate concentration of the observed rate constant, k_{obs} at 465 nm for the formation of TUPS reduced radical by ascorbate for 20 μM TUPS-N105C flavodoxin, in 20 mM MES pH 6.0.

marginally by the addition of salt, almost doubling with 50 mM NaCl, while the effect tailed off at approximately 100 mM NaCl.

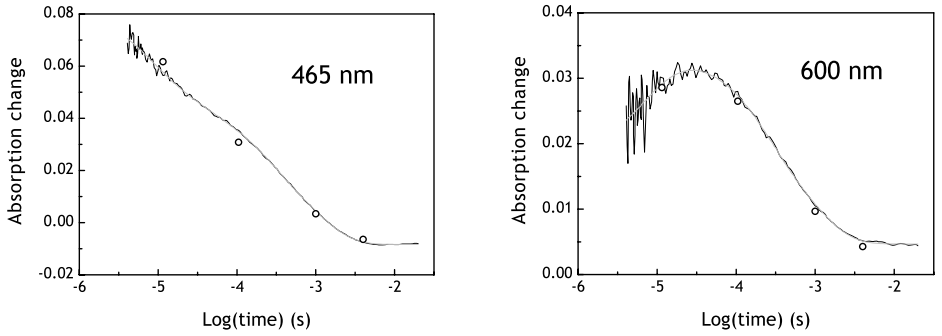

Fig. 7.5. Black lines: Changes in absorption of 20 μM TUPS-S178C flavodoxin in 20 mM MES pH 6.0 in the presence of 5 mM ascorbate and 50 mM NaCl, followed at 465 nm and 600 nm. Grey lines: Multi-exponential fit of absorption changes. Open circles: Normalized averages from the OMA spectra at 465 and 600 nm respectively.

The changes in absorption of the TUPS-flavodoxin over time were also followed at 465 and 600 nm, chosen on the basis of the transient spectra as good reporter wavelengths for the interconversion of the various species. Representative traces over a logarithmic timescale for the two wavelengths are shown as solid black lines in Fig. 7.5, for the TUPS-S178C flavodoxin. Absorption intensities at these two wavelengths could also be determined from averages of the transient spectra at the four different time points at which the spectra were taken. These are plotted as open circles in Fig. 7.5, and can be seen to correlate well with the continuous single wavelength traces. The traces showed multi-exponential behaviour, where a simple bi-exponential fit was insufficient for describing the traces. For kinetic traces at both 465 and 600 nm, up to five exponentials were required for a good fit, shown as solid grey lines in Fig. 7.5. Traces were taken at three different concentrations (20, 40 and 60 μM) of TUPS-flavodoxin for each mutant, and fitted as above. For all the mutants, the first two exponentials for both wavelengths were at 10^4 – 10^5 s^{-1} significantly faster than the last three, which were in turn of a similar order of magnitude between 10^2 and 10^3 s^{-1}, varying only in amplitude. Table 7.1 summarizes these rates for the various mutants, where a single decay exponential was obtained from a

Table 7.1. Observed rates of absorption change, k, in s^{-1}, for the four mutants of flavodoxin labelled with TUPS. $k1$ and $k2$ were fitted for both the wavelengths 465 and 600 nm simultaneously, and a weighted average of the rates $k3$, $k4$ and $k5$ was calculated as described for each of the two wavelengths individually.

	TUPS-V100C flavodoxin			TUPS-N105C flavodoxin			TUPS-S129C flavodoxin			TUPS-S178C flavodoxin		
	20 µM	40 µM	60 µM	20 µM	40 µM	60 µM	20 µM	40 µM	60 µM	20 µM	40 µM	60 µM
k1	4.29×10^{4}	4.77×10^{4}	6.31×10^{4}	1.79×10^{5}	1.83×10^{5}	1.27×10^{5}	9.29×10^{4}	1.02×10^{5}	2.59×10^{5}	1.25×10^{5}	9.59×10^{4}	1.40×10^{5}
k2	2.37×10^{4}	2.38×10^{4}	1.90×10^{4}	3.16×10^{4}	3.60×10^{4}	1.97×10^{4}	2.39×10^{4}	2.38×10^{4}	3.38×10^{4}	2.34×10^{4}	2.71×10^{4}	3.07×10^{4}
‹*k3-5*›												
465 nm	5.50×10^{3}	4.84×10^{3}	3.01×10^{3}	2.86×10^{3}	3.18×10^{3}	2.71×10^{3}	2.27×10^{3}	2.66×10^{3}	3.13×10^{3}	2.28×10^{3}	3.58×10^{3}	3.56×10^{3}
600 nm	4.82×10^{3}	5.24×10^{3}	4.99×10^{3}	2.29×10^{3}	2.99×10^{3}	3.00×10^{3}	2.24×10^{3}	3.17×10^{3}	3.52×10^{3}	2.59×10^{3}	4.36×10^{3}	4.90×10^{3}

weighted average of the last three decay exponentials. These values were found to be strikingly similar between the four mutants, considering the large variation in distance from the FMN co-factor of the various positions of the introduced cysteines.

Finally, the transient spectra could also be fitted using the spectra of the expected intermediates, thus deconvoluting them to their constituent components. This allowed the determination of the relative concentrations of each of the components at the four time points. These are plotted as symbols in Fig. 7.6, for 20 µM of TUPS-S178C flavodoxin, joined by lines.

Discussion and conclusions

The adapted procedure for generating $(TUPS)_2$-cystamine resulted in an excess of unreacted IPTS, which was important to remove as IPTS is capable of reacting with the many lysines on the surface of flavodoxin. The large amount of salt present

during the labelling reaction served to shield the charges on the negatively charged TUPS and flavodoxin molecules and promote their association, and increased the efficiency of labelling 4-fold when compared to a similar reaction in the absence of salt. Mass spectrometry confirmed that the flavodoxin mutants had successfully been labelled with TUPS via the cystamine linker to the free thiol groups of the introduced cysteines, and could successfully be purified from unlabelled flavodoxin.

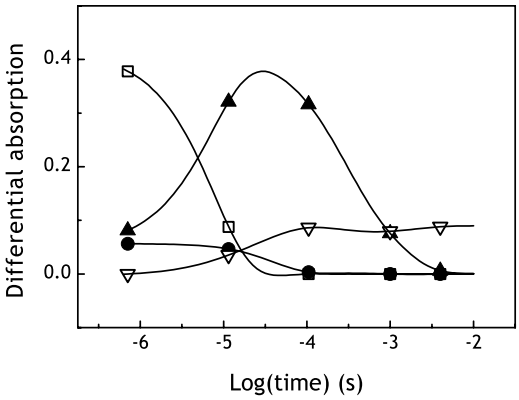

Fig. 7.6. Symbols joined by lines showing the relative amount of the various species present in time as determined from the deconvolution of the transient spectra where TUPS triplet is represented by open squares, TUPS reduced radical by closed triangles, TUPS oxidized radical plus flavodoxin semiquinone by closed circles and finally flavodoxin semiquinone alone by open triangles.

The absence of flavodoxin semiquinone upon excitation of any of the TUPS-flavodoxin mutants, even on relatively long timescales, may be explained by the fact that the driving force for the forward (750 mV for TUPS triplet to oxidized flavodoxin) reaction is smaller than that for the reverse (1050 mV for flavodoxin semiquinone to TUPS oxidized radical). These differences are plotted schematically in Fig. 7.7. In the case of TUPS-labelled cytochrome *c*, the reverse is true, leading to rate constants of haem reduction by TUPS triplet which were one to two orders of magnitude larger than its reoxidation [172]. In the case of the flavodoxin, the reverse reaction may in fact be faster than the forward, preventing the accumulation and detection of flavodoxin semiquinone.

The presence of ascorbate in the sample induces striking changes in the character of the transient spectra, where the overall reaction scheme is summarized in Fig. 7.6 and 7.8. TUPS triplet is found to have been formed immediately after the laser flash excitation, before being converted into TUPS negative radical through the oxidation of ascorbate. This process is largely completed by 10 μs [177]. The subsequent decrease in concentration of

TUPS reduced radical is mirrored by the emergence of the flavodoxin semiquinone, due to intramolecular electron transfer between the two redox centres, as confirmed by the dependence of this rate on the ascorbate concentration (Fig. 7.4). The intramolecular character of this reaction is confirmed by the concentration independence of this step (see Table 7.1).

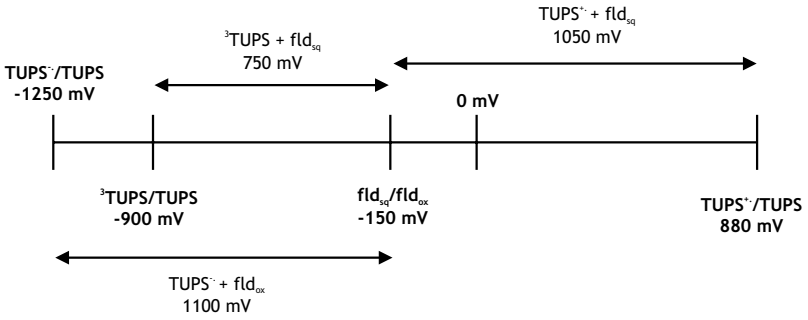

Fig. 7.7. Redox potentials of the various TUPS and flavodoxin couples, against NHE.

The spectral changes seen for the four TUPS-labelled flavodoxin mutants were qualitatively identical on both the experimental set-up used (see Materials and Methods), although the set-up for which all the results are shown had quantum efficiencies and thus signal amplitudes which were significantly higher. Through the deconvolution of the transient spectra, a small proportion of TUPS oxidized radical and flavodoxin semiquinone (Fig. 7.6, closed circles) was also found to be present immediately after excitation at 700 ns, decaying away by 100 μs. This may be due to the formation of solvated electrons, which is known to occur in high photon flux (›60 mJ/cm^2) [170]. It is likely that the resulting TUPS oxidized radical and flavodoxin semiquinone recombine, returning both species to their ground state by 100 μs.

The reason for the multi-exponential decay of TUPS reduced radical to form flavodoxin semiquinone was not immediately obvious, although similar behaviour has been observed for the reduction of TUPS positive radical by reduced haem in a system with TUPS covalently attached to cytochrome c via a cysteine-cystamine linkage [261]. There, molecular dynamics on the system indicated that TUPS could interact directly and occupy

several discrete positions on the protein surface due to the flexible linker, each of which may result in a different decay rate. A similar study to identify possible interactions between the surface of flavodoxin and TUPS is currently underway in our laboratory.

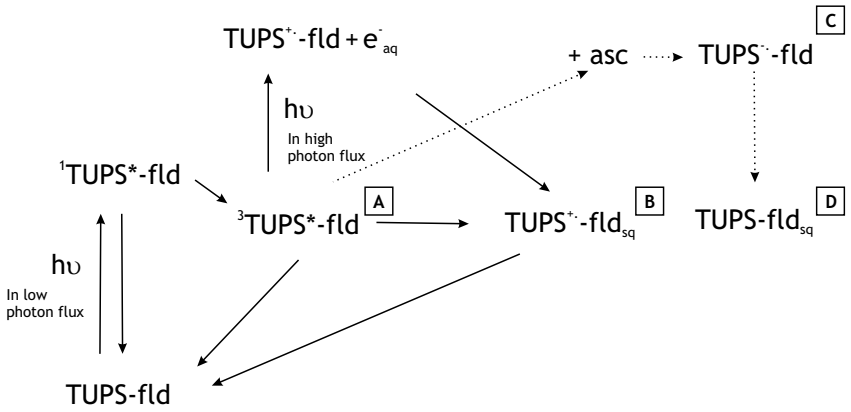

Fig. 7.8. Reaction scheme for TUPS-flavodoxin (annotated TUPS-fld). The singlet and triplet excited states of TUPS shown with the superscripts 1 and 3 respectively, with TUPS triplet also marked with the boxed letter A (see Fig. 7.3b). The oxidized and reduced radicals of TUPS are shown as $TUPS^{+\cdot}$ and $TUPS^{-\cdot}$, and are again marked B and C respectively. The solvated electron released in high photon flux is denoted e^-_{aq}. The dotted line shows the reduction route forming flavodoxin semiquinone (fld_{sq}, D) in the presence of ascorbate (asc).

More intriguing was the invariability of flavodoxin reduction rate by TUPS reduced radical, despite its various attachment points on flavodoxin. As can be seen from Fig. 7.1, the introduced cysteines vary greatly in their distance from the FMN cofactor. It is possible to use a generalized formula for the estimation of electron transfer rate [80]. With that, for an idealized activationless reaction where the driving force equals the reorganization energy, the rate of electron transfer could be expected to vary from 10^{10} s^{-1} for the distance of 6 Å for the N105C mutant, to 10^{-6} s^{-1} for the distance of 36 Å for the S178C mutant. The relatively slow reduction rates observed for the closest TUPS attachment positions, V100C and N105C, may be evidence of gating of the electron transfer reaction by the protonation of the FMN N5, effectively limiting the rate. The fact that the reduction rates for the more distant positions S128C and S178C remain within the same order of magnitude is however more of a surprise.

The reason for the unexpected independence of rate on distance is as yet unclear. One possible explanation could be that TUPS attached through the cystamine linker may have the freedom to sample different orientations with respect to the flavodoxin, or even associate preferentially with a positive patch on the flavodoxin surface and reside there for a longer time. The 10-bond length of the linker connecting TUPS and the cysteine residue would certainly allow a fair degree of flexibility in the mutants V100C, N105C and S128C, while the most cysteine most distant from the FMN, S178C, is in fact the penultimate residue at the C-terminus of the protein, which may afford even greater flexibility. Indeed, considerable mobility has previously been observed by EPR for a spin label attached to a surface cysteine on the redox protein azurin with a much shorter linker [262]. It is hoped that the molecular dynamics studies on TUPS-labelled flavodoxin currently being undertaken may clarify the situation further.

Chapter 8

A ^{31}P NMR study on monomeric *A. vinelandii* flavodoxin

Sharmini Alagaratnam, Gerard W. Canters and Marcellus Ubbink

Abstract

The electron self-exchange (e.s.e.) behaviour of the monomeric Cys69Ala mutant of flavodoxin II from *Azotobacter vinelandii* was characterised by using ^{31}P NMR. The ^{31}P spectrum of the protein, heterologously expressed in and purified from *E. coli*, showed a single peak deriving from the dianionic phosphate group of its FMN cofactor. The peak shape and position were similar to what has previously been observed for other flavodoxins, as were the changes observed upon reduction of the protein. E.s.e. was found to be slow ($<10^3$ $M^{-1}s^{-1}$), both between the oxidised and semiquinone and between the semiquinone and hydroquinone states of the protein, as deduced from the shape of the phosphorus peak upon reduction as well as T_1 measurements. The addition of salt did not affect the observed rate. However the addition of the small mediator methyl viologen accelerated e.s.e. of flavodoxin. This indicates that steric hindrance, rather than unfavourable electrostatics or a high energy barrier, is likely to be the cause of the slow rate seen in the absence of the mediator.

Introduction

The small flavoprotein flavodoxin has been widely applied as a model for studies on biological electron transfer, for a number of reasons including its ease of expression and purification, as well as its extensive physical and structural characterization (see [1] for a general review). The three redox states of flavodoxin, the oxidised form (ox), the one-electron reduced semiquinone (sq) and the two-electron reduced hydroquinone (hq), are spectroscopically distinct, allowing for direct monitoring of changes in the redox state of the flavin mononucleotide (FMN) cofactor bound to the protein. Flavodoxin in its semiquinone state has for example been used as an electron donor to cytochrome *c* from a number of sources [48], demonstrating the influence of electrostatic interactions and ionic strength in appropriately orienting proteins for electron transfer [263]. Flavodoxin can recognize and distinguish between potential partner proteins on the basis of these effects, and thus establish biological specificity.

Electrons can also be exchanged between the different redox forms of a single protein that are present in solution together. The system at equilibrium is perpetually self-generating and analysis is simple. While this reaction, known as electron self-exchange or e.s.e., is not of direct biological consequence, its study can nevertheless be informative. In one recent example, the rate of e.s.e., k_{ese}, was determined for different homo- and heterodimers of the blue copper protein azurin and allowed conclusions on the correlation between redox centre accessibility and orientation and rate to be drawn [126].

The downside of the simplified system involving a single protein self-exchanging is that spectroscopic or other changes that could otherwise be used to characterize the electron transfer reaction are now cancelled out, as below:

$$P_{ox} + P_{red} \overset{k_{ese}}{\leftrightarrows} P_{red} + P_{ox}$$

k_{ese} can be determined from the line broadening of the NMR signals of nuclei close to the redox centre when one of the species in the mixture is paramagnetic in character,

oxidized azurin in the example of the azurin dimers above. In short, the presence of a paramagnetic species leads to an additional mechanism for both spin-spin and spin-lattice relaxation of the nuclei in the NMR experiment. Changes in the relaxation time for a sample containing a known concentration of the paramagnetic species can be used to calculate k_{ese} [264].

This method has also been applied to the study of e.s.e. in flavodoxin from *Megasphaera elsdenii* [60], by following the ^{31}P resonance of the phosphorus group of the FMN cofactor. Contrasting behaviour was noted for the two redox couples, namely the ox/sq and sq/hq couples of flavodoxin. Partial one-electron reduction of flavodoxin resulted in a broad ^{31}P peak corresponding to the paramagnetic semiquinone form. This did not affect the oxidised protein ^{31}P resonance, which although reduced in intensity remained sharp and was superimposed onto the broad peak, indicative of a slow e.s.e. rate. Further reduction to a mixture of the sq and hq forms of flavodoxin however led to extensive line broadening of the phosphorus peak and no superimposed lines, as a result of the fast e.s.e. reaction between the two forms. k_{ese} for the two equilibria were quoted as unimolecular rates, however their relationship with the bimolecular process of e.s.e. was unclear. A follow-up proton NMR study of peaks corresponding to methyl groups of residues close to the FMN in the same protein showed k_{ese} between the quinone and semiquinone under the experimental conditions to be at least 350 times slower ($< 5.7 \times 10^3\ M^{-1}\ s^{-1}$) than between the semiquinone and hydroquinone ($> 20 \times 10^5\ M^{-1}\ s^{-1}$) [265].

In light of investigations into the kinetic behaviour of the C69A *Azotobacter vinelandii* flavodoxin II (here onwards referred to as the C69A flavodoxin) with free flavins, azurin and surface-attached photolabels carried out in our laboratory, an investigation into the ^{31}P NMR characteristics and behaviour of this protein was carried out. The C69A mutant has been shown to be spectroscopically and electrochemically identical to the wild type [26], but does not form disulphide dimers as the wild type does [217]. The changes observed upon reduction to its semiquinone and hydroquinone forms are described here and the resulting information on the kinetics of the e.s.e. reactions in this flavodoxin detailed. In contrast to the *M. elsdenii* flavodoxin, no line-broadening was observed for either the ox/sq or the sq/hq couples even under high salt conditions, signifying slow

exchange in both cases. Interestingly however, in a sample containing a mixture of sq/hq forms of flavodoxin, the presence of a small soluble mediator led to line-broadening of 10 Hz, indicative of e.s.e. between these two states. The addition of salt enhanced this effect further. These differences are discussed with reference to the structural characteristics of the *A. vinelandii* flavodoxin as well as differences around the redox centre in the two flavodoxins.

Materials and Methods

C69A flavodoxin II from *A. vinelandii* was expressed heterologously in *Escherichia coli* strain TG2 from a pUC19-derived plasmid containing the mutated Cys69Ala flavodoxin gene, kindly provided by Dr. Carlo van Mierlo of Wageningen University, the Netherlands. The culture was induced with 1 mM IPTG upon inoculation, and grown for 24 hours at 37°C before harvesting. The protein was purified according to described protocols and was considered to be pure when the absorption peaks showed a ratio A_{274}/A_{452} of 4.9 [12]. The extinction coefficient at 452 nm of 11.3 mM^{-1} cm^{-1} [12] was used to determine the concentration of flavodoxin in the ox form.

All experiments were performed in 100 mM Tris buffer pH 8.5, with flavodoxin at concentrations between 1 and 3 mM in a sample of approximately 500 µl. The samples also contained 6% D_2O to lock the magnetic field. An anaerobic stock of either 0.1 or 1 mM sodium dithionite was used to reduce flavodoxin. The high pH of the buffer solution has been noted to assist in achieving full reduction of flavodoxin with dithionite [20]. The protein was first made anaerobic by gentle bubbling with argon, then sealing the NMR tube with a rubber stopper. Two different approaches were then used to vary the level of reduction of the sample. The first involved fully reducing flavodoxin by anaerobic addition of the required amount of dithionite, typically between 3 – 5 equivalents, with a gas-tight Hamilton syringe. The sample could then be reoxidized in steps by the injection of small volumes of air into the sample tube with gentle mixing. Alternatively, sub-equimolar amounts of dithionite were consecutively added to the anaerobic flavodoxin sample, leading to increasing concentrations of reduced flavodoxin. The visible spectra of

flavodoxin at different levels of reduction were measured in the NMR tube in a custom-made holder with a PerkinElmer Lambda 800 UV-Vis spectrophotometer using fibre-optic cables fitted with immersion probes (Hellma GmbH & Co, Mülheim, Germany) to guide the beam to and from the spectrophotometer.

^{31}P NMR experiments were performed at 14.1 T on a Bruker DMX spectrometer, using a BBO probe. All spectra were taken at 298 K under proton decoupling conditions. All chemical shifts are quoted relative to a standard of 85% phosphoric acid. T_1 relaxation times were measured by the inversion recovery method, using delay times of 0.15s, 1s, 2s, 3.5s, 5.5s, 9s, 13s, 20s, 29s and 37s. Signal intensities were fitted to the single exponential:

$$y = A \cdot \left[1 - 2e^{-\left(\frac{x}{T_1}\right)} \right]$$

using Origin 7.5 (OriginLab Corporation, Northampton, MA). T_2 relaxation times were calculated from the estimated line width of the peak.

Results and Discussion

1D ^{31}P spectrum of oxidized C69A flavodoxin II

Fig. 8.1a shows the one dimensional ^{31}P spectrum of the heterologously expressed oxidised C69A flavodoxin. A single phosphorus resonance is observed at 6.0 ppm, deriving from the phosphate group at the 5'-terminal of the FMN ribityl side chain. The fact that the dianionic form of FMN free in solution at pH 8.0 resonates at a similar position of 5.1 ppm [32] strongly suggests that the FMN phosphate group in oxidized C69A flavodoxin is bound to the apoflavodoxin as a dianionic species. This value is similar both to that reported for the wild type flavodoxin II isolated directly from the same *A. vinelandii* strain, 6.05 ppm [12], and for the phosphate FMN resonances in flavodoxins from *M. elsdenii* [60], *C. beijerinckii* [266], *Anabaena* 7120 [32] and wild type flavodoxin from *A. vinelandii* OP [267]. In all these cases, the same conclusion was drawn on the charge of the phosphate group (see Table 8.1).

While ^{31}P NMR spectroscopy on flavodoxin purified from *A. vinelandii* OP cells grown under N_2-fixing conditions identified three phosphate groups either covalently or non-covalently bound to the protein [267], in flavodoxin II from *A. vinelandii* ATCC 478 only the FMN phosphate group has been identified, regardless of whether the cells were grown in the presence of ammonium or under N_2-fixing conditions [12]. The single phosphorus resonance in the ^{31}P spectrum of the C69A flavodoxin II expressed heterologously in *E. coli* confirms the absence of any other protein-associated phosphate groups in this protein.

Table 8.1. Phosphorus chemical shifts of FMN in the oxidized and reduced forms of flavodoxin (fld) from various sources, in ppm, relative to 85% phosphoric acid, with sample pH and temperature. Unavailable details are indicated by a dash.

Flavin	Oxidised	Reduced	pH	Temperature (K)
FMN [60,266]	5.1	5.1	9.0	298
A. vinelandii ATCC 478 C69A fld II	6.0	6.0	8.5	298
A. vinelandii ATCC 478 wt fld II [12]	6.0	–	7.5	278
A. vinelandii OP [267]	6.3	6.4	8.0	293
Anabaena 7120 [32]	5.4	5.9	8.0	–
C. beijerinckii [266]	5.7	5.8	8.0	298

Reduction of C69A flavodoxin II with dithionite

The two different approaches taken for achieving stepwise oxidation and/or reduction of flavodoxin had consequences both for the final extent of reduction achieved as well as the homogeneity of the sample. Addition of a small molar excess of dithionite over flavodoxin to an anaerobic sample of the protein resulted in the flavodoxin being almost fully reduced to its hydroquinone state (›98%), while the semiquinone represented ‹2% of the total flavodoxin. Subsequent injection of aliquots of air resulted in stepwise reoxidation of the sample. However, as the reoxidation process was relatively slow, despite mixing, the upper part of the samples continued to reoxidize in the NMR tube during measurement, leading to inhomogeneous samples. In addition, the extent of reoxidation by

this method was difficult to control. The alternative method of stepwise reduction of a fully oxidized flavodoxin sample by the addition of increasing amounts of dithionite was more easily controllable. This method however required the addition of much more dithionite to achieve the same level of reduction as the first method, most likely due to the small quantities of oxygen that are inadvertently introduced during the addition of dithionite. Also, the end point of flavodoxin reduction contained much higher concentrations of semiquinone, ranging from 8 to 30% depending on the experiment. The redox potential of dithionite is known to increase at higher concentrations [20], which may explain why flavodoxin hydroquinone reoxidized upon the addition of too large an excess of dithionite.

It is worth noting that flavodoxin is reduced by the dissociation product of dithionite, the SO_2^- radical, rather than by dithionite ion itself, $S_2O_4^{2-}$. Both species are however paramagnetic in character, which may affect the relaxation of the phosphorus nuclei as described above. Previous experiments on the *A. vinelandii* OP flavodoxin showed that addition of the paramagnetic ion Mn^{2+} up to a concentration of 0.1 mM had no effect on the line width of the FMN phosphorus group resonance [268], thus indicating that the phosphate group is buried within the protein

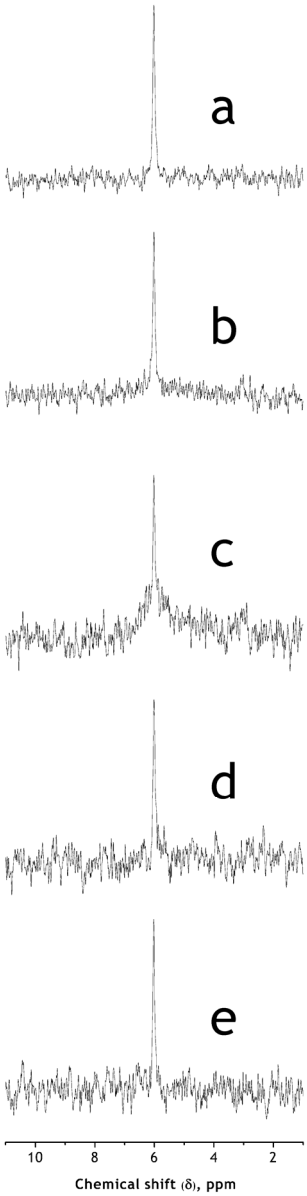

Fig. 8.1. ^{31}P NMR spectrum of 1 mM of C69A flavodoxin in 100 mM Tris, pH 8.5 at a) 100 % ox, b) 40% sq and 60% ox, c) 64% semiquinone and 36% ox and hq, d) 10% sq and 90% hq, and e) 2% sq and 98% hq.

and is not in contact with the solvent. Thus it is unlikely that the addition of dithionite over the course of the experiment will affect the relaxation properties of the flavodoxin.

Changes in the 1D spectrum upon reduction to the sq and hq

Upon reduction of C69A flavodoxin to its semiquinone form, a very broad peak emerges under the sharp oxidized flavodoxin peak. The latter decreases in intensity but remains sharp (see Fig. 8.1b and c). This broad peak represents the semiquinone form of flavodoxin, and as far as could be determined is also centred at 6.0 ppm. Similar effects have been observed for flavodoxins from *M. elsdenii* [60], *D. vulgaris* [269], and *A. vinelandii* OP [268], with line width of the semiquinone form increasing in that order. It has been suggested that this is due to the shorter distance between the phosphate group and the isoalloxazine moiety of the FMN in the different proteins [266]. However, the recently determined structure of the flavodoxin from *A. vinelandii* ATCC 478 ([246], see Chapter 4) has shown that this is not the case, and that in fact this distance is longest in this flavodoxin.

This is while the semiquinone peak is similar in width to that for the *A. vinelandii* OP flavodoxin semiquinone, which displays the broadest peak of all flavodoxin semiquinones. In general, the extent of line broadening is influenced not only by the distance-dependent dipolar relaxation mechanism, but also by contact relaxation through delocalization. A combination of the two mechanisms as a result of even partial electron delocalization may explain the observed line widths.

Further reduction to the hydroquinone results in the intensity gain of the FMN resonance as a sharp line at the same position (6.0 ppm) as the oxidized resonance, which increases again in intensity (See Fig. 8.1d and e). Marginal upfield shifts of the hydroquinone peak of between 0.1 to 0.2 ppm compared to the oxidized peak have been noted for the flavodoxins from *C. beijerinckii* [266], *M. elsdenii* [60] and *A. vinelandii* OP [268], while the reduction of the *Anabaena* flavodoxin shifted the FMN resonance by 0.5 ppm [32] (see Table 8.1). No such changes were observed for the C69A flavodoxin however, indicating that the phosphate group of FMN does not experience any significant changes

in its environment upon reduction from the oxidized to the hydroquinone state of the flavodoxin.

Effect of reduction on C69A flavodoxin II T_1 *and* T_2 *relaxation times*

Table 8.2. T_2 relaxation times for *A. vinelandii* C69A flavodoxin II at various reduction levels, with ox and hq after the percentage of semiquinone denoting the dominant species present in the sample.

Reduction level	T_2 (ms)
25% sq/ox	22.1 ± 0.2
40% sq/ox	18.2 ± 0.3
68% sq/q/hq	14.9 ± 0.4
25% sq/hq	22.2 ± 0.5
10% sq/hq	19.6 ± 0.4
6% sq/hq	20.4 ± 0.4

T_1 and T_2 relaxation times were determined for C69A flavodoxin with different degrees of reduction, and are summarized in Tables 2 and 3. The T_2 relaxation times were determined from the line widths of the FMN phosphorus peak at 6.0 ppm, and remain relatively unchanged regardless of the degree of reduction (see Table 8.2). Despite the fact that accurate determination of the line width was complicated by the presence of the broad semiquinone peak under the sharp quinone or hydroquinone peak, relaxation times of between 15 and 25 ms were found for all the samples. No line broadening could be detected in samples containing a mixture of either ox and sq or sq and hq flavodoxin, even at high concentrations of semiquinone. This behaviour corresponds to slow self-exchange for both the ox/sq and sq/hq equilibria, where an upper limit of 10^4 M^{-1} s^{-1} was determined for the exchange of electrons between the three different forms.

This is in stark contrast to the behaviour observed for the *M. elsdenii* flavodoxin, where line broadening of the FMN phosphorus was observed in samples containing a mixture of the sq and hq forms. While the presence of the semiquinone had no effect on the line width of the resonance line of the oxidized form like in the *A. vinelandii* C69A flavodoxin, a sample containing 98% hydroquinone and just 2% semiquinone exhibited extensive line broadening of the FMN phosphorus peak.

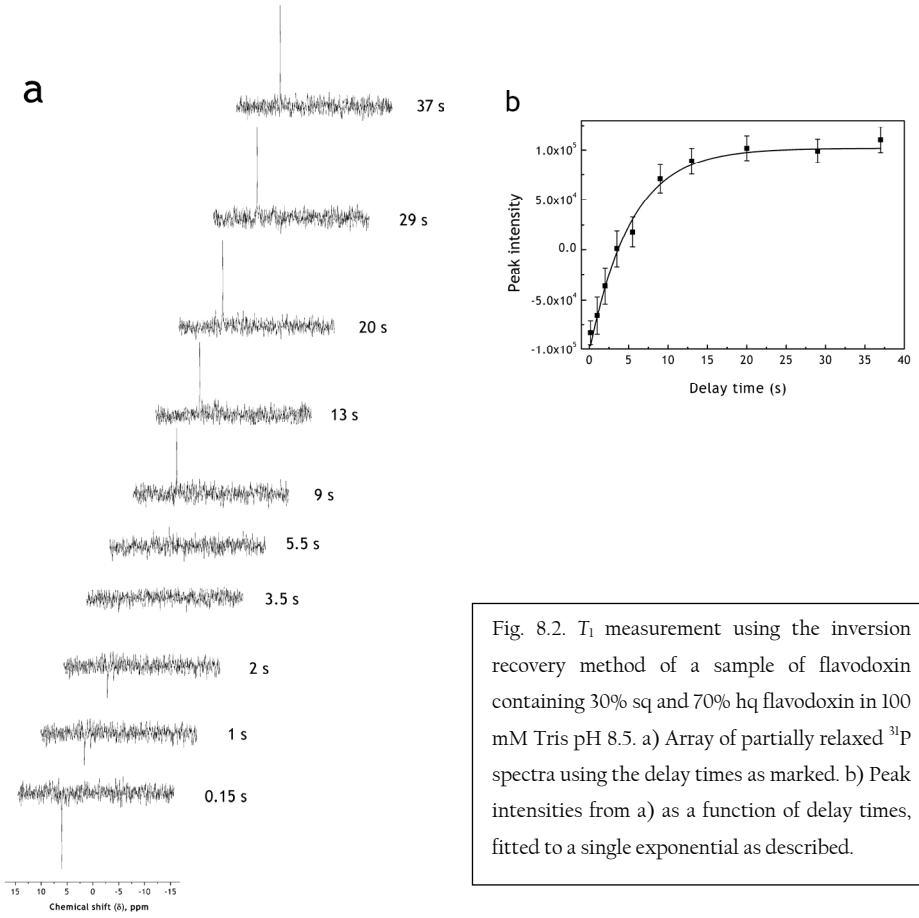

Fig. 8.2. T_1 measurement using the inversion recovery method of a sample of flavodoxin containing 30% sq and 70% hq flavodoxin in 100 mM Tris pH 8.5. a) Array of partially relaxed ^{31}P spectra using the delay times as marked. b) Peak intensities from a) as a function of delay times, fitted to a single exponential as described.

An example of the inversion recovery experiment performed to determine T_1 is shown in Fig. 8.2, including the fitting of the peak intensities as a function of delay times to a single exponential as described in Materials and Methods. As with the T_2 measurements above, the presence of the broad sq peak under the sharp ox or hq peak made accurate determination of the peak amplitudes more difficult at high concentrations of semiquinone. This may influence accurate determination of T_1 in particular and may be one reason for the observed large spread in the values obtained. Although at later stages of the experiment relatively high concentrations (up to 10s of mM) of dithionite are present, the paramagnetic dithionite ions are not expected to have direct access to the FMN phosphate group and affect. The line width of the FMN phosphorus peak was shown not to be affected by the addition of up to 0.1 mM of the paramagnetic manganese ion [268].

Table 8.3. T_1 relaxation times for *A. vinelandii* C69A flavodoxin II at various reduction levels, with ox and hq after the percentage of semiquinone denoting the dominant species present in the sample.

Reduction level	T_1 (s)
100% ox	7.3 ± 0.3
65% sq/ox	4.8 ± 0.3
83% sq	6 ± 1
59% sq/hq	4.6 ± 0.4
48% sq/hq	5.3 ± 0.6
31% sq/hq	5.5 ± 0.3

Importantly, T_1 remains relatively unchanged at different reduction levels both for the ox/sq and sq/hq couples (Table 8.3), corroborating the similar observation in T_2. This confirms the conclusion that e.s.e. for the C69A flavodoxin is slow on the NMR timescale ($< 10^3$ M^{-1} s^{-1}) both between the ox and sq as well as the sq and hq forms under the experimental conditions used. Earlier observations for several different flavodoxins [59,58,21] that the oxidized form of flavodoxin is reduced slower than the semiquinone form has been correlated to a backbone flip of a two-residue peptide upon one-electron reduction of flavodoxin to its semiquinone [41]. This effectively gates the ox/sq transition, while the absence of any such changes for the sq/hq transition allows this reaction to proceed at a higher rate.

Mutants of the *Anabaena* flavodoxin which have had the FMN-flanking tryptophan residue replaced showed slower reduction rates. This residue has direct interactions to the solvent exposed methyl groups of FMN that have been shown to be the entry point for electrons in flavodoxins, and apparently itself also plays a role in the kinetics of electron transfer [40]. The C69A flavodoxin from *A. vinelandii* carries a leucine at this position, and the *M. elsdenii* flavodoxin a methionine; the variation in sequence identity at this crucial position may be an additional cause of modulation for the rates of e.s.e. observed.

Effects of salt and a mediator on the sq/hq e.s.e rate

In this ^{31}P NMR study of C69A flavodoxin, e.s.e. was not observed either between the ox and sq or the sq and hq forms of the protein, with exchange in the latter couple apparently being slower than what has been observed for other flavodoxins. Structural features unique to this flavodoxin may contribute to this, such as a surface that is more negatively charged

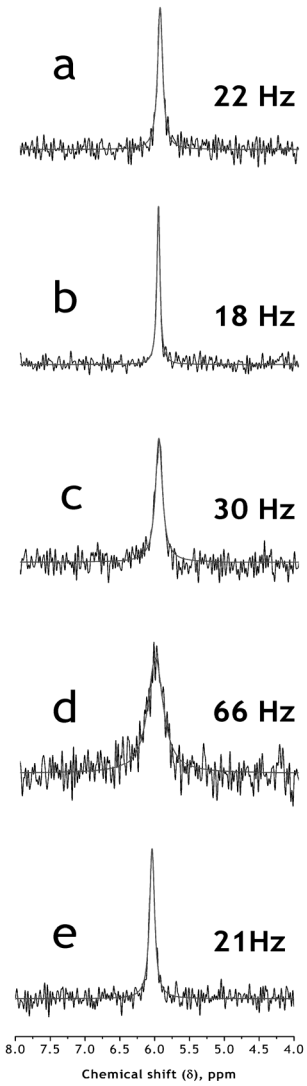

Fig. 8.3. The ^{31}P NMR spectrum of flavodoxin in 100 mM Tris, pH 8.5 containing a) 20% sq and 80% hq flavodoxin with no additives, b) 25% sq and 75 % hq flavodoxin in the presence of 0.5 M NaCl, c) 25% sq and 75% hq in the presence of 50 μM methyl viologen, d) 25% sq and 75% hq flavodoxin in the presence of 100 μM methyl viologen and 0.5 M NaCl and e) 100% ox flavodoxin in the presence of 0.1 mM $MnCl_2$. Each of the peaks was fitted to a Lorentzian function, and the resulting lines superimposed onto the spectra. The calculated line widths are indicated for each of the fits.

than in other flavodoxins, which hinders association between the flavodoxin molecules. This explanation was tested and excluded by comparison of the line-width of a sq/hq sample of flavodoxin in the absence and presence of 0.5 M NaCl (Fig. 8.3a and b). The salt would be expected to shield the surface charges on the flavodoxin, leading to faster e.s.e. were this the limiting factor in complex formation. However no significant difference in line-width could be detected with and without salt. By analogy, the addition of 1 M NaCl to the flavodoxin from *M. elsdenii* accelerated the rate of e.s.e. by more than 20-fold [265].

Interestingly, the addition of small amounts of methyl viologen, a small organic mediator often used in protein electrochemistry, caused significant broadening of the phosphorus resonance peak by 10 Hz to 30 Hz (Fig. 8.3c), although no simple relationship could be identified between the concentration of methyl viologen and line broadening. The combined action of methyl viologen and 0.5 M NaCl enhanced the effect further, leading to a line width of 65 Hz (Fig. 8.3d). This was despite the fact that methyl viologen and flavodoxin have opposing charges, and salt would be expected to disrupt rather than

promote complex formation. Importantly, the possibility that this could be caused by the paramagnetic character of methyl viologen was ruled out by a control in which no changes in line width could be observed for a sample of oxidised flavodoxin containing 0.1 mM of the paramagnet manganese (Fig. 8.3c). This result is significant as it shows that e.s.e. for this flavodoxin is limited by steric factors rather than inherent slow flavodoxin redox kinetics. The FMN cofactors bound by flavodoxin molecules do not appear to approach each other sufficiently for productive electron transfer, but the much smaller methyl viologen is capable of accessing the redox centres and shuttling electrons between the flavodoxin molecules. The structure of this flavodoxin was recently solved in our group, revealing a non-conserved extra loop adjacent to one of the FMN-binding loops [246]. This loop may hinder complex formation of flavodoxins in an orientation suitable for electron transfer.

Chapter 9

General Discussion and Conclusions

The FMN-containing redox protein flavodoxin from *Azotobacter vinelandii* has been used as a framework in this thesis around which a number of redox active models for the study of biological electron transfer has been built. Its amenability to such methods as flavin cofactor reconstitution and site-directed mutagenesis of surface residues without significantly affecting the global protein structure and function as well as the known spectroscopic changes associated with changes in redox state made flavodoxin an ideal molecule for this purpose. The aim of these studies was to better understand the factors that underpin not only how redox partners meet and interact, but also the ultimate process of electron transfer (ET) from one molecule to the other.

Protein structure as a determinant of redox potential

As groundwork for the interpretation of the kinetic data obtained later in the thesis, the three-dimensional structure of this flavodoxin was determined (Chapter 3). While the overall structure showed high similarity to other long chain flavodoxins, several unexpected structural details in the FMN-binding pocket came to light. In particular the unusual hydrogen bonding of the N5 in FMN was a case in point for the limitations of structure- and sequence-based protein alignments. The fine structure around the redox site, more specifically the hydrogen bonding pattern of the FMN group as well as its solvent accessibility, has been correlated with measured redox potentials for the different flavodoxins. Comparison of these structural details of the *A. vinelandii* flavodoxin to those in both long and short chain flavodoxins led to the conjecture that the destabilization of the protein-bound FMN group in its oxidised state by the absence of a crucial hydrogen bond is a primary determinant of the E_2 redox potential. Factors with opposing effects can also counterpoise each other. By analogy from other flavodoxins, the N1 atom of FMN is expected to be anionic in the hydroquinone state, and is likely to be destabilised by an unusually large cluster of negative residues in its vicinity; however the higher solvent-accessibility of the FMN group in this flavodoxin is expected to stabilize the anionic N1. These features demonstrate the delicate balance between factors in determining redox potential, borne out in this flavodoxin by an E_1 that is relatively unchanged. It should be noted however that the structural information only allows provisional conclusions to be

drawn on the relationship between redox potential and structure, where these would ideally be substantiated by combined mutational and functional studies on the protein.

Individual studies of the electron transfer properties of flavodoxin and azurin

The fate of electrons introduced into a resting system of redox proteins containing a photoexcitable electron donor by laser flash photolysis was the subject of Chapters 4, 5, 6 and 7. The systems under study varied in complexity, and character in Chapters 5 and 6 with regards to the means by which flavodoxin and azurin were linked. In all three studies, transient spectroscopy was used to trace the sequence of redox reactions after initiation by laser excitation. A thorough understanding of the ET behaviour of each individual component is however an absolute requirement for the deconvolution of the more complex kinetics obtained from the assembled heterodimeric system (see below). This was the basis for the work described in Chapters 4, 7 and 8.

In Chapter 4 the three different azurin species studied displayed ET activity in the order Im-Cu-H117G › wild type › Cu-H117G azurin towards the small soluble electron donor 5-deazariboflavin (5-dRf), demonstrating the importance of electronic coupling for efficient electron transfer. ET in azurin is known to occur through the hydrophobic patch on the protein that centres on histidine 117 [244], so changes in orientation or even the outright removal as in Cu-H117G azurin of this crucial copper ligand may be expected to affect the reactivity of the protein. The imidazole-reconstituted H117G was found to be more reactive than wild type protein towards 5-dRf, whereas the converse was found when using a large hydroxylase protein as the electron donor [76]. The two donors differ in mobility and ability to approach and complex with the protein acceptor, leading to the contrasting behaviour observed.

A protein-bound electron donor based on the photolabel TUPS was tested in Chapter 7, as an alternative to the soluble electron donor 5-dRf, or other known donors such as soluble ruthenium complexes. This affords the advantage of selective reduction of a particular (protein) component in a sample containing a mix of redox active centres, simply by close proximity. The results underlined the central role of driving force in

ensuring efficiency of reduction, where the route yielding the most flavodoxin semiquinone occurred through the production of the TUPS reduced radical in the presence of ascorbate. The surprising independence of reduction rate on distance can at this stage only be explained by the TUPS photolabel, attached to the protein via a relatively long linker, being very flexible and able to occupy positions closer to the FMN cofactor than would be expected solely on the basis of the cysteine attachment position. More rigid anchoring of labels such as with a double cysteine linkage has been shown to limit the dynamics of the label [270], much better defining its position in space with respect to the protein surface.

A ^{31}P NMR study of flavodoxin used the FMN cofactor terminal phosphate group as a reporter for the protein's electron self-exchange (e.s.e.) reactions (Chapter 8). Comparison of the results to those obtained from a similar study of the flavodoxin from *M. elsdenii* [60] showed how the two flavodoxins display relatively different behaviour, despite the homology between them. The most striking difference was a much slowed e.s.e. rate between the semiquinone and hydroquinone forms of the *A. vinelandii* flavodoxin, however this rate was greatly accelerated by the addition of a small mediator molecule. This again underlines the importance of accessibility for efficient ET, where even the addition of relatively short loops around the redox active site can result in steric hindrance and lead to large differences in reactivity.

Electron transfer in azurin-flavodoxin heterodimers

When more than one species or type of redox centre was present in the same sample as in Chapters 5 and 6, transient changes in absorbance were observed at different wavelengths to distinguish redox state changes of the various species. In this way, the progression of ET through the different redox centres of both the non-covalent heterodimer of azurin and flavodoxin in Chapter 5 (formed by the bi-functional linker IPAR that reconstitutes both the active sites simultaneously) as well as the heterodimers of the same two proteins linked via their termini by a flexible polypeptide chain in Chapter 6 could be followed. For the two types of construct, ET was observed from the flavodoxin to the azurin redox centres, as is expected from their relative redox potentials. The concentration-dependence of flavodoxin re-oxidation and azurin reduction showed that

inter-molecular ET dominated over intra-molecular ET, although the reasons for this were different for the different forms of heterodimer.

Linker length in the case of the peptide-linked heterodimers proved not only crucial for the formation of productive ET complexes between the two proteins of the heterodimer, but also determined the stability of the constructs to degradation (Chapter 6). The fact that ET between molecules was faster than ET within a molecule points towards the linkers being of insufficient length to allow significant population of ET-productive orientations within a single heterodimer. The molecular modelling indicated that the ET patches of azurin and flavodoxin are more likely to meet in the construct with the longest linker of 27 amino acids, however conditions for protecting the heterodimer from proteolysis need to be established before more studies can be undertaken.

The alternative modular approach taken to forming the non-covalent heterodimer of flavodoxin and azurin has the advantage of allowing the complex more flexibility, while not forcing the partner proteins into conformations that are unproductive for ET. This has previously been observed, among others for homodimers of azurin [126]. The use of cofactor reconstitution allows gentle linking of the various protein and non-protein components, where intermolecular ET between the reconstituted redox constituents was observed (Chapter 5).

Several points emerge from these experiments, in addition to the thorough characterization of the individual components as described above. There are limitations on the extent to which changes at the different redox centres may be individually tracked by following transient absorbances at different wavelengths. Non-covalent reconstitution results in a range of molecules with only slightly different absorption characteristics, which in practice can best be distinguished on the basis of their relative abundance with respect to the other components of the sample. Finally, in the context of a non-covalent heterodimeric system, tight binding (or low dissociation constants) between the proteins and their reconstituting elements is essential for the creation of a homogeneous system, and simplifies analysis.

Summary

This summary provides a brief introduction to the main subjects of this thesis, the proteins flavodoxin and azurin, as well as the techniques used to study them. This background allows better understanding of the questions on electron transfer in biological systems that were addressed here, and the conclusions that could be drawn from the results.

Together, azurin and flavodoxin are the basic building blocks of the systems under study in this thesis. They have in common that they are both redox active, or can accept and donate electrons, becoming in turn reduced and oxidized respectively. Such proteins act as electron shuttles or taxis in the cell's energetic processes, picking electrons up from donor proteins and delivering them to acceptor proteins which are often at a more distant location. Nature has evolved very well defined chains of electron transfer proteins for energy generation by oxidative phosphorylation in animals and photosynthesis in plants, algae and certain bacteria. The redox partners involved at each step are able to recognize, form complexes and dissociate from each other after the electron transfer reaction has occurred. This is achieved through the specific surface character of the partner proteins, defined by the presence of charged and hydrophobic groups. However the exact mechanism by which this recognition and complex formation is achieved remains a subject of intense study, with various techniques applied to a great number of redox protein pairs. Indications are that several types of encounter complexes exist, depending on the specific protein partners, where non-physiological partners can also transfer electrons at rates that are not insignificant.

The electron transfer reaction between azurin and flavodoxin is an example of the latter. The two proteins originate from different organisms, *Pseudomonas aeruginosa* and *Azotobacter vinelandii* respectively, where in the case of azurin, its physiological partner has not yet been identified. *In vitro* studies on electron transfer from flavodoxin to azurin in isolation, away from their natural setting, has however allowed the influence of various

factors on the reaction, ranging from charge shielding of the proteins to the viscosity of the solution, to be elucidated. The fact that both these proteins, like many other electron transfer proteins, change colour upon changing their oxidation state enabled quantitative detection of the electron transfer reaction. The work presented here takes this work a step further with the creation of several systems, so-called 'maquettes', where azurin and flavodoxin are either covalently or non-covalently linked, to emulate the complex of the proteins formed during electron transfer.

Previous attempts to link pairs of redox proteins by cross-linking or other covalent methods have occasionally resulted in the partners being locked into conformations that are unfavourable for electron transfer. As such, the two different approaches taken here to linking the partners focus on maintaining a high degree of rotational freedom between azurin and flavodoxin. The construction and characterization of both these systems is detailed in the next section, before describing the accompanying research on the individual components and their implications in a final section.

Two approaches to redox protein maquettes

The versatility and malleability of the redox centres, where the oxidation and reduction reactions are localized, of azurin (a single copper atom) and flavodoxin (the flavin cofactor FMN) as described in Chapter 1 facilitated very gentle linking of the two proteins (Chapter 5). This was achieved by slight modifications made to the redox centres. In the case of azurin a site-directed mutation (His117Gly) exchanged one of the co-ordinating ligands of the redox-active copper atom from its native histidine to the much smaller glycine, thus creating an aperture in the protein surface and rendering the protein's bound copper atom accessible to the solvent. Molecules similar in nature to the histidine side-chain, such as imidazole, have previously been found to be able to fill this gap, specifically binding the oxidized copper atom and apparently restoring the protein to its wild type state.

Taking this with the fact that the FMN cofactor of flavodoxin can be also removed and replaced with other flavins provided a scheme for a non-covalent link of the two

proteins. The bifunctional linker molecule IPAR was synthesized, comprising of a riboflavin moiety at one end which could bind to apoflavodoxin or the FMN-free flavodoxin, connected through an alkyl chain to an imidazole group. Visible spectroscopy and fluorescence studies were applied to quantify the reconstitution of the redox centres in each of the proteins by IPAR, through determination of their respective dissociation constants. Laser flash photolysis, the main method for introduction of electrons into the resting system, combined with transient visible spectroscopy methods, for detection of colour and thus redox state changes over time, allowed monitoring of the passage of the introduced electron from the flavodoxin to the azurin redox centre as expected. However, while the non-covalent linkage was successful in not introducing unnatural strain in the complex of the two proteins, it was also found to be at the loss of the formation of a tight ternary complex between flavodoxin, IPAR and azurin. Indeed, a large part of the redox changes observed was determined to result from inter-molecular reactions of the individual components of the complex. The balance between avoiding strain and maintaining sufficiently tight binding for a homogenous sample is a delicate one, and should be taken into consideration when designing such constructs in future.

An alternative approach was also taken by connecting the two proteins covalently, through the genetic introduction of a flexible peptide linker between the C-terminus of flavodoxin and the N-terminus of azurin (Chapter 6). Three different lengths for these linkers were chosen on the basis of a molecular dynamics study, and totalled 13, 23 and 27 mainly glycine amino acids respectively. The long linkers were necessary to sufficiently breach the length of both the proteins, as the termini are located at opposite ends of the proteins to the redox centres (see Fig. 6.1). All three chimeric proteins were successfully expressed in and purified from *E. coli*, and were found to show the visible spectral characteristics of both the flavodoxin and azurin redox centres. They were however found to differ greatly in stability, with the longer linkers being more susceptible to degradation. As a result, only the two shorter linker proteins could be functionally characterized for electron transfer, again by laser flash photolysis and transient spectroscopy, and inter-chimera flavodoxin to azurin electron transfer was found to dominate. Although the redox active patches of flavodoxin and azurin are known to

interact when the proteins are free in solution, these results indicate that when the proteins are linked a longer linker would be more favourable for electron transfer.

Complementary information from single molecule systems

Knowledge of a redox protein's three-dimensional structure is integral to understanding its molecular interactions with a partner protein. Only the secondary structure was known for the flavodoxin from *A. vinelandii* used in this thesis, while a model structure based on the structure of homologous flavodoxins could roughly be predicted. We determined the structure of this flavodoxin by X-ray crystallography for use in the molecular dynamics and other modelling studies as described in the previous section. The data was of sufficiently high resolution to enable close study of the structure, revealing several unexpected features, which may in part determine the redox potentials of the protein (Chapter 3). These include the absence of a hydrogen bond from the protein backbone to the FMN cofactor in the oxidized state, thus destabilizing that form of the protein, as well as a surprisingly large patch of acidic residues close to the N1 atom of FMN, which is expected to destabilize the doubly reduced hydroquinone form. This work demonstrates how comparisons of the structure of related redox proteins in conjunction with information on the amino acid sequences and redox potentials are powerful tools for furthering understanding of just how the protein coat determines the potential of the cofactor it binds.

Characterization of the electron transfer properties of the component proteins not only allowed for the deconvolution of the more complex data from the maquettes devised, but also permitted important conclusions to be drawn on the redox action of the individual proteins. A ^{31}P NMR study of the C69A flavodoxin in its various redox states showed markedly slowed electron self-exchange behaviour compared to other flavodoxins even between the semiquinone and hydroquinone forms (Chapter 8). However the presence of a simple mediator molecule in the flavodoxin sample resulted in a significant acceleration in rate, indicating that steric rather than thermodynamic factors govern this reaction. The reduction by an attached photolabel TUPS (Chapter 7) of oxidized to semiquinone flavodoxin, supposed gated by a peptide bond flip, was surprisingly independent of

distance from the FMN redox centre. The linker region connecting the photolabel to the protein may play a more important role in determining the label's position relative to the redox centre than is often recognized.

Finally, functional studies on the reduction of various copper-containing forms of the azurin mutant His117Gly revealed that the solvent-exposed species was, counter to intuition, less reactive to the external electron donor 5-deazariboflavin than its imidazole-bound or wild type cousins (Chapter 4). This demonstrates the extent to which electronic coupling as afforded by the arrangement of atoms around the redox centre can affect efficiency in electron transfer. These studies also underline the importance of functional studies of electron transfer proteins not just using various donors but also different techniques, which provide complementary information for better insight into how these proteins function.

Samenvatting

In deze samenvatting wordt een korte beschrijving gegeven van de eiwitten flavodoxine en azurine, van de technieken de gebruikt zijn om ze te onderzoeken en van de voornaamste resultaten van het onderzoek zoals beschreven in dit proefschrift.

Azurine en flavodoxine vormen de bouwstenen voor de moleculaire constructen die in dit proefschrift beschreven worden. Ze zijn allebei redoxactief, dwz ze kunnen elektronen opnemen en afstaan waardoor ze in de gereduceerde of geoxideerde vorm overgaan. Zij fungeren als 'pendels' of 'taxi's' voor elektronen in processen die een rol spelen in de energiehuishouding van de cel; eerst halen zij elektronen op bij donoreiwitten, later geven zij die weer af aan andere eiwitten, die vaak op een verder weg gelegen plek in de cel te vinden zijn. Voor de opwekking van energie in de cel heeft de natuur goed gedefinieerde ketens van elektronen overdragende eiwitten ontwikkeld. Energieopwekking vindt plaats middels een proces dat de naam draagt van "oxidatieve fosforylering" en dat in bijna alle aëroob levende organismen voorkomt. Een vergelijkbaar proces is de fotosynthese zoals die te vinden is in planten, algen en fotosynthetische bacteriën. Partners in de keten van elektronen overdragende eiwitten moeten elkaar eerst kunnen herkennen en complexen vormen (associëren), vervolgens een elektron uitwisselen en tenslotte weer uit elkaar gaan (dissociëren). Onderlinge herkenning wordt gereguleerd door specifieke kenmerken op het oppervlak van de partners, zoals de al of niet aanwezigheid van een specifiek patroon van geladen en/of hydrofobe groepen. Het precieze mechanisme van de herkenning en de vorming van complexen vormt een onderwerp van zeer intensief onderzoek op dit moment, waarbij gebruik gemaakt wordt van diverse geavanceerde technieken en veel combinaties van complementaire redoxeiwitten. De resultaten wijzen op het bestaan van specifieke complexen van fysiologische partners, maar ook niet-fysiologische partners blijken soms elektronen uit te kunnen wisselen met snelheden die in de buurt komen van die tussen fysiologische partners.

De elektronoverdracht tussen azurine en flavodoxine is hier een voorbeeld hiervan. Azurine en flavodoxine zijn afkomstig van twee verschillende organismen,

Pseudomonas aeruginosa (azurine) en *Azotobacter vinelandii* (flavodoxine) en dus niet elkaars natuurlijke partner (de fysiologische partner van azurine is niet bekend). Niettemin kon de *in vitro* elektronoverdracht tussen flavodoxine en azurine heel goed waargenomen en bestudeerd worden en de invloed op de reactiesnelheid van een aantal factoren, zoals de ladingsverdeling op de eiwitoppervlakken en de viscositeit van de oplossing, kon opgehelderd worden. Doordat beide eiwitten (zoals veel redox-eiwitten) van kleur veranderen met het veranderen van hun oxidatiestand kon de elektronoverdrachtsreactie kwantitatief gevolgd worden mbv optische technieken. Het onderzoek dat in dit proefschrift beschreven wordt vormt een uitbreiding van eerder onderzoek. Met de synthese van een aantal 'maquettes', waarin azurine en flavodoxine met elkaar verbonden zijn, covalent dan wel niet-covalent, hoopten wij de natuurlijke eiwitcomplexen te kunnen nabootsen en in detail te kunnen bestuderen.

Eerdere pogingen, door anderen, om redoxeiwitten dmv 'crossslinking' of mbv een andere techniek te koppelen hadden vaak tot gevolg dat de partners geïmmobiliseerd werden in conformaties die ongunstig waren voor de overdracht van elektronen. Om deze reden hebben we methodes gekozen om azurine en flavodoxine met elkaar te verbinden die een optimale bewegingsvrijheid garandeerden van de eiwitten tov elkaar. De synthese en de karakterisatie van de constructen ('maquettes') worden hieronder uitgelegd, gevolgd door een beschrijving van de resultaten van het onderzoek van de individuele componenten en de implicaties hiervan voor het begrip van de eigenschappen van de maquettes.

Twee manieren om maquettes te maken van redox-eiwitten

De redox centra van azurine (een koper atoom dat met vier liganden verankerd is in het eiwit) en flavodoxine (flavine mononucleotide (FMN)), zijn enigszins vervormbaar, zoals in Hoofdstuk 1 is uitgelegd. Dit maakt het mogelijk om azurine en flavodoxine op een subtiele manier te koppelen (Hoofdstuk 5) door het aanbrengen van kleine veranderingen in de redoxcentra. Een plaatsgerichte mutatie in azurine, His117Gly, verandert één van de coördinerende liganden van het koperatoom van een histidine in het veel kleinere glycine. Hierdoor ontstaat er een opening in het eiwit oppervlak die de koper van buitenaf toegankelijk maakt. Het is bekend dat moleculen die wat vorm en/of eigenschappen betreft

enigszins lijken op de zijketen van een histidine, zoals imidazool, deze opening kunnen vullen en aan het geoxideerde koperatoom kunnen binden waardoor ogenschijnlijk het 'wild type' toestand wordt hersteld.

Het feit dat de FMN cofactor in flavodoxine vervangen kan worden door andere flavines en de hierboven beschreven eigenschappen van His117Gly azurine hebben geleid tot een nieuwe strategie om de twee eiwitten langs niet-covalente weg te koppelen. Hiertoe werd het bifunctionele linkermolecuul 'IPAR' gesynthetiseerd, dat bestaat uit een alkyl keten met aan het ene uiteinde een riboflavine-groep, die aan apoflavodoxine (dwz het FMN-vrije flavodoxine) kan binden, en aan het andere uiteinde een imidazool-groep die aan het His117Gly azurine bindt. Optische absorptie- en fluorescentie-spectroscopie zijn gebruikt om de bindingsconstanten van IPAR met de twee eiwitten te bepalen. Laser flitsfotolyse, waarmee elektronen ingebracht kunnen worden in de gekoppelde eiwitten, is in combinatie met 'transient visible' absorptiespectroscopie gebruikt om de redoxreacties van de beide redoxcentra te volgen als functie van de tijd. Hiermee kon, zoals verwacht, de overdracht van een elektron van flavodoxine naar azurine gevolgd worden. Hoewel het mbv de niet-covalente koppeling lukte om sterische hindering in het complex te vermijden, resulteerde het ook in een afname van de bindingssterkte in het ternaire complex van azurine, flavodoxine en IPAR. Een groot deel van de waargenomen redoxreacties kon dan ook verklaard worden met het optreden van intermoleculaire reacties tussen individuele componenten van het complex. De balans tussen het verminderen van sterische hindering en een zo sterk mogelijke associatie van de samenstellende delen in het complex luistert zeer nauw en dient nauwlettend in het oog te worden gehouden bij het ontwerpen van zulke systemen.

Een andere methode om de twee eiwitten op een covalente manier te koppelen bestond uit de introductie op genetisch niveau van een flexibele peptide linker tussen de C-terminus van het flavodoxine en de N-terminus van het azurine (Hoofdstuk 6). Drie verschillende lengtes (van 13, 23 en 27 aminozuren, voornamelijk glycines) zijn gekozen op grond van een moleculair dynamica studie. Gedacht werd dat met de langere linkers de eiwitten zich zo zouden kunnen positioneren tov elkaar dat een complex gevormd zou worden dat optimaal is voor elektronoverdracht (zie Fig. 6.1). Alle drie de complexen

konden tot expressie worden gebracht in *E. coli* en daarna gezuiverd worden. Zij vertoonden de spectrale kenmerken van zowel de flavodoxine als de azurine redoxcentra. Grote verschillen in stabiliteit werden waargenomen tussen de drie constructen, waarbij de langere linkers gevoeliger bleken voor degradatie dan de kortste. Hierdoor was het alleen mogelijk om de twee eiwitten met de kortere linkers te bestuderen, waarbij van dezelfde technieken als hierboven beschreven gebruik gemaakt werd. De ***inter***moleculaire overdracht van elektronen van flavodoxine naar azurine bleek de ***intra***moleculaire reactie te overheersen. Deze resultaten maken het aannemelijk dat een langere linker gunstiger kan zijn voor elektronoverdracht.

Structuurinformatie

Kennis van de driedimensionale structuur van een redoxeiwit blijft essentieel voor een goed begrip van de interacties met partnereiwitten. Voorheen was slechts de secundaire structuur van de *A. vinelandii* flavodoxine bekend, en voor de driedimensionale structuur moesten we ons behelpen met een model dat gebouwd was op basis van de homologie met andere flavodoxines waarvan de structuur wél opgehelderd was. De exacte structuur van ons flavodoxine is in samenwerking met collega's in Parma en Groningen met behulp van X-ray kristallografie bepaald, en later gebruikt in moleculaire dynamica studies en theoretische analyses zoals beschreven in Hoofdstukken 5 en 6. De gegevens bleken zo nauwkeurig dat een aantal onverwachte eigenschappen naar voren kwamen die waarschijnlijk van invloed zijn op de redoxpotentialen van het eiwit (Hoofdstuk 3). Het gaat om details als de afwezigheid van een waterstofbrug tussen de 'backbone' van het eiwit en de geoxideerde FMN cofactor, die normaliter deze vorm van het eiwit stabiliseert, en de aanwezigheid van een groot aantal negatief geladen aminozuren vlak naast het N1 atoom van de FMN, die vermoedelijk de dubbel gereduceerde vorm van het flavodoxine destabiliseren. Dit deel van het onderzoek illustreert hoe de koppeling van structuurinformatie met informatie over aminozuursequenties en redoxpotentialen kan helpen om de invloed van een eiwit op de redoxpotentiaal van de gebonden cofactor beter te begrijpen.

De bestudering van de elektronoverdrachtseigenschappen van de individuele eiwitten was niet alleen belangrijk voor het begrijpen van de complexe resultaten afkomstig van de maquettes, maar leverde ook belangrijke conclusies op over de redoxreacties van de individuele eiwitten. Uit een ^{31}P NMR onderzoek van C69A flavodoxine in drie verschillende redoxtoestanden bleek dat de 'electron self exchange' reactie opvallend traag is in vergelijking met andere flavodoxines, zelfs die tussen de semichinon- en de hydrochinon-vormen (Hoofdstuk 8). De aanwezigheid van een mediator resulteerde in een aanmerkelijke versnelling van de reactie, en wijst erop dat sterische in plaats van thermodynamische factoren de snelheid van de reactie bepalen. De reductie van het geoxideerde flavodoxine door een aangehechte fotolabel (TUPS), waarvan de snelheid vermoedelijk afhangt van de omslag van een peptidebinding, bleek tegen de verwachting in onafhankelijk te zijn van de afstand van de label aan het FMN redoxcentrum. Het gebied op het eiwitoppervlak waarmee de linker uiteindelijk associeert blijkt een grotere rol te spelen in de lokalisatie van de label dan doorgaans wordt aangenomen.

Bestudering van de reductie van de azurinemutant His117Gly waarin verschillende externe liganden gebonden zijn, liet ook zien dat in afwezigheid van een ligand het Cu-centrum tegen de verwachting in minder reactief is met externe elektrondonoren (zoals 5-deazariboflavine) dan de imidazool-gebonden vorm of dan het wild type eiwit (Hoofdstuk 4). Dit laat zien dat de aard van de liganden rondom een redoxcentrum de efficiëntie van de elektronoverdracht sterk kan beïnvloeden. Deze studies benadrukken ook het belang van onderzoek van elektronoverdrachtseiwitten niet alleen met gebruikmaking van verschillende donoren, maar mbv ook verschillende technieken, waarmee een beter inzicht in het reactiemechanisme van deze eiwitten verkregen kan worden.

References

1. **Mayhew, S.G. and Tollin, G.** 1992. General properties of flavodoxins. 389-426. *In* Chemistry and Biochemistry of Flavoenzymes, Volume III, Müller, F. (eds). CRC Press, Boca Raton, FL, USA.

2. **Gomes, C.M., Giuffre, A., Forte, E., Vicente, J.B., Saraiva, L.M., Brunori, M. and Teixeira, M.** 2002. A novel type of nitric-oxide reductase: *Escherichia coli* flavorubredoxin. *J. Biol. Chem.* **277**:25273-6.

3. **Chapman, S.K., Reid, G.A. and Munro, A.W.** 1998. Flavocytochromes: Nature's electrical transformers. 165-84. *In* Biological Electron Transfer Chains: Genetics, Composition and Mode of Operation, Canters, G. W. and Vijgenboom, E. (eds). Kluwer Academic Publishers, the Netherlands.

4. **Astuti, Y., Topoglidis, E., Briscoe, P.B., Fantuzzi, A., Gilardi, G. and Durrant, J.R.** 2004. Proton-coupled electron transfer of flavodoxin immobilized on nanostructured tin dioxide electrodes: Thermodynamics versus kinetics control of protein redox function. *J. Am. Chem. Soc.* **126**:8001-9.

5. **Nogues, I., Martinez-Julvez, M., Navarro, J.A., Hervás, M., Armenteros, L., De la Rosa, M.A., Brodie, T.B., Hurley, J.K., Tollin, G., Gómez-Moreno, C. and Medina, M.** 2003. Role of hydrophobic interactions in the flavodoxin mediated electron transfer from photosystem I to ferredoxin-NADP+ reductase in *Anabaena* PCC 7119. *Biochemistry* **42**:2036-45.

6. **Medina, M. and Gómez-Moreno, C.** 2004. Interaction of ferredoxin-NADP$^+$ reductase with its substrates: Optimal interaction for efficient electron transfer. *Photosynth. Res.* **79**:113-31.

7. **Mayhew, S.G. and Ludwig, M.L.** 1975. Flavodoxins and electron-transferring flavoproteins. **3**:57-118. *In* The Enzymes Vol. XII, Boyer, P. D. (eds). Academic Press, Inc., New York.

8. **Hughes, N.J., Chalk, P.A., Clayton, C.L. and Kelly, D.J.** 1995. Identification of carboxylation enzymes and characterization of a novel four-subunit pyruvate:flavodoxin oxidoreductase from *Helicobacter pylori*. *J. Bacteriol.* **177**:3953-9.

9. **McIver, L., Leadbeater, C., Campopiano, D.J., Baxter, R.L., Daff, S.N., Chapman, S.K. and Munro, A.W.** 1998. Characterisation of flavodoxin NADP$^+$ oxidoreductase and flavodoxin; key components of electron transfer in *Escherichia coli*. *Eur. J. Biochem.* **257**:577-85.

10. **Benemann, J.R., Yoch, D.C., Valentin, R.C. and Arnon, D.I.** 1969. Electron transport system in nitrogen fixation by Azotobacter. 1.Azotoflavin as an electron carrier. *Proc. Natl. Acad. Sci. U. S. A.* **64**:1079-86.

11. **Bennett, L.T., Jacobson, M.R. and Dean, D.R.** 1988. Isolation, sequencing, and mutagenesis of the nifF gene encoding flavodoxin from *Azotobacter vinelandii*. *J. Biol. Chem.* **263**:1364-9.

12. **Klugkist, J., Voorberg, J., Haaker, H. and Veeger, C.** 1986. Characterization of three different flavodoxins from *Azotobacter vinelandii*. *Eur. J. Biochem.* **155**:33-40.

13. **Klugkist, J., Haaker, H. and Veeger, C.** 1986. Studies on the mechanism of electron transport to nitrogenase in *Azotobacter vinelandii*. *Eur. J. Biochem.* **155**:41-6.

14. **Lopez-Llano, J., Maldonado, S., Bueno, M., Lostao, A., Angeles-Jimenez, M., Lillo, M.P. and Sancho, J.** 2004. The long and short flavodoxins: I. The role of the differentiating loop in apoflavodoxin structure and FMN binding. *J. Biol. Chem.* **279**:47177-83.

15. **Peelen, S., Wijmenga, S., Erbel, P.J., Robson, R.L., Eady, R.R. and Vervoort, J.** 1996. Possible role of a short extra loop of the long-chain flavodoxin from *Azotobacter chroococcum* in electron transfer to nitrogenase: Complete ^{1}H, ^{15}N and ^{13}C backbone assignments and secondary solution structure of the flavodoxin. *J. Biomol. NMR* **7**:315-30.

16. **Lopez-Llano, J., Maldonado, S., Jain, S., Lostao, A., Godoy-Ruiz, R., Sanchez-Ruiz, J.M., Cortijo, M., Fernandez-Recio, J. and Sancho, J.** 2004. The long and short flavodoxins: II. The role of the differentiating loop in apoflavodoxin stability and folding mechanism. *J. Biol. Chem.* **279**:47184-91.

17. **Thompson, J.D., Higgins, D.G. and Gibson, T.J.** 1994. CLUSTAL W: Improving the sensitivity of progressive multiple sequence alignment through sequence weighting, position-specific gap penalties and weight matrix choice. *Nucleic Acids Res.* **22**:4673-80.

18. **Vervoort, J., Heering, D., Peelen, S. and van Berkel, W.** 1994. Flavodoxins. *Methods Enzymol.* **243**:188-203.

19. **Mayhew, S.G.** 1971. Studies on flavin binding in flavodoxins. *Biochim. Biophys. Acta* **235**:289-302.

20. **Mayhew, S.G.** 1978. The redox potential of dithionite and $SO2^{-}$ from equilibrium reactions with flavodoxins, methyl viologen and hydrogen plus hydrogenase. *Eur. J. Biochem.* **85**:535-47.

21. **Heering, H.A. and Hagen, W.R.** 1996. Complex electrochemistry of flavodoxin at carbon-based electrodes: Results from a combination of direct electron transfer, flavin-mediated electron transfer and comproportionation. *J. Electroanal. Chem.* **404**:249-60.

22. **Massey, V., Stankovich, M. and Hemmerich, P.** 1978. Light-mediated reduction of flavoproteins with flavins as catalysts. *Biochemistry* **17**:1-8.

23. **Anderson, R.F., Massey, V. and Schopfer, L.M.** 1987. Pulse radiolysis studies on flavodoxin. 279-82. *In* Flavins and Flavoproteins 1987, Edmondson, D. E. and McCormick, D. B. (eds). Walter de Gruyter, Berlin.

24. **Hall, D.A., Vander Kooi, C.W., Stasik, C.N., Stevens, S.Y., Zuiderweg, E.R. and Matthews, R.G.** 2001. Mapping the interactions between flavodoxin and its physiological partners flavodoxin reductase and cobalamin-dependent methionine synthase. *Proc. Natl. Acad. Sci. U. S. A.* **98**:9521-6.

25. **Nogues, I., Campos, L.A., Sancho, J., Gómez-Moreno, C., Mayhew, S.G. and Medina, M.** 2004. Role of neighboring FMN side chains in the modulation of flavin reduction potentials and in the energetics of the FMN:apoprotein interaction in *Anabaena* flavodoxin. *Biochemistry* **43**:15111-21.

26. **Steensma, E., Heering, H.A., Hagen, W.R. and van Mierlo, C.P.** 1996. Redox properties of wild-type, Cys69Ala, and Cys69Ser *Azotobacter vinelandii* flavodoxin II as measured by cyclic voltammetry and EPR spectroscopy. *Eur. J. Biochem.* **235**:167-72.

27. **Ludwig, M.L., Pattridge, K.A., Metzger, A.L., Dixon, M.M., Eren, M., Feng, Y. and Swenson, R.P.** 1997. Control of oxidation-reduction potentials in flavodoxin from *Clostridium beijerinckii*: The role of conformation changes. *Biochemistry* **36**:1259-80.

28. **Watt, W., Tulinsky, A., Swenson, R.P. and Watenpaugh, K.D.** 1991. Comparison of the crystal structures of a flavodoxin in its three oxidation states at cryogenic temperatures. *J. Mol. Biol.* **218**:195-208.

29. **Hoover, D.M., Drennan, C.L., Metzger, A.L., Osborne, C., Weber, C.H., Pattridge, K.A. and Ludwig, M.L.** 1999. Comparisons of wild-type and mutant flavodoxins from *Anacystis nidulans*. Structural determinants of the redox potentials. *J. Mol. Biol.* **294**:725-43.

30. **Rao, S.T., Shaffie, F., Yu, C., Satyshur, K.A., Stockman, B.J., Markley, J.L. and Sundarlingam, M.** 1992. Structure of the oxidized long-chain flavodoxin from *Anabaena* 7120 at 2 Å resolution. *Protein Sci.* **1**:1413-27.

31. **Chang, F.C. and Swenson, R.P.** 1999. The midpoint potentials for the oxidized-semiquinone couple for Gly57 mutants of the *Clostridium beijerinckii* flavodoxin correlate with changes in the hydrogen-bonding interaction with the proton on N(5) of the reduced flavin mononucleotide cofactor as measured by NMR chemical shift temperature dependencies. *Biochemistry* **38**:7168-76.

32. **Stockman, B.J., Westler, W.M., Mooberry, E.S. and Markley, J.L.** 1988. Flavodoxin from *Anabaena* 7120: Uniform nitrogen-15 enrichment and hydrogen-1, nitrogen-15, and phosphorus-31 NMR investigations of the flavin mononucleotide binding site in the reduced and oxidized states. *Biochemistry* **27**:136-42.

33. **Hutchinson, E.G. and Thornton, J.M.** 1994. A revised set of potentials for beta-turn formation in proteins. *Protein Sci.* **3**:2207-16.

34. **Hoover, D.M. and Ludwig, M.L.** 1997. A flavodoxin that is required for enzyme activation: The structure of oxidized flavodoxin from *Escherichia coli* at 1.8 Å resolution. *Protein Sci.* **6**:2525-37.

35. **Franken, H.D., Ruterjans, H. and Müller, F.** 1984. Nuclear-magnetic-resonance investigation of ^{15}N-labeled flavins, free and bound to *Megasphaera elsdenii* apoflavodoxin. *Eur. J. Biochem.* **138**:481-9.

36. **Ludwig, M.L., Schopfer, L.M., Metzger, A.L., Pattridge, K.A. and Massey, V.** 1990. Structure and oxidation-reduction behavior of 1-deaza-FMN flavodoxins: Modulation of redox potentials in flavodoxins. *Biochemistry* **29**:10364-75.

37. **Zhou, Z. and Swenson, R.P.** 1995. Electrostatic effects of surface acidic amino acid residues on the oxidation-reduction potentials of the flavodoxin from *Desulfovibrio vulgaris* (Hildenborough). *Biochemistry* **34**:3183-92.

38. **Zhou, Z. and Swenson, R.P.** 1996. Evaluation of the electrostatic effect of the 5'-phosphate of the flavin mononucleotide cofactor on the oxidation-reduction potentials of the flavodoxin from *Desulfovibrio vulgaris* (Hildenborough). *Biochemistry* **35**:12443-54.

39. **Swenson, R.P. and Krey, G.D.** 1994. Site-directed mutagenesis of tyrosine-98 in the flavodoxin from *Desulfovibrio vulgaris* (Hildenborough): Regulation of oxidation-reduction properties of the bound FMN cofactor by aromatic, solvent, and electrostatic interactions. *Biochemistry* **33**:8505-14.

40. **Lostao, A., Gómez-Moreno, C., Mayhew, S.G. and Sancho, J.** 1997. Differential stabilization of the three FMN redox forms by tyrosine 94 and tryptophan 57 in flavodoxin from *Anabaena* and its influence on the redox potentials. *Biochemistry* **36**:14334-44.

41. **Ludwig, M.L. and Luschinsky, C.L.** 1992. Structure and redox properties of Clostridial flavodoxin. 427-66. *In* Chemistry and Biochemistry of Flavoenzymes, Volume III, Muller, F. (eds). CRC Press, Boca Raton, FL, USA.

42. **Jung, J. and Tollin, G.** 1981. Transient kinetics of electron-transfer reactions of flavodoxins. *Biochemistry* **20**:5124-31.

43. **Medina, M., Hervás, M., Navarro, J.A., De la Rosa, M.A., Gómez-Moreno, C. and Tollin, G.** 1992. A laser flash absorption-spectroscopy study of *Anabaena* Sp PCC 7119 flavodoxin photoreduction by photosystem I particles from spinach. *FEBS Lett.* **313**:239-42.

44. **Tollin, G., Meyer, T.E. and Cusanovich, M.A.** 1986. Elucidation of the factors which determine reaction-rate constants and biological specificity for electron-transfer proteins. *Biochim. Biophys. Acta* **853**:29-41.

45. **Cheddar, G., Meyer, T.E., Cusanovich, M.A., Stout, C.D. and Tollin, G.** 1986. Electron-transfer reactions between flavodoxin semiquinone and *c*-type cytochromes: Comparisons between various flavodoxins. *Biochemistry* **25**:6502-7.

46. **Zöllner, A., Nogues, I., Heinz, A., Medina, M., Gómez-Moreno, C. and Bernhardt, R.** 2004. Analysis of the interaction of a hybrid system consisting of bovine adrenodoxin reductase and flavodoxin from the cyanobacterium *Anabaena* PCC 7119. *Bioelectrochemistry* **63**:61-5.

47. **Feng, Y.C. and Swenson, R.P.** 1997. Evaluation of the role of specific acidic amino acid residues in electron transfer between the flavodoxin and cytochrome *c*3 from Desulfovibrio vulgaris (Hildenborough). *Biochemistry* **36**:13617-28.

48. **Tollin, G., Cheddar, G., Watkins, J.A., Meyer, T.E. and Cusanovich, M.A.** 1984. Electron transfer between flavodoxin semiquinone and *c*-type cytochromes: Correlations between electrostatically corrected rate constants, redox potentials, and surface topologies. *Biochemistry* **23**:6345-9.

49. **Prudencio, M. and Ubbink, M.** 2004. Transient complexes of redox proteins: structural and dynamic details from NMR studies. *J. Mol. Recognit.* **17**:524-39.

50. **De Francesco, R., Tollin, G. and Edmondson, D.E.** 1987. Influence of 8 alpha-imidazole substitution of the FMN cofactor on the rate of electron transfer from the neutral semiquinones of two flavodoxins to cytochrome *c*. *Biochemistry* **26**:5036-42.

51. **Leadbeater, C., McIver, L., Campopiano, D.J., Webster, S.P., Baxter, R.L., Kelly, S.M., Price, N.C., Lysek, D.A., Noble, M.A., Chapman, S.K. and Munro, A.W.** 2000. Probing the NADPH-binding site of *Escherichia coli* flavodoxin oxidoreductase. *Biochem. J.* **352**:257-66.

52. **Sadeghi, S.J., Valetti, F., Cunha, C.A., Romao, M.J., Soares, C.M. and Gilardi, G.** 2000. Ionic strength dependence of the non-physiological electron transfer between flavodoxin and cytochrome *c*553 from *D. vulgaris*. *J. Biol. Inorg. Chem.* **5**:730-7.

53. **Gómez-Moreno, C., Martinez-Julvez, M., Medina, M., Hurley, J.K. and Tollin, G.** 1998. Protein-protein interaction in electron transfer reactions: The ferredoxin/flavodoxin/ferredoxin:NADP$^+$ reductase system from *Anabaena*. *Biochimie* **80**:837-46.

54. **Jenkins, C.M., Genzor, C.G., Fillat, M.F., Waterman, M.R. and Gómez-Moreno, C.** 1997. Negatively charged *Anabaena* flavodoxin residues (Asp^{144} and Glu^{145}) are important for reconstitution of cytochrome P450 17 alpha-hydroxylase activity. *J. Biol. Chem.* **272**:22509-13.

55. **Meimberg, K., Fischer, N., Rochaix, J.D. and Muhlenhoff, U.** 1999. Lys35 of PsaC is required for the efficient photoreduction of flavodoxin by photosystem I from *Chlamydomonas reinhardtii*. *Eur. J. Biochem.* **263**:137-44.

56. **Meyer, T.E., Przysiecki, C.T., Watkins, J.A., Bhattacharyya, A., Simondsen, R.P., Cusanovich, M.A. and Tollin, G.** 1983. Correlation between rate constant for reduction and redox potential as a basis for systematic investigation of reaction mechanisms of electron transfer proteins. *Proc. Natl. Acad. Sci. U. S. A.* **80**:6740-4.

57. **Casaus, J.L., Navarro, J.A., Hervás, M., Lostao, A., De la Rosa, M.A., Gómez-Moreno, C., Sancho, J. and Medina, A.** 2002. *Anabaena* sp PCC 7119 flavodoxin as electron carrier from photosystem I to ferredoxin-NADP$^+$ reductase. Role of Trp57 and Tyr94. *J. Biol. Chem.* **277**:22338-44.

58. **Dubourdieu, M., le Gall, J. and Favaudon, V.** 1975. Physicochemical properties of flavodoxin from *Desulfovibrio vulgaris*. *Biochim. Biophys. Acta* **376**:519-32.

59. **Mayhew, S.G. and Massey, V.** 1973. Studies on the kinetics and mechanism of reduction of flavodoxin from *Peptostreptococcus elsdenii* by sodium dithionite. *Biochim. Biophys. Acta* **315**:181-90.

60. **Moonen, C.T. and Müller, F.** 1982. Structural and dynamic information on the complex of *Megasphaera elsdenii* apoflavodoxin and riboflavin 5'-phosphate. A phosphorus-31 nuclear magnetic resonance study. *Biochemistry* **21**:408-14.

61. **Navarro, J.A., Hervás, M., Pueyo, J.J., Medina, M., Gómez-Moreno, C., De la Rosa, M.A. and Tollin, G.** 1994. Laser flash-induced photoreduction of photosynthetic ferredoxins and flavodoxin by 5-deazariboflavin and by a viologen analogue. *Photochem. Photobiol.* **60**:231-6.

62. **Vijgenboom, E., Busch, J.E. and Canters, G.W.** 1997. In vivo studies disprove an obligatory role of azurin in denitrification in *Pseudomonas aeruginosa* and show that azu expression is under control of RpoS and ANR. *Microbiology (Reading, U. K.)* **143**:2853-63.

63. **Winkler, J.R., Wittung-Stafshede, P., Leckner, J., Malmstrom, B.G. and Gray, H.B.** 1997. Effects of folding on metalloprotein active sites. *Proc. Natl. Acad. Sci. U. S. A* **94**:4246-9.

64. **Pozdnyakova, I., Guidry, J. and Wittung-Stafshede, P.** 2000. Copper-triggered beta-hairpin formation: Initiation site for azurin folding? *J. Am. Chem Soc.* **122**:6337-8.

65. **Maxwell, K.L., Wildes, D., Zarrine-Afsar, A., los Rios, M.A., Brown, A.G., Friel, C.T., Hedberg, L., Horng, J.C., Bona, D., Miller, E.J., Vallee-Belisle, A., Main, E.R.G., Bemporad, F., Qiu, L.L., Teilum, K., Vu, N.D., Edwards, A.M., Ruczinski, I., Poulsen, F.M., Kragelund, B.B., Michnick, S.W., Chiti, F., Bai, Y.W., Hagen, S.J., Serrano, L., Oliveberg, M., Raleigh, D.P., Wittung-Stafshede, P., Radford, S.E., Jackson, S.E., Sosnick, T.R., Marqusee, S., Davidson, A.R. and Plaxco, K.W.** 2005. Protein folding: Defining a "standard" set of experimental conditions and a preliminary kinetic data set of two-state proteins. *Protein Sci.* **14**:602-16.

66. **Zhao, J.W., Davis, J.J., Sansom, M.S.P. and Hung, A.** 2004. Exploring the electronic and mechanical properties of protein using conducting atomic force microscopy. *J. Am. Chem. Soc.* **126**:5601-9.

67. **Andolfi, L., Bruce, D., Cannistraro, S., Canters, G.W., Davis, J.J., Hill, H.A.O., Crozier, J., Verbeet, M.P., Wrathmell, C.L. and Astier, Y.** 2004. The electrochemical characteristics of blue copper protein monolayers on gold. *J. Electroanal. Chem.* **565**:21-8.

68. **Farver, O., Skov, L.K., van de Kamp, M., Canters, G.W. and Pecht, I.** 1992. The effect of driving force on intramolecular electron transfer in proteins. Studies on single-site mutated azurins. *Eur. J. Biochem* **210**:399-403.

69. **Farver, O., Jeuken, L.J., Canters, G.W. and Pecht, I.** 2000. Role of ligand substitution on long-range electron transfer in azurins. *Eur. J. Biochem* **267**:3123-9.

70. **Tollin, G., Meyer, T.E., Cheddar, G., Getzoff, E.D. and Cusanovich, M.A.** 1986. Transient kinetics of reduction of blue copper proteins by free flavin and flavodoxin semiquinones. *Biochemistry* **25**:3363-70.

71. **Bjerrum, M.J., Casimiro, D.R., Chang, I.J., Dibilio, A.J., Gray, H.B., Hill, M.G., Langen, R., Mines, G.A., Skov, L.K., Winkler, J.R. and Wuttke, D.S.** 1995. Electron transfer in ruthenium-modified proteins. *J. Bioenerg. Biomembr.* **27**:295-302.

72. **den Blaauwen, T., van de, K.M. and Canters, G.W.** 1991. Type I and II copper sites obtained by external addition of ligands to a His117Gly azurin mutant. *J. Am. Chem. Soc.* **113**:5050-2.

73. **Jeuken, L.J.C., Ubbink, M., Bitter, J.H., van Vliet, P., Meyer-Klaucke, W. and Canters, G.W.** 2000. The structural role of the copper-coordinating and surface-exposed histidine residue in the blue copper protein azurin. *J. Mol. Biol.* **299**:737-55.

74. **Jeuken, L.J.C., van Vliet, P., Verbeet, M.P., Camba, R., McEvoy, J.P., Armstrong, F.K. and Canters, G.W.** 2000. Role of the surface-exposed and copper-coordinating histidine in blue copper proteins: The electron-transfer and redox-coupled ligand binding properties of His117Gly azurin. *J. Am. Chem. Soc.* **122**:12186-94.

75. **den Blaauwen, T. and Canters, G.W.** 1993. Creation of Type-I and Type-II copper sites by addition of exogenous ligands to the *Pseudomonas aeruginosa* azurin His117Gly mutant. *J. Am. Chem. Soc.* **115**:1121-9.

76. **Gorren, A.C., den Blaauwen, T., Canters, G.W., Hopper, D.J. and Duine, J.A.** 1996. The role of His117 in the redox reactions of azurin from *Pseudomonas aeruginosa*. *FEBS Lett.* **381**:140-2.

77. **van Pouderoyen, G., denBlaauwen, T., Reedijk, J. and Canters, G.W.** 1996. Dimerization of a His117Gly azurin mutant by external addition of 1,omega-di(imidazol-1-yl)alkanes. *Biochemistry* **35**:13205-11.

78. **Marcus, R.A. and Sutin, N.** 1985. Electron transfers in chemistry and biology. *Biochim. Biophys. Acta* **811**:265-322.

79. **Moser, C.C., Keske, J.M., Warncke, K., Farid, R.S. and Dutton, P.L.** 1992. Nature of biological electron transfer. *Nature* **355**:796-802.

80. **Page, C.C., Moser, C.C., Chen, X. and Dutton, P.L.** 1999. Natural engineering principles of electron tunnelling in biological oxidation-reduction. *Nature* **402**:47-52.

81. **Page, C.C., Moser, C.C. and Dutton, P.L.** 2003. Mechanism for electron transfer within and between proteins. *Curr. Opin. Chem. Biol.* **7**:551-6.

82. **Beratan, D.N., Betts, J.N. and Onuchic, J.N.** 1991. Protein electron transfer rates set by the bridging secondary and tertiary structure. *Science* **252**:1285-8.

83. **Winkler, J.R. and Gray, H.B.** 1992. Electron transfer in ruthenium-modified proteins. *Chem. Rev.* **92**:369-79.

84. **Gray, H.B. and Winkler, J.R.** 2003. Electron tunneling through proteins. *Q. Rev. Biophys.* **36**:341-72.

85. **Farver, O. and Pecht, I.** 1992. Long-range intramolecular electron transfer in azurins. *J. Am. Chem. Soc.* **114**:5764-7.

86. **Farver, O., Skov, L.K., Gilardi, G., van Pouderoyen, G., Canters, G.W., Wherland, S. and Pecht, I.** 1996. Structure-function correlation of intramolecular electron transfer in wild type and single-site mutated azurins. *Chem. Phys.* **204**:271-7.

87. **Regan, J.J. and Onuchic, J.N.** 1999. Electron-transfer tubes. *Adv. Phys. Chem.* **107**:497-553.

88. **Daizadeh, I., Guo, J.X. and Stuchebrukhov, A.** 1999. Vortex structure of the tunneling flow in long-range electron transfer reactions. *J. Chem. Phys.* **110**:8865-8.

89. **Kawatsu, T., Kakitani, T. and Yamato, T.** 2001. Worm model for electron tunneling in proteins: Consolidation of the pathway model and the Dutton plot. *J. Phys. Chem. B* **105**:4424-35.

90. **Ho, S.P. and DeGrado, W.F.** 1987. Design of a 4-helix bundle protein: Synthesis of peptides which self-associate into a helical protein. *J. Am. Chem. Soc.* **109**:6751-8.

91. **Summa, C.M., Lombardi, A., Lewis, M. and DeGrado, V.F.** 1999. Tertiary templates for the design of diiron proteins. *Curr. Opin. Struct. Biol.* **9**:500-8.

92. **DeGrado, W.F., Summa, C.M., Pavone, V., Nastri, F. and Lombardi, A.** 1999. De novo design and structural characterization of proteins and metalloproteins. *Annual Review of Biochemistry* **68**:779-819.

93. **Kennedy, M.L. and Gibney, B.R.** 2001. Metalloprotein and redox protein design. *Curr. Opin. Struct. Biol.* **11**:485-90.

94. **Benson, D.E., Wisz, M.S. and Hellinga, H.W.** 2000. Rational design of nascent metalloenzymes. *Proc. Natl. Acad. Sci. U. S. A.* **97**:6292-7.

95. **Worrall, J.A.R., Diederix, R.E.M., Prudêncio, M., Lowe, C.E., Ciofi-Baffoni, S., Ubbink, M. and Canters, G.W.** 2005. The effects of ligand exchange and mobility on the peroxidase activity of a bacterial cytochrome *c* upon unfolding. *ChemBioChem* **6**:747-58.

96. **Wijma, H.J., Boulanger, M.J., Molon, A., Fittipaldi, M., Huber, M., Murphy, M.E.P., Verbeet, M.P. and Canters, G.W.** 2003. Reconstitution of the type-1 active site of the H145G/A variants of nitrite reductase by ligand insertion. *Biochemistry* **42**:4075-83.

97. **Feng, C.J., Kedia, R.V., Hazzard, J.T., Hurley, J.K., Tollin, G. and Enemark, J.H.** 2002. Effect of solution viscosity on intramolecular electron transfer in sulfite oxidase. *Biochemistry* **41**:5816-21.

98. **Bhattacharyya, A., Tollin, G., Davis, M. and Edmondson, D.E.** 1983. Laser flash photolysis studies of intramolecular electron transfer in xanthine oxidase. *Biochemistry* **22**:5270-9.

99. **Govindaraj, S. and Poulos, T.L.** 1997. The domain architecture of cytochrome P450BM-3. *J. Biol. Chem.* **272**:7915-21.

100. **Hazzard, J.T., Govindaraj, S., Poulos, T.L. and Tollin, G.** 1997. Electron transfer between the FMN and heme domains of cytochrome P450BM-3. Effects of substrate and CO. *J. Biol. Chem.* **272**:7922-6.

101. **Sadeghi, S.J., Meharenna, Y.T., Fantuzzi, A., Valetti, F. and Gilardi, G.** 2000. Engineering artificial redox chains by molecular 'Lego'. *Faraday Discuss.* **116**:135-53.

102. **Gilardi, G., Fantuzzi, A. and Sadeghi, S.J.** 2001. Engineering and design in the bioelectrochemistry of metalloproteins. *Curr. Opin. Struct. Biol.* **11**:491-9.

103. **Hamachi, I., Nakamura, K., Fujita, A. and Kunitake, T.** 1993. Anisotropic incorporation of lipid-anchored myoglobin into a phospholipid-bilayer membrane. *J. Am. Chem. Soc.* **115**:4966-70.

104. **Hamachi, I. and Shinkai, S.** 1999. Chemical modification of the structures and functions of proteins by the cofactor reconstitution method. *Eur. J. Org. Chem.* 539-49.

105. **Boerakker, M.J., Hannink, J.M., Bomans, P.H., Frederik, P.M., Nolte, R.J., Meijer, E.M. and Sommerdijk, N.A.** 2002. Giant amphiphiles by cofactor reconstitution. *Angew. Chem. Int. Ed. Engl.* **41**:4239-41.

106. **Hamachi, I., Tajiri, Y. and Shinkai, S.** 1994. Sugar-responsive semisynthetic myoglobin bearing phenylboronic acid groups as recognition sites. *J. Am. Chem. Soc.* **116**:7437-8.

107. **Hamachi, I., Nagase, T., Tajiri, Y. and Shinkai, S.** 1997. Incorporation of an artificial receptor into a native protein: New strategy for the design of semisynthetic enzymes with allosteric properties. *Bioconjugate Chem.* **8**:862-8.

108. **Hayashi, T., Takimura, T. and Ogoshi, H.** 1995. Photoinduced singlet electron-transfer in a complex formed from zinc myoglobin and methyl viologen - Artificial recognition by a chemically-modified porphyrin. *J. Am. Chem. Soc.* **117**:11606-7.

109. **Hayashi, T., Hitomi, Y., Takimura, T., Tomokuni, A., Mizutani, T., Hisaeda, Y. and Ogoshi, H.** 1999. New approach to the construction of an artificial hemoprotein complex. *Coord. Chem. Rev.* **192**:961-74.

110. **Hayashi, T., Hitomi, Y. and Ogoshi, H.** 1998. Artificial protein-protein complexation between a reconstituted myoglobin and cytochrome c. *J. Am. Chem. Soc.* **120**:4910-5.

111. **Hayashi, T., Tomokuni, A., Mizutani, T., Hisaeda, Y. and Ogoshi, H.** 1998. Interfacial recognition between reconstituted myoglobin having charged binding domain and electron acceptor via electrostatic interaction. *Chem. Lett.* 1229-30.

112. **Hayashi, T., Hitomi, Y., Ando, T., Mizutani, T., Hisaeda, Y., Kitagawa, S. and Ogoshi, H.** 1999. Peroxidase activity of myoglobin is enhanced by chemical mutation of heme-propionates. *J. Am. Chem. Soc.* **121**:7747-50.

113. **Monzani, E., Alzuet, G., Casella, L., Redaelli, C., Bassani, C., Sanangelantoni, A.M., Gullotti, M., De Gioia, L., Santagostini, L. and Chillemi, F.** 2000. Properties and reactivity of myoglobin reconstituted with chemically modified protohemin complexes. *Biochemistry* **39**:9571-82.

114. **Katz, E., Riklin, A., Heleg-Shabtai, V., Willner, I. and Buckmann, A.F.** 1999. Glucose oxidase electrodes via reconstitution of the apo-enzyme: Tailoring of novel glucose biosensors. *Anal. Chim. Acta* **385**:45-58.

115. **Willner, I., I and Katz, E.** 2000. Integration of layered redox proteins and conductive supports for bioelectronic applications. *Angew. Chem. Int. Ed. Engl.* **39**:1180-218.

116. **Edmondson, D.E., Barman, B. and Tollin, G.** 1972. On the importance of the N-5 position in flavin coenzymes. Properties of free and protein-bound 5-deaza analogs. *Biochemistry* **11**:1133-8.

117. **De Francesco, R. and Edmondson, D.E.** 1988. pK_a values of the 8 alpha-imidazole substituents in selected flavoenzymes containing 8 alpha-histidylflavins. *Arch. Biochem. Biophys.* **264**:281-7.

118. **Lostao, A., El Harrous, M., Daoudi, F., Romero, A., Parody-Morreale, A. and Sancho, J.** 2000. Dissecting the energetics of the apoflavodoxin-FMN complex. *J. Biol. Chem.* **275**:9518-26.

119. **Nar, H., Huber, R., Messerschmidt, A., Filippou, A.C., Barth, M., Jaquinod, M., Vandekamp, M. and Canters, G.W.** 1992. Characterization and crystal structure of zinc azurin, a by-product of heterologous expression in *Escherichia coli* of *Pseudomonas aeruginosa* copper azurin. *Eur. J. Biochem.* **205**:1123-9.

120. **Salgado, J., Kroes, S.J., Berg, A., Moratal, J.M. and Canters, G.W.** 1998. The dynamic properties of the M121H azurin metal site as studied by NMR of the paramagnetic Cu(II) and Co(II) metalloderivatives. *J. Biol. Chem.* **273**:177-85.

121. **Jorgensen, L.E., Ubbink, M. and Danielsen, E.** 2004. Amicyanin metal-site structure and interaction with MADH: PAC and NMR spectroscopy of Ag-, Cd-, and Cu-amicyanin. *J. Biol. Inorg. Chem.* **9**:27-38.

122. **van de Velde, F., Könemann, L., van Rantwijk, F. and Sheldon, R.A.** 2000. The rational design of semisynthetic peroxidases. *Biotechnol. Bioeng.* **67**:87-96.

123. **Dickerson, J.L., Kornuc, J.J. and Rees, D.C.** 1985. Complex formation between flavodoxin and cytochrome *c*. Cross-linking studies. *J. Biol. Chem* **260**:5175-8.

124. **Furukawa, Y., Matsuda, F., Ishimori, K. and Morishima, I.** 2002. Investigation of the electron-transfer mechanism by cross-linking between Zn-substituted myoglobin and cytochrome *b*5. *J. Am. Chem. Soc.* **124**:4008-19.

125. **Qin, L. and Kostic, N.M.** 1993. Importance of protein rearrangement in the electron-transfer reaction between the physiological partners cytochrome *f* and plastocyanin. *Biochemistry* **32**:6073-80.

126. **van Amsterdam, I.M., Ubbink, M., Einsle, O., Messerschmidt, A., Merli, A., Cavazzini, D., Rossi, G.L. and Canters, G.W.** 2002. Dramatic modulation of electron transfer in protein complexes by crosslinking. *Nat. Struct. Biol.* **9**:48-52.

127. **Walker, M.C., Pueyo, J.J., Gómez-Moreno, C. and Tollin, G.** 1990. Comparison of the kinetics of reduction and intramolecular electron-transfer in electrostatic and covalent complexes of ferredoxin-NADP+ reductase and flavodoxin from *Anabaena* PCC 7119. *Arch. Biochem. Biophys.* **281**:76-83.

128. **Pappa, H.S. and Poulos, T.L.** 1995. Site-specific cross-linking as a method for studying intramolecular electron transfer. *Biochemistry* **34**:6573-80.

129. **Massey, V. and Hemmerich, P.** 1978. Photoreduction of flavoproteins and other biological compounds catalyzed by deazaflavins. *Biochemistry* **17**:9-16.

130. **Blankenhorn, G.** 1976. Nicotinamide-dependent one-electron and two-electron (flavin) oxidoreduction: Thermodynamics, kinetics, and mechanism. *Eur. J. Biochem.* **67**:67-80.

131. **Tollin, G., Hurley, J.K., Hazzard, J.T. and Meyer, T.E.** 1993. Use of laser flash photolysis time-resolved spectrophotometry to investigate interprotein and intraprotein electron transfer mechanisms. *Biophys. Chem* **48**:259-79.

132. **Tollin, G.** 1995. Use of flavin photochemistry to probe intraprotein and interprotein electron transfer mechanisms. *J. Bioenerg. Biomembr.* **27**:303-9.

133. **Meyer, T.E., Watkins, J.A., Przysiecki, C.T., Tollin, G. and Cusanovich, M.A.** 1984. Electron-transfer reactions of photoreduced flavin analogues with *c*-type cytochromes: Quantitation of steric and electrostatic factors. *Biochemistry* **23**:4761-7.

134. **Roncel, M., Hervás, M., Navarro, J.A., De la Rosa, M.A. and Tollin, G.** 1990. Flavin-photosensitized oxidation of reduced *c*-type cytochromes. Reaction mechanism and comparison with photoreduction of oxidized cytochromes by flavin semiquinones. *Eur. J. Biochem.* **191**:531-6.

135. **Navarro, J.A., De la Rosa, M.A. and Tollin, G.** 1991. Transient kinetics of flavin-photosensitized oxidation of reduced redox proteins. Comparison of *c*-type cytochromes and plastocyanins. *Eur. J. Biochem.* **199**:239-43.

136. **Navarro, J.A., Cheddar, G. and Tollin, G.** 1989. Laser flash photolysis studies of the kinetics of reduction of spinach and *Clostridium* ferredoxins by a viologen analogue: Electrostatically controlled nonproductive complex formation and differential reactivity among the iron-sulfur clusters. *Biochemistry* **28**:6057-65.

137. **Hazzard, J.T., Poulos, T.L. and Tollin, G.** 1987. Kinetics of reduction by free flavin semiquinones of the components of the cytochrome *c*-cytochrome *c* peroxidase complex and intracomplex electron transfer. *Biochemistry* **26**:2836-48.

138. **Walker, M.C., Pueyo, J.J., Navarro, J.A., Gómez-Moreno, C. and Tollin, G.** 1991. Laser flash photolysis studies of the kinetics of reduction of ferredoxins and ferredoxin-NADP+ reductases from Anabaena PCC 7119 and spinach: Electrostatic effects on intracomplex electron transfer. *Arch. Biochem. Biophys.* **287**:351-8.

139. **van den Berg, P.A., van Hoek, A., Walentas, C.D., Perham, R.N. and Visser, A.J.** 1998. Flavin fluorescence dynamics and photoinduced electron transfer in *Escherichia coli* glutathione reductase. *Biophys. J.* **74**:2046-58.

140. **Bellelli, A., Brunori, M., Brzezinski, P. and Wilson, M.T.** 2001. Photochemically induced electron transfer. *Methods* **24**:139-52.

141. **Verkhovsky, M.I., Morgan, J.E. and Wikstrom, M.** 1996. Redox transitions between oxygen intermediates in cytochrome-*c* oxidase. *Proc. Natl. Acad. Sci. U. S. A.* **93**:12235-9.

142. **Brunori, M., Giuffre, A., Malatesta, F. and Sarti, P.** 1998. Investigating the mechanism of electron transfer to the binuclear center in Cu-heme oxidases. *J. Bioenerg. Biomembr.* **30**:41-5.

143. **Xiao, K.H., Engstrom, G., Rajagukguk, S., Yu, C.A., Yu, L., Durham, B. and Millett, F.** 2003. Effect of famoxadone on photoinduced electron transfer between the iron-sulfur center and cytochrome *c*1 in the cytochrome *bc*1 complex. *J. Biol. Chem.* **278**:11419-26.

144. **Di Bilio, A.J., Hill, M.G., Bonander, N., Karlsson, B.G., Villahermosa, R.M., Malmström, B.G., Winkler, J.R. and Gray, H.B.** 1997. Reorganization energy of blue copper: Effects of temperature and driving force on the rates of electron transfer in ruthenium- and osmium-modified azurins. *J. Am. Chem. Soc.* **119**:9921-2.

145. **Durham, B., Pan, L.P., Long, J.E. and Millett, F.** 1989. Photoinduced electron-transfer kinetics of singly labeled ruthenium bis(bipyridine) dicarboxybipyridine cytochrome *c* derivatives. *Biochemistry* **28**:8659-65.

146. **Pan, L.P., Hibdon, S., Liu, R.Q., Durham, B. and Millett, F.** 1993. Intracomplex electron transfer between ruthenium-cytochrome *c* derivatives and cytochrome *c* oxidase. *Biochemistry* **32**:8492-8.

147. **Geren, L., Hahm, S., Durham, B. and Millett, F.** 1991. Photoinduced electron transfer between cytochrome *c* peroxidase and yeast cytochrome *c* labeled at Cys 102 with (4-bromomethyl-4'-methylbipyridine)[bis(bipyridine)]ruthenium^{2+}. *Biochemistry* **30**:9450-7.

148. **Scott, J.R., Willie, A., McLean, M., Sligar, S.G. and Durham, B.** 1993. Intramolecular electron-transfer in cytochrome *b*5 labeled with Ruthenium(II) polypyridine complexes - Rate measurements in the Marcus Inverted Region. *J. Am. Chem. Soc.* **115**:6820-4.

149. **Hamachi, I., Tanaka, S., Tsukiji, S., Shinkai, S. and Oishi, S.** 1998. Design and semisynthesis of photoactive myoglobin bearing ruthenium tris(2,2 '-bipyridine) using cofactor-reconstitution. *Inorg. Chem.* **37**:4380-8.

150. **Immoos, C.E., Di Bilio, A.J., Cohen, M.S., van der Veer, W., Gray, H.B. and Farmer, P.J.** 2004. Electron-transfer chemistry of Ru-linker-(heme)-modified myoglobin: Rapid intraprotein reduction of a photogenerated porphyrin cation radical. *Inorg. Chem.* **43**:3593-6.

151. **Wilker, J.J., Dmochowski, I.J., Dawson, J.H., Winkler, J.R. and Gray, H.B.** 1999. Substrates for rapid oxidation and reduction of buried active sites in proteins. *J. Inorg. Biochem.* **74**:338.

152. **Geren, L.M., Beasley, J.R., Fine, B.R., Saunders, A.J., Hibdon, S., Pielak, G.J., Durham, B. and Millett, F.** 1995. Design of a ruthenium-cytochrome *c* derivative to measure electron transfer to the initial acceptor in cytochrome *c* oxidase. *J. Biol. Chem.* **270**:2466-72.

153. **Babini, E., Bertini, I., Borsari, M., Capozzi, F., Luchinat, C., Zhang, X.Y., Moura, G.L.C., Kurnikov, I.V., Beratan, D.N., Ponce, A., Di Bilio, A.J., Winkler, J.R. and Gray, H.B.** 2000. Bond-mediated electron tunneling in ruthenium-modified high-potential iron-sulfur protein. *J. Am. Chem. Soc.* **122**:4532-3.

154. **Regan, J.J., Di Bilio, A.J., Winkler, J.R., Richards, J.H. and Gray, H.B.** 1998. Electron tunneling in Ru-modified His46Asp azurin. Coupling through the Cu ligands. *Inorg. Chim. Acta* **276**:470-80.

155. **Winkler, J.R., Di Bilio, A.J., Farrow, N.A., Richards, J.H. and Gray, H.B.** 1999. Electron tunneling in biological molecules. *Pure Appl. Chem.* **71**:1753-64.

156. **Winkler, J.R., Malmstrom, B.G. and Gray, H.B.** 1995. Rapid electron injection into multisite metalloproteins: Intramolecular electron transfer in cytochrome oxidase. *Biophys. Chem.* **54**:199-209.

157. **Liu, R.Q., Geren, L., Anderson, P., Fairris, J.L., Peffer, N., McKee, A. and Durham, B.** 1995. Design of ruthenium-cytochrome *c* derivatives to measure electron transfer to cytochrome *c* peroxidase. *Biochimie* **77**:549-61.

158. **Mei, H., Wang, K., Peffer, N., Weatherly, G., Cohen, D.S., Miller, M., Pielak, G., Durham, B. and Millett, F.** 1999. Role of configurational gating in intracomplex electron transfer from cytochrome *c* to the radical cation in cytochrome *c* peroxidase. *Biochemistry* **38**:6846-54.

159. **Millett, F. and Durham, B.** 2002. Design of photoactive ruthenium complexes to study interprotein electron transfer. *Biochemistry* **41**:11315-24.

160. **Wang, K., Mei, H., Geren, L., Miller, M.A., Saunders, A., Wang, X., Waldner, J.L., Pielak, G.J., Durham, B. and Millett, F.** 1996. Design of a ruthenium-cytochrome *c* derivative to measure electron transfer to the radical cation and oxyferryl heme in cytochrome *c* peroxidase. *Biochemistry* **35**:15107-19.

161. **Dmochowski, I.J., Dunn, A.R., Wilker, J.J., Crane, B.R., Green, M.T., Dawson, J.H., Sligar, S.G., Winkler, J.R. and Gray, H.B.** 2002. Sensitizer-linked substrates and ligands: Ruthenium probes of cytochrome P450 structure and mechanism. 357 120-33. *In* Methods Enzym., Elsevier Science (USA),

162. **Zhou, J.S. and Kostic, N.M.** 1992. Photoinduced electron-transfer from zinc cytochrome *c* to plastocyanin is gated by surface-diffusion within the metalloprotein complex. *J. Am. Chem. Soc.* **114**:3562-3.

163. **Bellelli, A., Brzezinski, P., Arese, M., Cutruzzola, F., Silvestrini, M.C. and Brunori, M.** 1996. Electron transfer in zinc-reconstituted nitrite reductase from *Pseudomonas aeruginosa*. *Biochem. J.* **319**:407-10.

164. **Takashima, H., Tanaka, M., Hasegawa, Y. and Tsukahara, K.** 2003. Remarkably stereoselective photoinduced electron-transfer reaction between zinc myoglobin and optically active binaphthyl bisviologen. *J. Biol. Inorg. Chem.* **8**:499-506.

165. **Sokerina, E.V., Ullmann, G.M., van Pouderoyen, G., Canters, G.W. and Kostic, N.M.** 1999. Electrostatic effects on the kinetics of photoinduced electron-transfer reactions of the triplet state of

zinc cytochrome *c* with wild-type and mutant forms of *Pseudomonas aeruginosa* azurin. *J. Biol. Inorg. Chem.* **4**:111-21.

166. **Hayashi, T., Takimura, T., Ohara, T., Hitomi, Y. and Ogoshi, H.** 1995. Photoinduced electron transfer from zinc porphyrin to a linked quinone in myoglobin. *J. Chem. Soc. ,Chem. Commun.* 2503-4.

167. **Hayashi, T. and Ogoshi, H.** 1997. Molecular modelling of electron transfer systems by noncovalently linked porphyrin-acceptor pairing. *Chem. Soc. Rev.* **26**:355-64.

168. **Hayashi, T., Ando, T., Matsuda, T., Yonemura, H., Yamada, S. and Hisaeda, Y.** 2000. Introduction of a specific binding domain on myoglobin surface by new chemical modification. *J. Inorg. Biochem.* **82**:133-9.

169. **Hayashi, T. and Hisaeda, Y.** 2002. New functionalization of myoglobin by chemical modification of heme-propionates. *Acc. Chem. Res.* **35**:35-43.

170. **Kotlyar, A.B., Borovok, N., Raviv, S., Zimányi, L. and Gutman, M.** 1996. Fast redox perturbation of aqueous solution by photoexcitation of pyranine. *Photochem. Photobiol.* **63**:448-54.

171. **Kotlyar, A.B. and Borovok, N.** 1995. Light-induced oxidation of cytochrome *c*. *Biochim. Biophys. Acta* **1228**:87-90.

172. **Kotlyar, A.B., Borovok, N. and Hazani, M.** 1997. Use of thiouredopyrenetrisulfonate photochemistry for driving electron transfer reactions in aqueous solutions. *Biochemistry* **36**:15823-7.

173. **Kotlyar, A.B., Borovok, N. and Hazani, M.** 1997. Photoinduced electron transfer in singly labeled thiouredopyrenetrisulfonate cytochrome *c* derivatives. *Biochemistry* **36**:15828-33.

174. **Borovok, N., Kotlyar, A.B., Pecht, I., Skov, L.K. and Farver, O.** 1999. Photoinduced electron transfer in singly labeled thiouredopyrenetrisulfonate azurin derivatives. *FEBS Lett.* **457**:277-82.

175. **Kotlyar, A., Borovok, N., Hazani, M., Szundi, I. and Einarsdottir, O.** 2000. Photoinduced intracomplex electron transfer between cytochrome *c* oxidase and TUPS-modified cytochrome *c*. *Eur. J. Biochem.* **267**:5805-9.

176. **Szundi, I., Cappuccio, J.A., Borovok, N., Kotlyar, A.B. and Einarsdottir, O.** 2001. Photoinduced electron transfer in the cytochrome *c*/cytochrome *c* oxidase complex using thiouredopyrenetrisulfonate-labeled cytochrome *c*. Optical multichannel detection. *Biochemistry* **40**:2186-93.

177. **Kotlyar, A.B., Borovok, N., Khoroshyy, P., Tenger, K. and Zimányi, L.** 2004. Redox photochemistry of thiouredopyrenetrisulfonate. *Photochem. Photobiol.* **79**:489-93.

178. **Denisov, I.G., Makris, T.M. and Sligar, S.G.** 2001. Cryotrapped reaction intermediates of cytochrome P450 studied by radiolytic reduction with phosphorus-32. *J. Biol. Chem.* **276**:11648-52.

179. **Silkstone, G., Stanway, G., Brzezinski, P. and Wilson, M.T.** 2002. Production and characterisation of Met80X mutants of yeast iso-1-cytochrome *c*: Spectral, photochemical and binding studies on the ferrous derivatives. *Biophys. Chem.* **98**:65-77.

180. **Nastri, F., Lombardi, A., Morelli, G., Maglio, O., D'Auria, G., Pedone, C. and Pavone, V.** 1997. Hemoprotein models based on a colvalent helix-heme-helix sandwich: 1. Design, synthesis and characterisation. *Chem. Eur. J.* **3**:340-9.

181. **Sharp, R.E., Moser, C.C., Rabanal, F. and Dutton, P.L.** 1998. Design, synthesis, and characterization of a photoactivatable flavocytochrome molecular maquette. *Proc. Natl. Acad. Sci. U. S. A.* **95**:10465-70.

182. **Rau, H.K., DeJonge, N. and Haehnel, W.** 1998. Modular synthesis of de novo-designed metalloproteins for light-induced electron transfer. *Proc. Natl. Acad. Sci. U. S. A.* **95**:11526-31.

183. **Sykes, G.A. and Rogers, L.J.** 1984. Redox potentials of algal and cyanobacterial flavodoxins. *Biochem. J.* **217**:845-50.

184. **Burnett, R.M., Darling, G.D., Kendall, D.S., LeQuesne, M.E., Mayhew, S.G., Smith, W.W. and Ludwig, M.L.** 1974. The structure of the oxidized form of clostridial flavodoxin at 1.9-Å resolution. *J. Biol. Chem* **249**:4383-92.

185. **Fukuyama, K., Matsubara, H. and Rogers, L.J.** 1992. Crystal structure of oxidized flavodoxin from a red alga *Chondrus crispus* refined at 1.8 Å resolution. Description of the flavin mononucleotide binding site. *J. Mol. Biol.* **225**:775-89.

186. **Freigang, J., Diederichs, K., Schafer, K.P., Welte, W. and Paul, R.** 2002. Crystal structure of oxidized flavodoxin, an essential protein in *Helicobacter pylori*. *Protein Sci.* **11**:253-61.

187. **van Mierlo, C.P., Lijnzaad, P., Vervoort, J., Müller, F., Berendsen, H.J. and de Vlieg, J.** 1990. Tertiary structure of two-electron reduced *Megasphaera elsdenii* flavodoxin and some implications, as determined by two-dimensional 1H-NMR and restrained molecular dynamics. *Eur. J. Biochem.* **194**:185-98.

188. **Smith, W.W., Pattridge, K.A., Ludwig, M.L., Petsko, G.A., Tsernoglou, D., Tanaka, M. and Yasunobu, K.T.** 1983. Structure of oxidized flavodoxin from *Anacystis nidulans*. *J. Mol. Biol.* **165**:737-53.

189. **Romero, A., Caldeira, J., Legall, J., Moura, I., Moura, J.J. and Romao, M.J.** 1996. Crystal structure of flavodoxin from *Desulfovibrio desulfuricans* ATCC 27774 in two oxidation states. *Eur. J. Biochem.* **239**:190-6.

190. **Smith, W.W., Burnett, R.M., Darling, G.D. and Ludwig, M.L.** 1977. Structure of the semiquinone form of flavodoxin from *Clostridum* MP. Extension of 1.8 Å resolution and some comparisons with the oxidized state. *J. Mol. Biol.* **117**:195-225.

191. **Zhou, Z. and Swenson, R.P.** 1996. The cumulative electrostatic effect of aromatic stacking interactions and the negative electrostatic environment of the flavin mononucleotide binding site is a major determinant of the reduction potential for the flavodoxin from *Desulfovibrio vulgaris* (Hildenborough). *Biochemistry* **35**:15980-8.

192. **McCarthy, A.A., Walsh, M.A., Verma, C.S., O'Connell, D.P., Reinhold, M., Yalloway, G.N., D'Arcy, D., Higgins, T.M., Voordouw, G. and Mayhew, S.G.** 2002. Crystallographic investigation of the role of aspartate 95 in the modulation of the redox potentials of *Desulfovibrio vulgaris* flavodoxin. *Biochemistry* **41**:10950-62.

193. **Steensma, E., Nijman, M.J., Bollen, Y.J., de Jager, P.A., van den Berg, W.A., van Dongen, W.M. and van Mierlo, C.P.** 1998. Apparent local stability of the secondary structure of *Azotobacter vinelandii* holoflavodoxin II as probed by hydrogen exchange: implications for redox potential regulation and flavodoxin folding. *Protein Sci.* **7**:306-17.

194. **Duyvis, M.G., Wassink, H. and Haaker, H.** 1998. Nitrogenase of *Azotobacter vinelandii*: Kinetic analysis of the Fe protein redox cycle. *Biochemistry* **37**:17345-54.

195. **Barman, B.G. and Tollin, G.** 1972. Flavine-protein interactions in flavoenzymes - Thermodynamics and kinetics of reduction of *Azotobacter* flavodoxin. *Biochemistry* **11**:4755-9.

196. **Pueyo, J.J., Curley, G.P. and Mayhew, S.G.** 1996. Kinetics and thermodynamics of the binding of riboflavin, riboflavin 5'-phosphate and riboflavin 3',5'-bisphosphate by apoflavodoxins. *Biochem. J.* **313**:855-61.

197. **van Mierlo, C.P., van den Oever, J.M. and Steensma, E.** 2000. Apoflavodoxin (un)folding followed at the residue level by NMR. *Protein Sci.* **9**:145-57.

198. **Bollen, Y.J., Sanchez, I.E. and van Mierlo, C.P.** 2004. Formation of on- and off-pathway intermediates in the folding kinetics of *Azotobacter vinelandii* apoflavodoxin. *Biochemistry* **43**:10475-89.

199. **Drummond, M.H.** 1986. Structure predictions and surface charge of nitrogenase flavodoxins from *Klebsiella pneumoniae* and *Azotobacter vinelandii*. *Eur. J. Biochem.* **159**:549-53.

200. **van Mierlo, C.P., van Dongen, W.M., Vergeldt, F., van Berkel, W.J. and Steensma, E.** 1998. The equilibrium unfolding of *Azotobacter vinelandii* apoflavodoxin II occurs via a relatively stable folding intermediate. *Protein Sci.* **7**:2331-44.

201. **Tollin, G. and Edmondson, D.E.** 1980. Purification and properties of flavodoxins. *Methods Enzymol.* 392-406.

202. **Otwinowski, Z. and Minor, W.** 1997. Processing of X-ray diffraction data collected in oscillation mode. *Methods Enzymol.* 307-26.

203. **French, S.W.K.** 1978. On the treatment of negative intensity observations. *Acta Crystallogr. A* **34**:517-24.

204. **Burkhart, B.M.** 1995. Structure of the trigonal form of recombinant oxidized flavodoxin from *Anabaena* 7120 at 1.40 Å resolution. *Acta Crystallogr. D. Biol. Crystallogr.* **51**:318-30.

205. **Kelley, L.A., MacCallum, R.M. and Sternberg, M.J.** 2000. Enhanced genome annotation using structural profiles in the program 3D-PSSM. *J. Mol. Biol.* **299**:499-520.

206. **Bower, M.J., Cohen, F.E. and Dunbrack, R.L., Jr.** 1997. Prediction of protein side-chain rotamers from a backbone-dependent rotamer library: A new homology modeling tool. *J. Mol. Biol.* **267**:1268-82.

207. **Kissinger, C.R., Gehlhaar, D.K. and Fogel, D.B.** 1999. Rapid automated molecular replacement by evolutionary search. *Acta Crystallogr. D. Biol. Crystallogr.* **55**:484-91.

208. **Brunger, A.T., Adams, P.D., Clore, G.M., DeLano, W.L., Gros, P., Grosse-Kunstleve, R.W., Jiang, J.S., Kuszewski, J., Nilges, M., Pannu, N.S., Read, R.J., Rice, L.M., Simonson, T. and Warren, G.L.** 1998. Crystallography & NMR system: A new software suite for macromolecular structure determination. *Acta Crystallogr. D. Biol. Crystallogr.* **54**:905-21.

209. **Jones, T.A., Zou, J.Y., Cowan, S.W. and Kjeldgaard.** 1991. Improved methods for building protein models in electron density maps and the location of errors in these models. *Acta Crystallogr. A* **47**:110-9.

210. **Murshudov, G.N.** 1997. Refinement of macromolecular structures by the maximum-likelihood method. *Acta Crystallogr. D. Biol. Crystallogr.* **53**:240-55.

211. **Laskowski, R.A., Moss, D.S. and Thornton, J.M.** 1993. Main-chain bond lengths and bond angles in protein structures. *J. Mol. Biol.* **231**:1049-67.

212. **Berman, H.M., Westbrook, J., Feng, Z., Gilliland, G., Bhat, T.N., Weissig, H., Shindyalov, I.N. and Bourne, P.E.** 2000. The Protein Data Bank. *Nucleic Acids Res.* **28**:235-42.

213. **Hubbard, S.J. and Thornton, J.M.** 1993. NACCESS, Computer Program, Department of Biochemistry and Molecular Biology, University College London.

214. **Kabsch, W. and Sander, C.** 1983. Dictionary of Protein Secondary Structure - Pattern-recognition of hydrogen-bonded and geometrical features. *Biopolymers* **22**:2577-637.

215. **Altschul, S.F., Gish, W., Miller, W., Myers, E.W. and Lipman, D.J.** 1990. Basic local alignment search tool. *J. Mol. Biol.* **215**:403-10.

216. **Thorneley, R.N.F., Ashby, G.A., Drummond, M.H., Eady, R.R., Hughes, D.L., Ford, G., Harrison, P.M., Shaw, A., Robson, R.L., Kazlauskaite, J. and Hill, H.A.O.** 1994. Flavodoxins and nitrogen fixation - Structure, electrochemistry and post-translational modification by coenzyme A. 343-54. *In* Flavins and Flavoproteins, Walter de Gruyter, Berlin.

217. **Yoch, D.C.** 1975. Dimerization of *Azotobacter vinelandii* flavodoxin (azotoflavin). *Arch. Biochem. Biophys.* **170**:326-33.

218. **Taylor, M.F., Boylan, M.H. and Edmondson, D.E.** 1990. *Azotobacter vinelandii* flavodoxin: Purification and properties of the recombinant, dephospho form expressed in *Escherichia coli*. *Biochemistry* **29**:6911-8.

219. **Drennan, C.L., Pattridge, K.A., Weber, C.H., Metzger, A.L., Hoover, D.M. and Ludwig, M.L.** 1999. Refined structures of oxidized flavodoxin from *Anacystis nidulans*. *J. Mol. Biol.* **294**:711-24.

220. **Bruns, C.M., Hubatsch, I., Ridderstrom, M., Mannervik, B. and Tainer, J.A.** 1999. Human glutathione transferase A4-4 crystal structures and mutagenesis reveal the basis of high catalytic efficiency with toxic lipid peroxidation products. *J. Mol. Biol.* **288**:427-39.

221. **Artali, R., Bombieri, G., Meneghetti, F., Gilardi, G., Sadeghi, S.J., Cavazzini, D. and Rossi, G.L.** 2002. Comparison of the refined crystal structures of wild-type (1.34 Å) flavodoxin from *Desulfovibrio vulgaris* and the S35C mutant (1.44 Å) at 100 K. *Acta Crystallogr. D. Biol. Crystallogr.* **58**:1787-92.

222. **Vervoort, J., van Berkel, W.J., Mayhew, S.G., Müller, F., Bacher, A., Nielsen, P. and LeGall, J.** 1986. Properties of the complexes of riboflavin 3',5'-bisphosphate and the apoflavodoxins from *Megasphaera elsdenii* and *Desulfovibrio vulgaris*. *Eur. J. Biochem.* **161**:749-56.

223. **Mayhew, S.G., OConnell, D.P., OFarrell, P.A., Yalloway, G.N. and Geoghegan, S.M.** 1996. Regulation of the redox potentials of flavodoxins: Modification of the flavin binding site. *Biochem. Soc. Trans.* **24**:122-7.

224. **Hu, Y.Z., Tsukiji, S., Shinkai, S., Oishi, S. and Hamachi, I.** 2000. Construction of artificial photosynthetic reaction centers on a protein surface: Vectorial, multistep, and proton-coupled electron transfer for long-lived charge separation. *J. Am. Chem. Soc.* **122**:241-53.

225. **Shumyantseva, V.V., Bulko, T.V., Bachmann, T.T., Bilitewski, U., Schmid, R.D. and Archakov, A.I.** 2000. Electrochemical reduction of flavocytochromes 2B4 and 1A2 and their catalytic activity. *Arch. Biochem. Biophys.* **377**:43-8.

226. **Chowdhury, A., Peteanu, L.A., Webb, M.A. and Loppnow, G.R.** 2001. Stark spectroscopic studies of blue copper proteins: Azurin. *J. Phys. Chem. B* **105**:527-34.

227. **Kroes, S.J., Salgado, J., Parigi, G., Luchinat, C. and Canters, G.W.** 1996. Electron relaxation and solvent accessibility of the metal site in wild-type and mutated azurins as determined from nuclear magnetic relaxation dispersion experiments. *J. Biol. Inorg. Chem.* **1**:551-9.

228. **den Blaauwen, T., Hoitink, C.W., Canters, G.W., Han, J., Loehr, T.M. and Sanders-Loehr, J.** 1993. Resonance Raman-spectroscopy of the azurin His117Gly mutant - Interconversion of Type-1 and Type-2 copper sites through exogenous ligands. *Biochemistry* **32**:12455-64.

229. **van de Kamp, M., Hali, F.C., Rosato, N., Agro, A.F. and Canters, G.W.** 1990. Purification and characterization of a non-reconstitutable azurin, obtained by heterologous expression of the *Pseudomonas aeruginosa* azu gene in *Escherichia coli*. *Biochim. Biophys. Acta* **1019**:283-92.

230. **Williamson, G. and Edmondson, D.E.** 1985. Effect of pH on oxidation-reduction potentials of 8α-N-imidazole-substituted flavins. *Biochemistry* **24**:7790-7.

231. **Dutton, P.L.** 1978. Redox potentiometry: determination of midpoint potentials of oxidation-reduction components of biological electron-transfer systems. *Methods Enzymol.* **54**:411-35.

232. **Navarro, J.A., Hervás, M., De la, C.B. and De la Rosa, M.A.** 1995. Purification and physicochemical properties of the low-potential cytochrome c_{549} from the cyanobacterium *Synechocystis* sp. PCC 6803. *Arch. Biochem. Biophys.* **318**:46-52.

233. **Draper, R.D. and Ingraham, L.L.** 1968. A potentiometric study of the flavin semiquinone equilibrium. *Arch. Biochem. Biophys.* **125**:802-8.

234. **Walker, W.H., Singer, T.P., Ghisla, S. and Hemmerich, P.** 1972. Studies on succinate dehydrogenase. 8 -Histidyl-FAD as the active center of succinate dehydrogenase. *Eur. J. Biochem.* **26**:279-89.

235. **Edmondson, D.E. and De Francesco, R.** 1991. Structure, synthesis and physical properties of covalently bound flavins and 6- and 8-hydroxyflavins. 73-103. *In* Chemistry and Biochemistry of Flavoenzymes, Müller, F. (eds). CRC Press, Boca Raton, FL, USA.

236. **Michaelis, L. and Schubert, M.P.** 1938. The theory of reversible two-step oxidation involving free radicals. *Chem. Rev.* **22**:437-70.

237. **Diederix, R.E.M., Ubbink, M. and Canters, G.W.** 2002. Peroxidase activity as a tool for studying the folding of *c*-type cytochromes. *Biochemistry* **41**:13067-77.

238. **Beratan, D.N. and Onuchic, J.N.** 1996. The protein bridge between redox centres. 23-42. *In* Protein Electron Transfer, Bendall, D. S. (eds). BIOS Scientific Publishers, Oxford.

239. **Peeters, E., van Hal, P.A., Meskers, S.C.J., Janssen, R.A.J. and Meijer, E.W.** 2002. Photoinduced electron transfer in a mesogenic donor-acceptor-donor system. *Chem. Eur. J.* **8**:4470-4.

240. **Duncan, T.V., Rubtsov, I.V., Uyeda, H.T. and Therien, M.J.** 2004. Highly conjugated (polypyridyl)metal-(porphinato)zinc(II) compounds: Long-lived, high oscillator strength, excited-state absorbers having exceptional spectral coverage of the near-infrared. *J. Am. Chem. Soc.* **126**:9474-5.

241. **Hu, Y.Z., Takashima, H., Tsukiji, S., Shinkai, S., Nagamune, T., Oishi, S. and Hamachi, I.** 2000. Direct comparison of electron transfer properties of two distinct semisynthetic triads with non-protein based triad: Unambiguous experimental evidences on protein matrix effects. *Chem. Eur. J.* **6**:1907-16.

242. **Canters, G.W., Kalverda, A.P. and Hoitink, C.W.G.** 1993. Structure and activity of Type I Cu sites. 30-7. *In* The Chemistry of the Copper and Zinc Triads, Welch, A. J. and Chapman, S. K. (eds). The Royal Society of Chemistry, Cambridge.

243. **Farver, O.** 1996. Copper proteins. 161-88. *In* Protein Electron Transfer, Bendall, D. S. (eds). BIOS Scientific Publishers, Oxford.

244. **van de Kamp, M., Floris, R., Hali, F.C. and Canters, G.W.** 1990. Site-directed mutagenesis reveals that the hydrophobic patch of azurin mediates electron transfer. *J. Am. Chem. Soc.* **112**:907-8.

245. **Nar, H., Messerschmidt, A., Huber, R., van de Kamp, M. and Canters, G.W.** 1991. X-ray crystal structure of the two site-specific mutants His35Gln and His35Leu of azurin from *Pseudomonas aeruginosa*. *J. Mol. Biol.* **218**:427-47.

246. **Alagaratnam, S., van Pouderoyen, G., Pijning, T., Dijkstra, B.W., Cavazzini, D., Rossi, G.L. and Canters, G.W.** 2005. Crystallographic study of Cys69Ala flavodoxin II of *Azotobacter vinelandii*: Structural determinants of redox potential. *Protein Sci.*

247. **Adman, E.T. and Jensen, L.H.** 1981. Structural features of azurin at 2.7 Å resolution. *Isr. J. Chem.* 8-12.

248. **Edmondson, D.E., Kenney, W.C. and Singer, T.P.** 1976. Structural elucidation and properties of 8α-(N1-histidyl)riboflavin: The flavin component of thiamine dehydrogenase and beta-cyclopiazonate oxidocyclase. *Biochemistry* **15**:2937-45.

249. **Mayhew, S.G.** 1999. The effects of pH and semiquinone formation on the oxidation-reduction potentials of flavin mononucleotide. A reappraisal. *Eur. J. Biochem.* **265**:698-702.

250. **Curley, G.P., Carr, M.C., Mayhew, S.G. and Voordouw, G.** 1991. Redox and flavin-binding properties of recombinant flavodoxin from *Desulfovibrio vulgaris* (Hildenborough). *Eur. J. Biochem.* **202**:1091-100.

251. **Sibbesen, O., De Voss, J.J. and Montellano, P.R.O.** 1996. Putidaredoxin reductase-putidaredoxin-cytochrome P450cam triple fusion protein. Construction of a self-sufficient *Escherichia coli* catalytic system. *J. Biol. Chem.* **271**:22462-9.

252. **Bizub, D., Weber, I.T., Cameron, C.E., Leis, J.P. and Skalka, A.M.** 1991. A range of catalytic efficiencies with avian retroviral protease subunits genetically linked to form single polypeptide chains. *J. Biol. Chem.* **266**:4951-8.

253. **Bovia, F., Bui, N. and Strub, K.** 1994. The heterodimeric subunit SRP9/14 of the signal recognition particle functions as permuted single polypeptide chain. *Nucleic Acids Res.* **22**:2028-35.

254. **Robinson, C.R. and Sauer, R.T.** 1996. Covalent attachment of Arc repressor subunits by a peptide linker enhances affinity for operator DNA. *Biochemistry* **35**:109-16.

255. **Sieber, M. and Allemann, R.K.** 1998. Single chain dimers of MASH-1 bind DNA with enhanced affinity. *Nucleic Acids Res.* **26**:1408-13.

256. **Kuntz, M.A. and Shapiro, D.J.** 1997. Dimerizing the estrogen receptor DNA binding domain enhances binding to estrogen response elements. *J. Biol. Chem.* **272**:27949-56.

257. **Pantoliano, M.W., Bird, R.E., Johnson, S., Asel, E.D., Dodd, S.W., Wood, J.F. and Hardman, K.D.** 1991. Conformational stability, folding, and ligand-binding affinity of single-chain Fv immunoglobulin fragments expressed in *Escherichia coli*. *Biochemistry* **30**:10117-25.

258. **Jana, R., Hazbun, T.R., Fields, J.D. and Mossing, M.C.** 1998. Single-chain lambda Cro repressors confirm high intrinsic dimer-DNA affinity. *Biochemistry* **37**:6446-55.

259. **Sambrook, J., Fritsch, E.F. and Maniatis, T.** 1989. Molecular cloning: A laboratory manual. Cold Spring Harbor Laboratory Press, Cold Spring Harbor, New York.

260. **Ho, S.N., Hunt, H.D., Horton, R.M., Pullen, J.K. and Pease, L.R.** 1989. Site-directed mutagenesis by overlap extension using the polymerase chain reaction. *Gene* **77**:51-9.

261. **Tenger, K., Khoroshyy, P., Leitgeb, B., Rákhely, G., Borovok, N., Kotlyar, A., Dolgikh, D.A. and Zimányi, L.** 2005. Complex kinetics of the electron transfer between the photoactive redox label TUPS and the heme of cytochrome *c*. *Submitted*

262. **Finiguerra, M.G., van Amsterdam, I.M.C., Alagaratnam, S., Ubbink, M. and Huber, M.** 2003. Anisotropic spin label mobilities in azurin from 95 GHz electron paramagnetic resonance spectroscopy. *Chemical Physics Letters* **382**:528-33.

263. **Ahmad, I., Cusanovich, M.A. and Tollin, G.** 1982. Laser flash photolysis studies of electron transfer between semiquinone and fully reduced free flavins and the cytochrome *c*-cytochrome oxidase complex. *Biochemistry* **21**:3122-8.

264. **Ubbink, M., Worrall, J.A.R., Canters, G.W., Groenen, E.J.J. and Huber, M.** 2002. Paramagnetic resonance of biological metal centers. *Annu. Rev. Bioph. Biom.* **31**:393-422.

265. **Moonen, C.T. and Müller, F.** 1984. On the intermolecular electron transfer between different redox states of flavodoxin from *Megasphaera elsdenii*. A 500-MHz ^{1}H NMR study. *Eur. J. Biochem.* **140**:303-9.

266. **Vervoort, J., Müller, F., Mayhew, S.G., van den Berg, W.A., Moonen, C.T. and Bacher, A.** 1986. A comparative carbon-13, nitrogen-15, and phosphorus-31 nuclear magnetic resonance study on the flavodoxins from *Clostridium* MP, *Megasphaera elsdenii* and *Azotobacter vinelandii*. *Biochemistry* **25**:6789-99.

267. **Edmondson, D.E. and James, T.L.** 1979. Covalently bound non-coenzyme phosphorus residues in flavoproteins: 31P nuclear magnetic resonance studies of *Azotobacter* flavodoxin. *Proc. Natl. Acad. Sci. U. S. A.* **76**:3786-9.

268. **Edmondson, D.E. and James, T.L.** 1982. Physical and chemical studies on the FMN and non-flavin phosphate residues in *Azotobacter f*lavodoxin. 111-8. *In* Flavins and Flavoproteins, Massey, V. and Williams, C. H. (eds). Elsevier, North Holland, New York.

269. **Favaudon, V., LeGall, J. and Lhoste, J.M.** 1980. 373-86. *In* Flavins and Flavoproteins, Yagi, K. and Yamano, T. (eds). Japan Scientific Societies Press, Tokyo.

270. **Prudêncio, M., Rohovec, J., Peters, J.A., Tocheva, E., Boulanger, M.J., Murphy, M.E.P., Hupkes, H.J., Kosters, W., Impagliazzo, A. and Ubbink, M.** 2004. A caged lanthanide complex as a paramagnetic shift agent for protein NMR. *Chem. Eur. J.* **10**:3252-60.

List of Publications

1. Finiguerra, M.G., van Amsterdam, I.M.C., **Alagaratnam, S.**, Ubbink, M. and Huber, M. 2003. Anisotropic spin label mobilities in azurin from 95 GHz electron paramagnetic resonance spectroscopy. *Chem. Phys Lett.* **382:** 528-533.

2. **Alagaratnam, S.**, van Pouderoyen, G., Pijning, T., Dijkstra, B.W., Cavazzini, D., Rossi, G.L., van Dongen, W.M.A.M., van Mierlo, C.P.M., van Berkel, W.J.H. and Canters, G.W. 2005. A crystallographic study of Cys69Ala flavodoxin II from *Azotobacter vinelandii*: Structural determinants of redox potential. *Protein Sci.* **14**: 2284-2295.

3. Schmauder, R., **Alagaratnam, S.**, Chan, C., Schmidt, T., Canters, G.W. and Aartsma, T.J. 2005. Sensitive detection of the redox state of copper proteins using fluorescence. *J. Biol. Inorg. Chem.* In press.

4. **Alagaratnam, S.**, van Vliet, P., Meeuwenoord, N.J., Navarro, J.A., Hervás, M., De la Rosa, M.A., Ubbink, M. and Canters, G.W. 2005. Probing the reactivity of different forms of azurin by flavin photoreduction. *In preparation.*

5. **Alagaratnam, S.**, de Waal, E., Navarro, Navarro, J.A., Hervás, M., De la Rosa, M.A., Tenger, K., Khoroshyy, P., Zimányi, L., Ubbink, M. and Canters, G.W. 2005. Photoinduced electron transfer in TUPS-labelled flavodoxin derivatives. *In preparation.*

Curriculum vitæ

Sharmini Alagaratnam was born in Singapore on the 17th of March, 1975 and lived there until the age of two, when she moved with her family to Kuala Lumpur, Malaysia. She started her education at Assunta Primary and Secondary Schools in Petaling Jaya, Selangor, before going on to obtain three 'A' levels in Biology, Chemistry and Mathematics at Penrhos College in North Wales, UK in 1994. Following this, she embarked upon a Bachelor of Science degree in Biotechnology at Imperial College in London. She conducted her final-year research project on the heterologous expression of ferredoxin from *R. rubrum* under the supervision of Prof. Stefan Nordlund at the Department of Biochemistry of Stockholm University. In 1997, she went on to do a one year's Masters degree in Biochemical Research again at Imperial College, completing three research projects, variously in plasposon mutagenesis in *P. putida*, development of a trimethylogen dehydrogenase biosensor and methionine auxotrophy in clinical isolates of *P. aeruginosa*. She was awarded a Distinction grade for this work.

In 1998, she started as a PhD student in the Metalloproteins group at the Leiden Institute of Chemistry, University of Leiden, under the supervision of Prof. G. W. Canters. The study focused on the creation of a number of covalent and non-covalent constructs of the redox proteins flavodoxin and azurin, and the subsequent characterization of their electron transfer properties. She carried out this work in collaboration with several other groups, including that of Prof. Silvia Braslavsky at the Max Planck Institute for Bioinorganic Chemistry in Mülheim, Germany, the Structural and Functional Proteomics group at the Institute of Plant Biochemistry and Photosynthesis (IBVF-CSIC) at the University of Seville, Spain, and the Institute of Biophysics at the Biological Research Center of the Hungarian Academy of Sciences in Szeged, Hungary. She also attended a number of conferences both in the Netherlands and abroad, most notably winning the poster prize at the Protein Research Study Group Meeting of the NWO (the Dutch Organization for Scientific Research) in 2000 and attending the Gordon Research Conference on Electron Donor Acceptor Interactions in the United States of America in 2000.

Since the 16th of September, 2005, she has been employed as a post-doctoral researcher at the Leiden University Medical Centre (LUMC), working towards the development of an improved method for the diagnosis of neuromuscular diseases based on the presence of particular proteins in blood serum.

Acknowledgments

My experience during my PhD research period while at the University of Leiden would not have been the same without the numerous personal interactions, both short and long, that allowed the completion of this thesis. For this, I would like to acknowledge the following:

The environment and people at Metprot, which allowed me the freedom to expand my work in directions I was interested in as well as giving the nudges to keep it on track when necessary, and for asking all the right questions (usually!) at the right time,

Martin and Erik, for the kick start in molecular biology, and being the perfect sounding boards when making decisions on the microbiological side of the work,

Ellen, Gertrūd, and more recently Yvonne, for every single errand and task you helped me with, this thesis would not be here without you.

Miguel Ángel, por su constante apoyo y por poner siempre a mi disposición tanto los equipos como la experiencia de su laboratorio del IBVF de Sevilla,

Pepe y Manolo, por ser los perfectos mentores "flach" para una completa novata, pero también por vuestro entusiasmo incesante, inspiración y optimismo que me dieron tanta fuerza para mí y para mi trabajo,

y pa tos los habitantes del Laboratorio 5 (y visitantes asociaos), no zolo por estar siempre preparaos, sino también por encontrarme ezo aparato y disoluzione que nececezitaba, y zobre tó por compartí vuetro maravillozo rincón der mundo conmigo con lo brazo abierto ¡Sevilla tendrá ziempre un lugá muy especiá en mi corasón!

Sasha and László, for your interest and inexhaustible ideas and input both on the theoretical and practical aspects of the flavodoxin-TUPS project, and László, for being the best guide to Hungary anyone could wish for, köszönöm!

Kees and Fons, for their invaluable NMR support,

Silvia, por tu entusiasmo por aprender, y por ser la prueba viviente de que la mejor manera de aprender es enseñar.

my parents, sister and 'brother', Yngve, family (in-law) and friends, whether in the lab, in Leiden, or an e-mail away across the globe, for your encouragement and support but also for all our shared extra-curricular activities that were the perfect counter to the challenges and worries of a PhD.

You mean the world to me.